

JRC TECHNICAL REPORTS

JRC Testing and Demonstration Hub for the EU GNSS Programmes

Inventory of GNSS Testing Capabilities

Directorate Space, Security, and Migration
Unit Technology Innovation in Security
Galileo Sector



Year 2021



This publication is a Technical report by the Joint Research Centre (JRC), the European Commission's science and knowledge service. It aims to provide evidence-based scientific support to the European policymaking process. The scientific output expressed does not imply a policy position of the European Commission. Neither the European Commission nor any person acting on behalf of the Commission is responsible for the use that might be made of this publication. For information on the methodology and quality underlying the data used in this publication for which the source is neither Eurostat nor other Commission services, users should contact the referenced source. The designations employed and the presentation of material on the maps do not imply the expression of any opinion whatsoever on the part of the European Union concerning the legal status of any country, territory, city or area or of its authorities, or concerning the delimitation of its frontiers or boundaries.

Contact information

Name: Joaquim Fortuny-Guasch
Address: Via Enrico Fermi, 2749, I-21027 Ispra (VA), Italy
Email: Joaquim.Fortuny-Guasch@ec.europa.eu
Tel.: +39 0332 785104

EU Science Hub

<https://ec.europa.eu/jrc>

JRC125180

EUR 30747 EN

PDF ISBN 978-92-76-39185-2 ISSN 1831-9424 doi:10.2838/93444

Luxembourg: Publications Office of the European Union, 2021

© European Union, 2021



The reuse policy of the European Commission is implemented by the Commission Decision 2011/833/EU of 12 December 2011 on the reuse of Commission documents (OJ L 330, 14.12.2011, p. 39). Except otherwise noted, the reuse of this document is authorised under the Creative Commons Attribution 4.0 International (CC BY 4.0) licence (<https://creativecommons.org/licenses/by/4.0/>). This means that reuse is allowed provided appropriate credit is given and any changes are indicated. For any use or reproduction of photos or other material that is not owned by the EU, permission must be sought directly from the copyright holders.

All content © European Union 2021, unless otherwise specified.

How to cite this report: Luca Cucchi, Ciro Gioia, Melania Susi, Sophie Damy, Lukasz Bonenberg, Karen Boniface, Marco Basso, Matteo Sgammini, Matteo Paonni and Joaquim Fortuny, JRC Testing and Demonstration Hub for the EU GNSS Programmes - *Inventory of GNSS Testing Capabilities*, EUR 30747 EN, Luxembourg: Publications Office of the European Union, 2021, ISBN 978-92-76-39185-2, doi:10.2838/93444, JRC125180.

Contents

Abstract	5
1 Introduction.....	7
1.1 Scope of the document.....	7
1.2 Structure of the document.....	7
2 General terms and conditions.....	8
2.1 Preparatory activities	8
2.2 General conditions	9
2.3 Contact points for general inquiries and logistics.....	9
3 Testing capabilities catalogue.....	11
3.1 Antenna measurements and characterisation	11
3.1.1 The EMSL Laboratory	11
3.1.2 Antenna measurements with a Vector Network Analyser.....	14
3.1.3 Antenna measurements with a GNSS simulator	15
3.1.4 Antenna array measurements	16
3.2 Conformance testing and performance assessment	19
3.2.1 Conformance testing of eCall devices	19
3.2.2 Performance assessment of Galileo-enabled ship-borne GNSS receivers ...	23
3.2.3 Performance assessment of smartphones exposing raw measurements	26
3.3 Retrieval of reference trajectory solutions	31
3.3.1 GNSS/IMU based reference solution: an agriculture case study	31
3.3.2 GNSS based reference solution: a drone case study	33
3.3.3 Total station based surveying: a 5G case study	35
3.4 RTK/PPP high accuracy positioning.....	37
3.4.1 RTK processing with high-end base and rover receivers.....	37
3.4.2 RTK/PPP post-processing	38
3.4.3 Simulation of Galileo E6 signal and navigation message.....	39
3.4.4 Galileo E6 signal reception quality analysis.....	41
3.5 Testing of GNSS timing receivers.....	43
3.5.1 Local oscillator characterisation	43
3.5.2 Pulse Per Second (PPS) signal analysis	45
3.5.3 GNSS intersystem time bias evaluation	46
3.6 Laboratory testing with RFI and spoofing signals	48
3.6.1 Testing of GNSS receivers with RFI signals.....	48
3.6.2 Testing of GNSS receivers with spoofing signals	51
3.7 GNSS signal record & replay testing	55
3.8 Testing of OSNMA-enabled receivers	57
3.8.1 Generation of the Galileo OSNMA data stream	57

3.8.2 OSNMA-enabled receivers	57
3.8.3 Post processing tools.....	58
3.8.4 Modular set-up for OSNMA testing	59
3.9 JRC Living Labs	61
3.9.1 SARA drone flight trials in the JRC Campus	62
3.9.2 Testing of an indoor navigation app on a smartphone.....	63
3.10 Future updates on the inventory of GNSS testing capabilities	66
References	69
List of Abbreviations	75
List of Figures	77
List of Tables	81

Acknowledgements

The development of the testing capabilities and associated laboratory infrastructures subject of this report has only been possible thanks to the constant support and trust from the colleagues at the Satellite Navigation Unit of the European Commission (EC) Directorate General Defence Industry and Space (DEFIS), and the European GNSS Agency (GSA). Over the last few years, thanks to this fruitful cooperation, the JRC has established a scientific and technical team that is actively supporting the implementation of the EU Global Navigation Satellite System (GNSS) Programmes.

Likewise, the support from the colleagues at the Strategy, Work Programme and Resources (JRC.A) and the Space, Security and Migration (JRC.E) Directorates of the JRC is also acknowledged.

Finally, some of the testing capabilities reported in this document are based on software defined radio instruments with a dedicated firmware developed in-house by an FPGA consultant. The support of Fausto Bonavitacola, affiliated to Fincons Italia S.p.A. and working as a consultant at the JRC, is acknowledged.

Authors

Luca Cucchi, Ciro Gioia, Melania Susi, Sophie Damy, Lukasz Bonenberg, Karen Boniface, Marco Basso, Matteo Sgammini, Matteo Paonni and Joaquim Fortuny

European Commission, Joint Research Centre, Directorate E, Space, Security and Migration, Italy

Abstract

The European Commission (EC) Joint Research Centre (JRC), in the frame of a scientific and technical support activity with the Satellite Navigation Unit of the EC Directorate General Defence Industry and Space (DEFIS) and the European GNSS Agency (GSA), has agreed to facilitate testing and demonstrations activities of Research and Development (R&D) Actions under the European Union (EU) Global Navigation Satellite System (GNSS) Programmes. This facilitation is provided on a voluntary basis to H2020 and Galileo Fundamental Elements project consortia interested in accessing the GNSS testing facilities based at the JRC's Ispra Site. In this context, the availability of a document providing an up-to-date inventory of the GNSS testing capabilities available at the JRC has been identified as an urgent need. This report is aimed specifically at addressing this gap and has two main components: firstly, setting the general terms and conditions to request the access to the testing facilities, and secondly, the provision of a comprehensive summary of the GNSS testing capabilities that are currently available at the JRC. A reference to past testing campaigns is made to illustrate the typical testbeds and results that were produced. With this reference document at hand, interested project consortia are expected to be set in a position to be able to specify an initial test plan with the required level of detail.

Lastly, the portfolio of the testing capabilities available at the JRC provided in this document is expected to evolve in the coming years. Therefore, regular reviews to integrate any new addition or change in the portfolio of testing capabilities are planned, with the corresponding release of the updated versions of the document.

1 Introduction

1.1 Scope of the document

The scope of the document is to provide an overall description of the portfolio of Global Navigation Satellite System (GNSS) testing capabilities currently available at the European Commission's Joint Research Centre (JRC), at the premises of its Ispra Site.

The facilitation of testing and demonstration activities in the context of R&D Actions under the European Union (EU) GNSS Programmes started back in 2012. At that time, the JRC could make available the anechoic chamber of the European Microwave Signature Laboratory (EMSL) and a GNSS simulator. The first testing campaign that was supported was that of the GSA FP7 Project DETECTOR [1], in July 2012. This project was aimed at prototyping a low-cost solution to detect and characterise radio-frequency interference (RFI) to protect and increase the use of GNSS in critical road applications. Likewise, in January 2014, the JRC facilitated the testing and demonstrations planned in an R&D action of the European Commission (EC) developing GNSS Receivers with integrity monitoring capabilities for vehicular and pedestrian platforms, in the frame of the iGNSSRx Project [2]. Other relevant EC R&D actions that were supported subsequently were FOSTER [3], TACOT [4], TRITON [5], and AALECS [6], [7].

This initial support activity was consolidated and led to a formal agreement with the Directorate General (DG) of the Commission in charge of the management of the EU GNSS Programmes (i.e., currently DG DEFIS, and previously DG ENTR and DG GROW) and the European GNSS Agency (GSA). Over the last 8 years, a scientific team at the JRC was established and over the years has developed a wide range of testing capabilities on the user-segment of GNSS. In parallel with this development, the JRC has integrated state of the art GNSS test equipment combined with indoor test facilities, where measurements can be conducted under full control and in isolation from the outside electromagnetic environment.

Project consortia potentially interested in conducting tests and demonstrations at the JRC need to have access to a reference document where the testing capabilities available are thoroughly reported, with use case examples and results from test campaigns facilitated in the past. This document is aimed at addressing this need and provide a comprehensive set of information that can set the potential users in the position to specify a test plan with the required level of detail at the submission of a project proposal.

At a later stage, project consortia that were successful in the evaluation process and planned the tests and demonstrations at the JRC will be asked to share the test plan. This is required to assess the feasibility in terms of the equipment needed and the temporal availability of the laboratory sufficiently in advance.

Finally, the evolution of the support activity with DG DEFIS and the GSA will entail the development of new testing capabilities at the JRC. Consequently, to integrate these changes, this document is expected to be reviewed and updated on a regular basis in the coming years.

1.2 Structure of the document

This document has been structured as follows. In Section 2, the general terms and conditions to get granted the access to the GNSS testing facilities of the JRC are given. Here, an indication of times and protocol to be followed during the entire process of preparation, execution, and finalisation of the tests. Section 3 provides a thorough description of a total of 9 main categories of the testing capabilities available to date at the JRC, these include GNSS antenna measurements and characterisation, GNSS receiver testing, measurement of reference trajectories, high accuracy positioning, GNSS timing receiver characterisation, radio frequency interference testing, radio frequency signal record and replay, Galileo Open Service Navigation Message Authentication (OSNMA) testing capabilities, and the outdoor facilities of the JRC Living Labs. As pointed out earlier on, the inventory of subject of this document will be reviewed on a regular basis and, for that reason, a final section presenting a summary of the expected updates has been included.

2 General terms and conditions

2.1 Preparatory activities

An overall description of typical interactions with actor having planned to access the laboratory for the verification and validation phase of the on-going project are described in the steps reported in Table 1, where T_v denotes the date of the event to be held at the JRC premises. The scheduling made in this table are to be considered as indicative only, and therefore, modifications to the proposed timeline are expected to be agreed on a case by case with the Project Consortium.

Table 1. Typical interactions between JRC and the project consortium requesting the facilitation of testing and demonstration activities.

Start Event	End Event	Actions
$T_v - 3m$	$T_v - 2.5m$	JRC expects to receive the following items: <ul style="list-style-type: none"> - Test plan with test cases description including: objectives, overall description, test facility, test set-up, step-by-step procedure, pass/fail criteria if applicable - Control software/Drivers/Datasheet/user manual of relevant hardware (HW) equipment under test from Project Consortia.
$T_v - 2.5m$	$T_v - 2m$	JRC examines the documentation and provides a feedback. Possible interactions between JRC and consortium via email exchanges and/or teleconference might be arranged to agree pending issues such as the test plan, logistics, the booking of test facilities and the readiness of the equipment under test.
$T_v - 2m$	$T_v - 1m$	JRC expects to receive the Device Under Test (DUT) and the necessary HW equipment at the Reception & Shipment of Goods Desk of JRC's Ispra Site.
$T_v - 1m$	$T_v - 0.5m$	JRC is in charge of setting up the test bed and facilitating a preparatory dry-run. In case of need, during these preparatory phase, remote access to the test equipment can be granted to the consortium. Log data and analysis results are exchanged and verified. Meetings with consortium are scheduled at regular basis to assess that the results are in line with the expectations.
T_v	$T_v + 3d$	Execution of the test campaign or demonstration event at the JRC premises in Ispra. Typical duration of the test campaign is 2 to 3 days.
$T_v + 3d$	$T_v + 5d$	JRC collects and shares the data logs and tests results other than those already gathered directly by the consortium during the test campaign.
$T_v + 5d$	$T_v + 10d$	The Project Consortium arranges the pick up of the test equipment from the Reception & Shipment of Goods Desk of JRC's Ispra Site. The test equipment is returned to the Consortium.

2.2 General conditions

- JRC facilities and support from the technical staff are available to facilitate testing and demonstration activities under EC initiatives as Horizon 2020 and Galileo Fundamental Elements R&D Actions.
- This document is intended to be used as a guideline during the preparation of the test plan, which is under the responsibility of the Project Consortium requesting the access to the JRC testing facilities.
- The facilitation of the testing and demonstration activities proposed by the Project Consortium is subject to the feasibility of the test plan and the availability of required testing facilities and equipment. Although there is no specific limit on the duration of the test campaign, since the test facilities are made available to multiple project consortia, for obvious reasons, it is suggested to keep the duration to a minimum.
- In case of testing activities to be carried out in the JRC premises, it is worth underlining that the final Demo-event represents just the last step of a set of preparatory activities aimed at defining and configuring the test environment properly.

2.3 Contact points for general inquiries and logistics

The contact point details for any inquiries regarding the access to the GNSS testing facilities of the JRC is as follows:

Joaquim Fortuny
e-mail: Joaquim.Fortuny@ec.europa.eu
Phone: +39 0332 785104
Via Enrico Fermi, 2749
I-21027 Ispra, Italy
Galileo Sector
Directorate Space, Security and Migration
EC Joint Research Centre

Any shipments of equipment needed for the testing campaigns at the JRC shall be addressed to:

e-mail: JRC-ISPRA-RICEVIMENTO-MERCI@ec.europa.eu
Phone: +39 0332 786164
EC Joint Research Centre
Reception & Shipment of Goods Service
Via Enrico Fermi, 2749
I-21027, Italy

It is important to keep in mind that all parcels shall arrive accompanied with a pro-forma invoice listing the items shipped to the JRC and a note stating that "All the goods are entering the JRC Ispra Site temporary for testing purposes". In the absence of the pro-forma invoice, please be aware that parcels might be rejected at the JRC Customs and returned to the sender.

3 Testing capabilities catalogue

This section gives a comprehensive overview of the GNSS receiver testing capabilities that are currently available at the JRC and are considered relevant in the frame of the EU R&D Actions under the EU GNSS Programmes. A total of 9 different categories of the testing capabilities are presented, illustrated with a description the test set-ups, the test procedures and a selection of the results that were obtained.

The evolution of the support activity with the DG of the EC in charge of the management of the EU GNSS Programmes (i.e., DG DEFIS) and the GSA will entail the development of new testing capabilities at the JRC. Consequently, the present portfolio must be considered as a first selection of testing capabilities and thus will be subject to regular revisions and updates in the coming years.

3.1 Antenna measurements and characterisation

This section provides a description of the main testing facility in the GNSS laboratory of the JRC, the European Microwave Signature Laboratory (EMSL), and the different measurement configurations aimed at characterising GNSS antennas and GNSS antenna arrays in an anechoic room.

3.1.1 The EMSL Laboratory

The main testing facility to conduct antenna measurements at the JRC is EMSL. The overall structure of the EMSL anechoic chamber is the conjunction of a hemi-spherical and a cylindrical dome, with a diameter of 20 meters. The centre of the hemi-spherical dome is located at 5 meters above the floor. The Devices Under Test (DUTs) are positioned on top of a rotating tower that can move in and out the dome. An interesting feature of the EMSL is that, in the gap between the hemi-spherical and cylindrical domes, it has two separate antenna sleds with transmit and receive antennas that can move independently along a circular rail on the dome of the anechoic chamber, maintaining its pointing at the centre or focal point. The high load capacity of the rotating tower, it can hold a maximum load is 3.0 tons, allows the testing of antennas integrated in vehicles. A 3-D sketch of the exploded view of the EMSL along with a photograph of the rotating tower inside the anechoic chamber are shown in Figure 1.

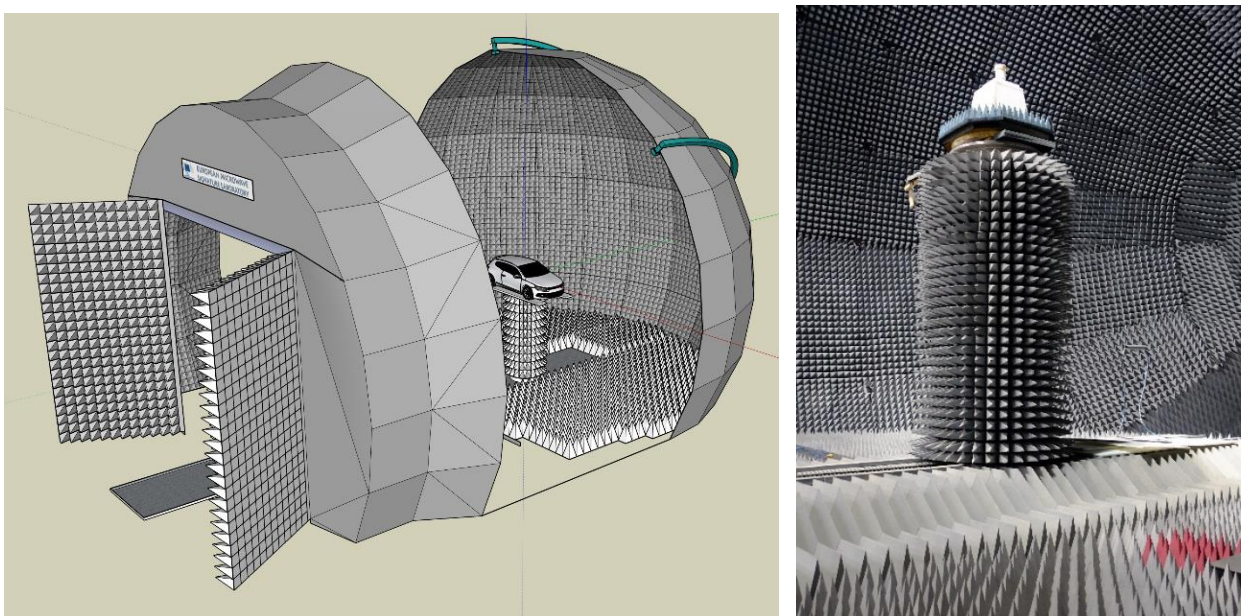


Figure 1. 3-D sketch of an exploded view of the EMSL with a car on top of the rotating tower (left). A photograph of the rotating tower with an antenna under test (right).

The EMSL laboratory was built in 1992 and was originally designed for antenna and electromagnetic scattering measurements. Since its inauguration and until 2008, the testing activities were focused on the fields of radar remote sensing and, more in particular, on

polarimetric Synthetic Aperture Radar (SAR) to support the development of new applications of spaceborne SAR missions [8]–[11]. More recently, in 2008, the EMSL was upgraded to initiate the current testing activity on GNSS receivers and, more precisely, those integrating Galileo and EGNOS. The first main upgrade made at that time was the integration of a GNSS simulation platform in the laboratory, such that over-the-air measurements to assess the performance of GNSS receivers with their antennas could be carried out in a controlled, automated, and repeatable manner [12]. These measurements are conducted with one of the probe antennas that can be moved along the circular rail transmitting the signals from the GNSS simulator. The second main upgrade was that of adding a new set of antennas on the sled A to be used in antenna measurements in the frequency range from 700 MHz up to 4.0 GHz. A close view of the antennas, video cameras, and laser pointer currently installed in the sleds A and B of the EMSL is shown in Figure 2.

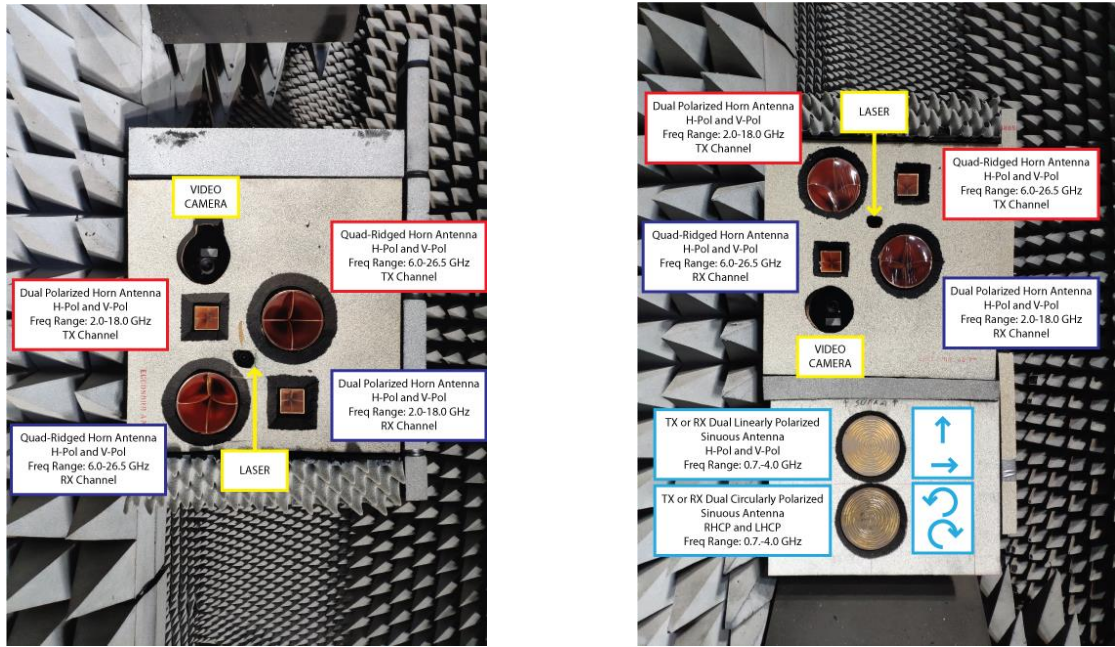


Figure 2. Close view of the antennas, video camera and laser pointer in the sleds A (left) and B (right) of the EMSL laboratory.

The electromechanical sub-system of the EMSL consists of four brushless DC motors that actuate the movement of four mechanical axes individually (i.e., sled A, sled B, linear axis of the tower, and rotation of the tower). A dedicated control software interfaces with a Programmable Logic Controller (PLC) over the network such that the antenna measurements can be conducted in a fully automated manner. The positioning ranges and accuracy of the four mechanical axes of the EMSL are summarised in Table 2.

Table 2. Specification of the positioning ranges and accuracies of the four mechanical axes of the EMSL.

Axis	Positioning Range	Accuracy
Linear axis of measurement tower	$-8500 \text{ mm} \leq L \leq +2500 \text{ mm}$	$\pm 0.5 \text{ mm}$
Azimuth Scan Angle of measurement tower	$-20^\circ \leq \Phi \leq +360^\circ$	0.05°
Zenith Scan Angle of Sleds A and B	$-112^\circ \leq \theta \leq +112^\circ$	0.005°

The EMSL laboratory has three Radio Frequency (RF) signal paths, two identical paths routed to each one of the antenna sleds plus a third one that is routed to the measurement tower. The RF

paths routed to the antenna sleds include four RF cables: one Transmitting (TX) channel, two Receiving (RX) channels and one return channel for the external reference. The third RF path to the measurement tower includes just one RF cable that can be used on TX and RX modes depending on what is the device under test. The routing of the RF signal paths and that in the sleds to the probe antenna is managed with a network of 32 electromechanical microwave switches. The configuration of the routing of the three RF paths can be programmed and is remotely controlled with a microwave switch driver instrument interfaced over the intranet of the laboratory.

A common measurement set-up for the characterisation of a GNSS antenna is that of combining a 180 degree zenith scan of the probe antenna with a 180 degree azimuth scan of the measurement tower, as it is depicted in Figure 3. This combination allows to have a set of measurement points uniformly sampled in the azimuth and zenith angles, covering the entire upper hemisphere.

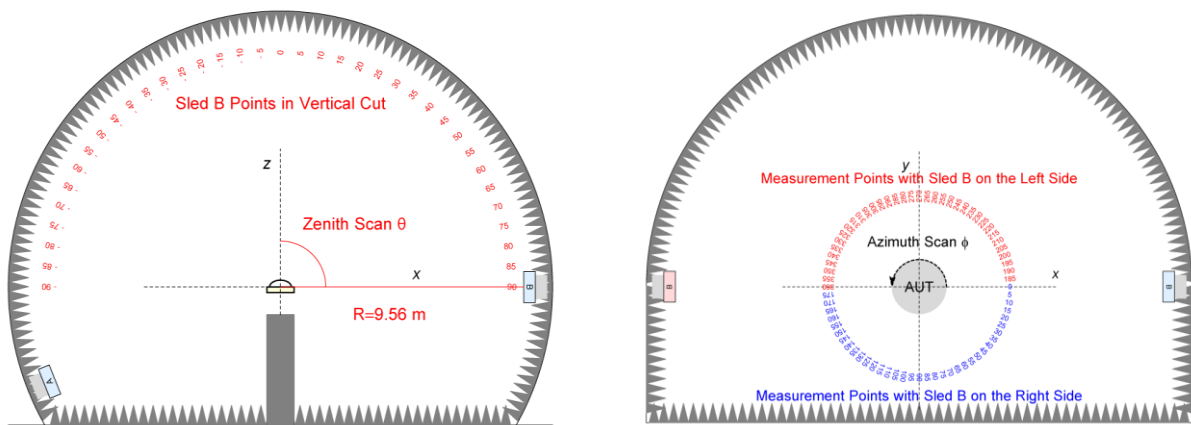


Figure 3. Sketch of the side view (left) and top view (right) of the two circular scans in an antenna measurement in the EMSL, which correspond to the zenith and azimuth angles.

Two 3D sketches identifying the four mechanical axes of the EMSL and the measurement points in an antenna measurement with combined zenith/azimuth scans are shown in Figure 4.

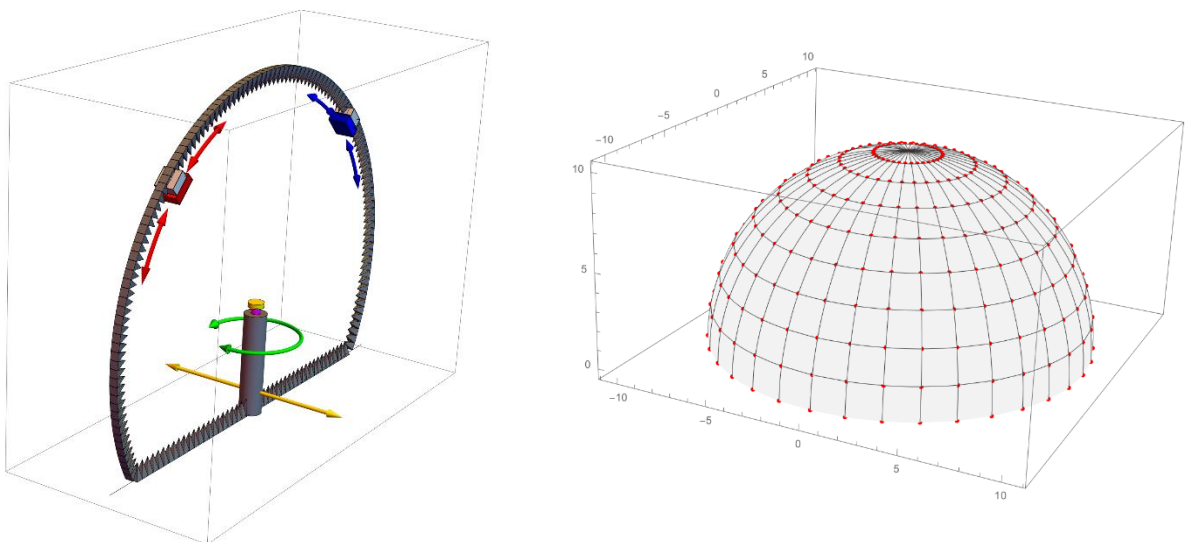


Figure 4. 3D sketches identifying the four mechanical axes of the EMSL (left) and the spherical grid of measurement points in an antenna measurement with combined azimuth/zenith scans (right).

At present, the two core RF instruments of the EMSL that can be used to characterise a GNSS antenna are a vector network analyser and the GNSS simulator. Measurements with the vector network analyser can be carried out in two configurations, depending whether the antenna to be tested integrates a low noise amplifier on reception (i.e., as it is the case in many GNSS

antenna systems) or not. A third configuration that can be used is that where the source of the RF signals received by the antenna under test is that coming either from the GNSS simulator or a rooftop geodetic antenna installed in the building hosting the EMSL.

3.1.2 Antenna measurements with a Vector Network Analyser

A sketch of the set-ups for the antenna measurements with the Vector Network Analyser (VNA), in the configuration to characterise a passive or an active reference antenna, are shown in Figure 5. More precisely, it shows the set-up of a calibration measurement with a reference antenna with gain vs frequency characteristic known from a previous measurement or has been provided by an accredited laboratory.

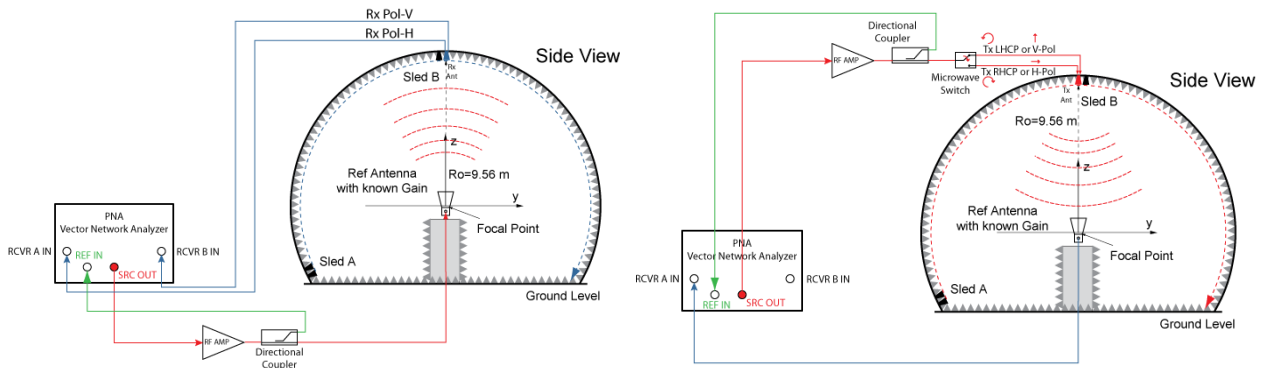


Figure 5. Sketches of the set-up of a calibration measurement with the vector network analyser: reference antenna with known gain on transmit (left) and receive (right) modes.

There is commonality in the two configurations of the measurements with the VNA that is important to underline. In both set-ups there is an amplifier in the RF transmit path with a directional coupler located right after. This coupled return path is routed to the external reference input of the VNA to filter out any variations of the amplifier amplitude and phase response during the measurement, improving the overall stability and accuracy of the system. This is particularly important when the characterisation made is that of estimating the variations of the phase centre and phase centre offset of the antenna under test. In these measurements, the entire RF chain of the measurement system excluding the device under test has to exhibit an extremely high phase and amplitude stability.

A VNA is an instrument that allows to characterise the S-parameters of a device under test. In the antenna measurements, it is then possible to characterise the gain by measuring the complex ratios A/R1 and B/R1 versus frequency, where A and B are the test port receivers of the VNA and R1 is the external reference input of port 1. Measurements of the return loss or impedance matching versus frequency of the antenna under test can also be carried out. This measurement though requires a prior calibration of the VNA at the location of the RF port of the antenna, which must be carried out using an S-parameter calibration kit covering the frequency range of interest.

An illustrative example of the results obtained in the measurements of a choke-ring GNSS antenna are given in Figure 6. The characterisation made on this antenna was that of measuring the gain in the Left Hand Circular Polarisation (LHCP) and Right Hand Circular Polarisation (RHCP) modes at two vertical cuts spaced 90 degrees. This is a measurement of the overall gain of the antenna plus filter and the low noise amplifier that has integrated. The vertical cuts of the measured antenna gain pattern correspond to the frequency of 1578.0 MHz.

Choke-Ring Antenna Elevation Cuts at L1 (1.578 GHz)

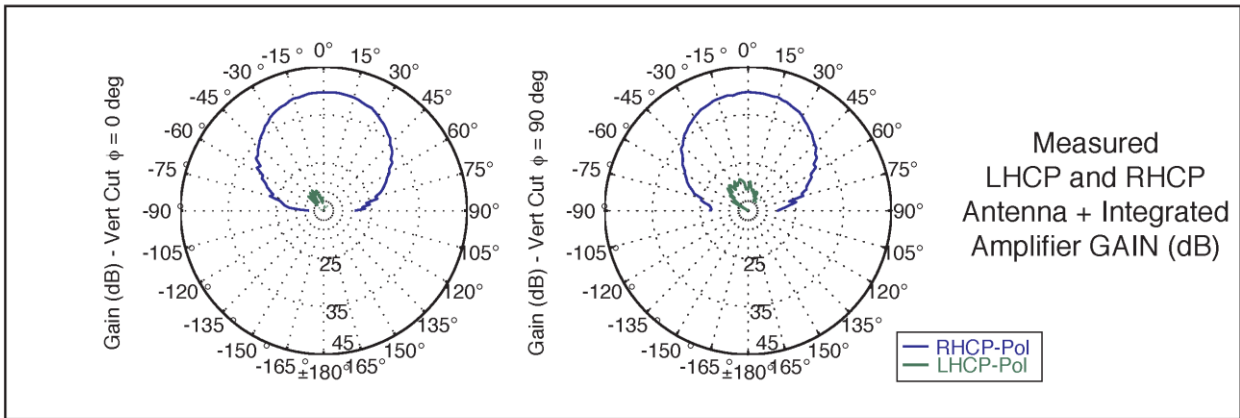


Figure 6. Two vertical cuts of the LHCP and RHCP gain of a choke-ring antenna at the frequency of 1578.0 MHz: vertical cuts at azimuth 0 deg (left) and azimuth 90 deg (right).

The measurements on this choke-ring antenna were made in a frequency range covering entirely all the GNSS bands. The result of the antenna RHCP gain versus the frequency at the boresight is shown in Figure 7, where the effects of the highly selective pass band filters integrated in the antenna are clearly noticeable.

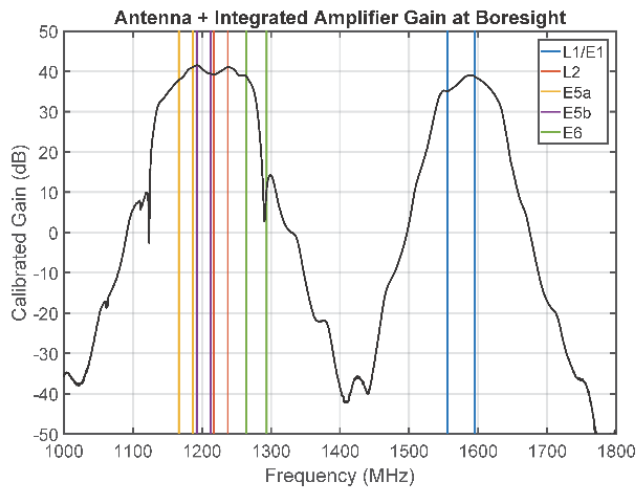


Figure 7. RHCP gain versus frequency of a choke-ring antenna measured at boresight in the EMSL.

3.1.3 Antenna measurements with a GNSS simulator

A second modality of conducting the characterisation of an antenna is that of using a GNSS simulator as the signal source. The EMSL laboratory is equipped with a state-of-the-art GNSS simulator that is currently capable to generate Galileo E1/E5/E6, GPS L1/L2/L5, and Satellite Based Augmentation System (SBAS) signals [13]. A dedicated room behind the dome of the EMSL is the host of the GNSS simulation rack, which includes the simulator, its controller, an RF signal combiner, two vector signal generators, a Rubidium frequency standard, a GNSS timing receiver and Network Time Protocol (NTP) server, and a server station hosting Dynamic Host Configuration Protocol (DHCP), Domain Name System (DNS) and Network Attached Storage (NAS) services. A sketch of the configuration of the laboratory when the GNSS simulator is used as the signal source to characterise a GNSS antenna, and a photograph of the GNSS simulation rack are shown in Figure 8.

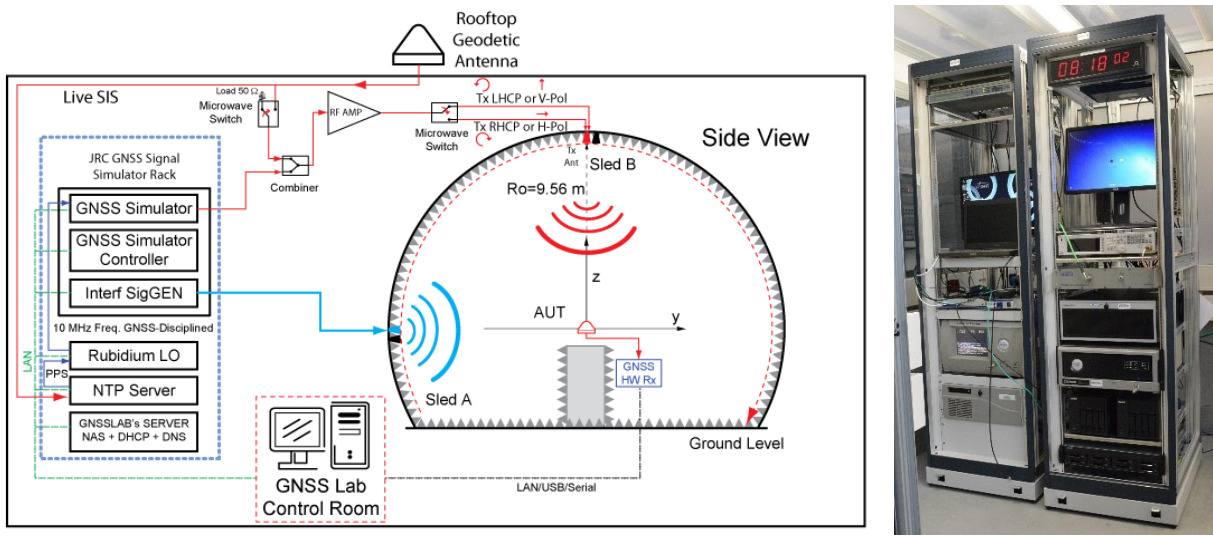


Figure 8. Sketch of the laboratory set-up to characterise an antenna using a GNSS simulator as a signal source (left) and photograph of the GNSS simulation rack behind the dome of the EMSL (right).

The use of the signal generator and RF combiner is an interesting option in case one wants to assess the performance of a GNSS receiver and its antenna when there are other signals present either in band or in adjacent bands (e.g., a GNSS jamming or spoofing signal). In this type of tests, it is possible to channel separately the signal from the GNSS simulator and that from the RF signal generator to the two antenna sleds, as illustrated in Figure 8.

An aspect that deserves special attention when conducting RF compatibility tests is the calibration of the power levels of the GNSS signals broadcast inside the anechoic chamber of the EMSL. Here, it is important to note that it is possible to calibrate the transmit power level at the probe antenna in the sled. This will ensure that the radiated power level at the position of the antenna under test is closely aligned with that specified in the Interface Control Document (ICD) of the GNSS systems enabled in the simulator.

A variant of the configuration of the test set-up using a GNSS simulator that is worth noting is the one using a GNSS playback platform as the signal source. In this test modality, the GNSS playback device broadcasts a signal that has been synthesised or recorded in advance. Just as it is done with a GNSS simulator, the power level of the GNSS playback device can be calibrated to obtain radiated power levels close to the antenna under test that are aligned with those specified in the ICD.

A last observation on the antenna measurements using a GNSS simulator as the signal source is that some of the KPIs that can be characterised are very close to those using a vector network analyser. Examples of these are the group delay and phase centre variation of the antenna under test. An investigation on the stability and cross-validity of this type of measurements with those using a vector network analyser is currently on-going at the JRC. A more detailed description of this antenna characterisation capability illustrated with some example results will be provided in a future revision of this document.

3.1.4 Antenna array measurements

The testing and characterisation of GNSS antenna arrays is an important capability of the anechoic chamber of the EMSL. Example Key Performance Indicators (KPIs) that one may want to assess are the performance of the antenna array to implement effectively null-steering or digital beamforming [14]. A possible approach to assess these KPIs is to characterise each antenna element separately. This characterisation can only be carried out when the RF port of all the elements of the antenna array are interfaceable with the vector network analyser. The EMSL laboratory is equipped with a microwave switch driver instrument and an 11-port microwave switch that have been specifically designed for antenna array measurements. This multi-port microwave switch device can be installed next to the antenna array under test and can be controlled remotely during the tests. For the sake of illustration, a sketch of the multi-

port microwave switch and a photograph of a 7-element antenna array mounted on the measurement tower are shown in Figure 9. During the tests run on this antenna array, the radiation pattern of every antenna element was characterised sequentially, scanning all the elements with the multi-port switch at each position of the probe antenna in the sled and rotation angle of the measurement tower. The current version of the control software used for the antenna measurements allows a fully automated switching across an arbitrary number of antenna elements, which at present is limited to 11.

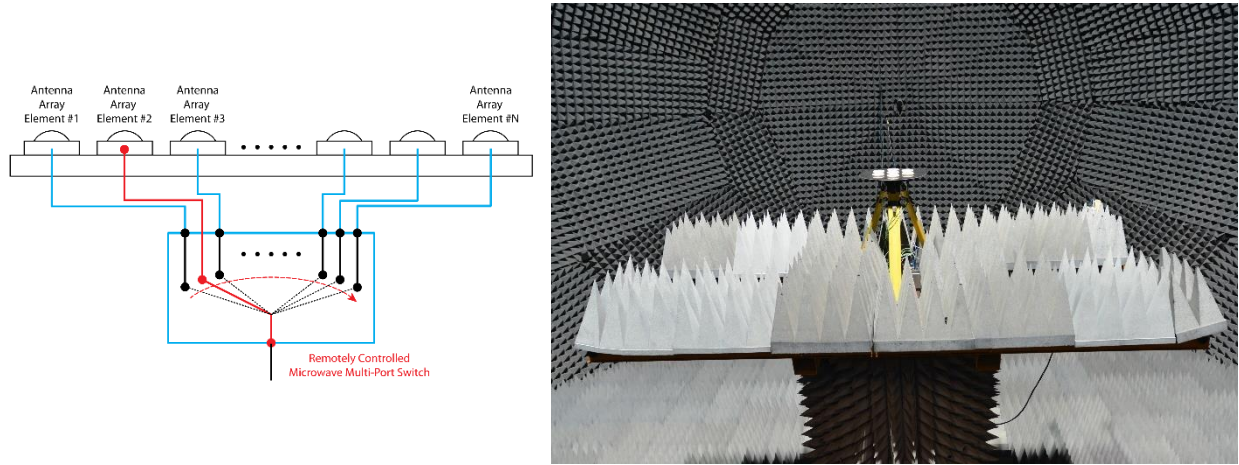


Figure 9. a sketch of the multi-port microwave switch (left) and a photograph of a 7-element antenna array mounted on the measurement tower of the EMSL (right).

A closer view of the 7-element array and the microwave switch driver, and the horizontal and vertical cuts of the RHCP measured gain pattern of the central element (blue lines) and one of the peripheral elements (red lines) are shown in Figure 10. These results correspond to an azimuth angle of the vertical cuts of 0 deg, and an elevation angle of the horizontal cuts of 40 deg. The elements of the array are active GNSS antennas with dual-polarisation (LHCP-RHCP) receive ports.

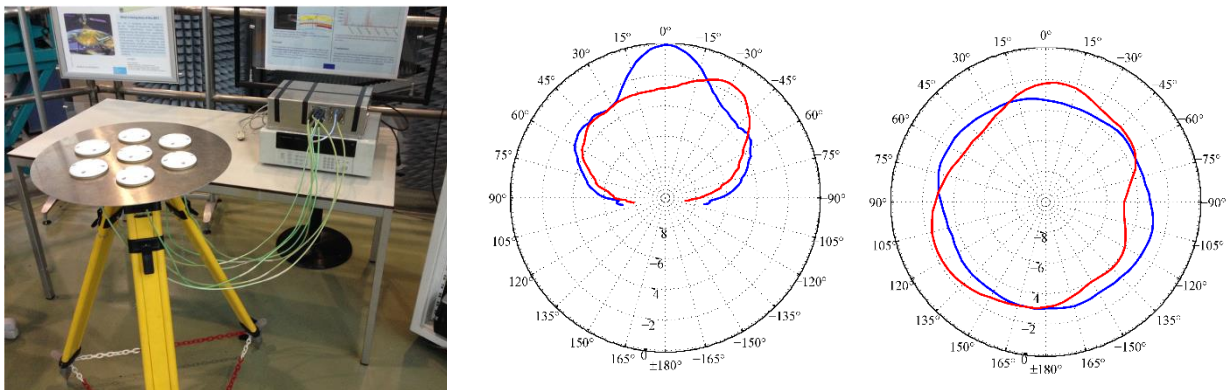


Figure 10. Close view of the 7-element antenna array interfaced with the microwave switch driver (left); vertical cuts of the RHCP gain pattern of the central and a peripheral element at azimuth 0 deg (center); horizontal cuts of the gain of the central and a peripheral element at 40 deg elevation (right).

An interesting and pretty unique feature of the EMSL anechoic chamber is that, in addition to the two sleds with the Tx/Rx probe antennas, it also has an array of 36 dual-polarised antennas that are distributed in a half of the hemi-spherical dome. These additional probe antennas are dual linearly polarised standard gain horns that can be used in the frequency range 1 to 18 GHz. This fixed antenna array was originally installed to conduct multi-static radar cross section measurements of targets under test. A dedicated network of a total of 7 six-port electromechanical microwave switches allows the routing of the Tx or Rx signals to/from any individual probe antenna. The entire set of multi-port switches can be interfaced remotely and the signal routing can be changed during the course of a measurement. A 3-D sketch of the RF

signal routing network, with the 7 electromechanical switches on the dome of the EMSL, and a photograph of the interior of the EMSL, indicating the arrangement of the 36 probe antennas, are shown in Figure 11.

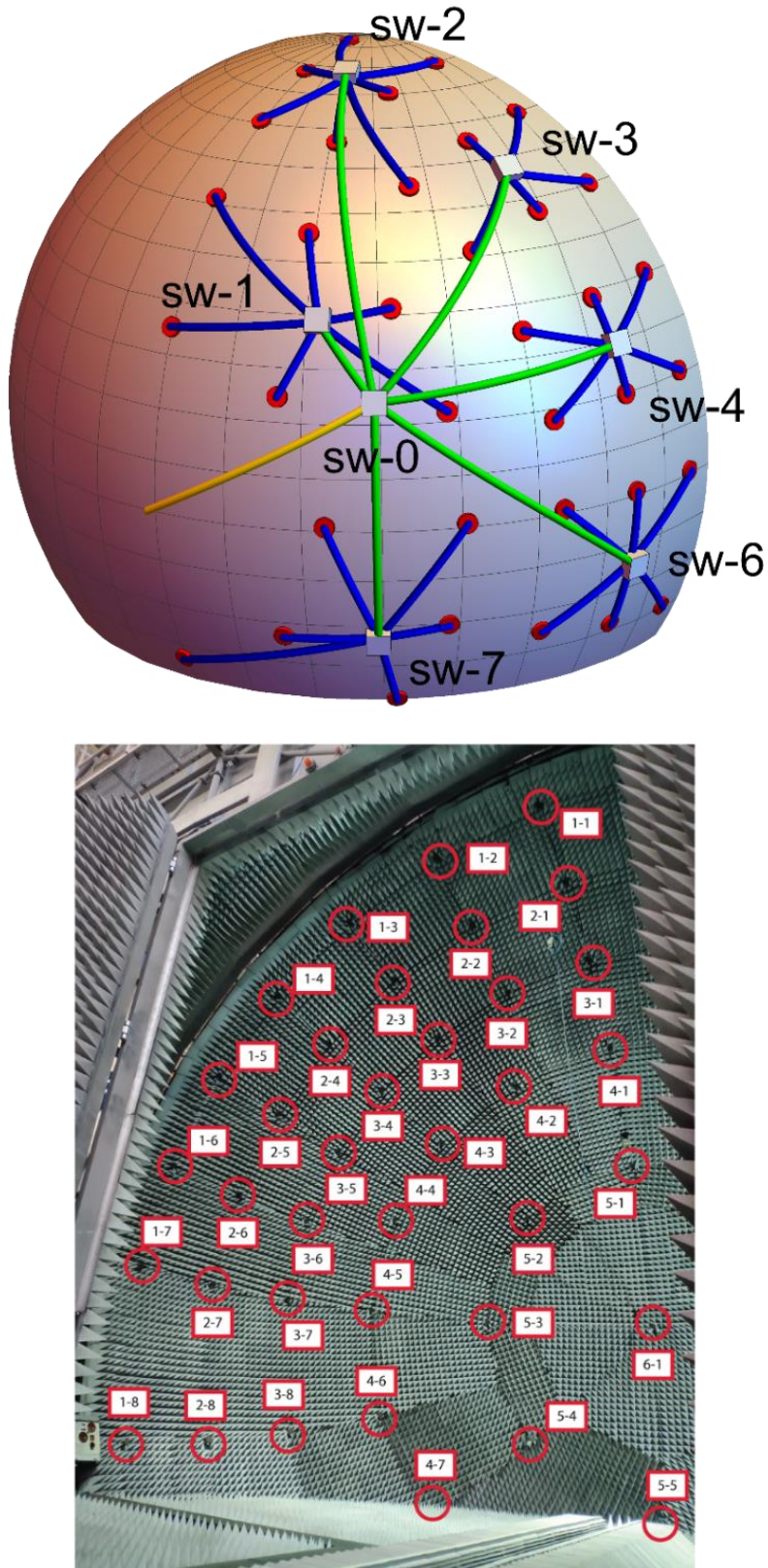


Figure 11. 3-D sketch of the signal routing network of the array of the 36 fixed antennas on the outer surface of the dome (top), and photograph showing the arrangement of the fixed probe antennas as seen inside the anechoic chamber (bottom).

3.2 Conformance testing and performance assessment

This section gives three examples of recent test campaigns where multiple GNSS receivers were assessed simultaneously with the aim to illustrate the testing capabilities currently available at the JRC. A description of the scope of the test campaign, the test scenarios, and the KPIs assessed are provided.

The three test campaigns in question that have been selected are:

- Conformance testing of the eCall devices, which was aimed at assessing the compliance of the available devices prior to the entry in force of the EU regulatory framework on the eCall.
- Performance assessment of Galileo-enabled ship-borne GNSS receivers. The goal of this campaign was to assess the conformity of Galileo-enabled devices to the requirements set in an existing International Electrotechnical Committee (IEC) standard.
- Performance assessment of Android smartphones providing access to GNSS raw measurements.

3.2.1 Conformance testing of eCall devices

The eCall Commission Delegated Regulation (EU) 2017/79 [15] is one of the first EU regulatory frameworks enforcing the adoption of Galileo and EGNOS in the road sector. The practical implication of this is that, starting in April 2018, all new models of light vehicles sold in the EU must integrate an eCall on board unit with a GNSS receiver using Galileo and EGNOS. Noting the significant impact that the adoption of this and other EU regulatory frameworks have, the EGNSS Programmes have streams of targeted actions aimed at facilitating the implementation of regulatory frameworks that are considered strategic. In the case of the eCall, there was the need to support both on-board unit manufacturers and technical centres and help them be ready for the type-approval process specified in the regulation. In 2017, in close coordination with the GSA, the JRC facilitated a preparatory test campaign to assess the conformance of the on-board units made available to the technical requirements set in the Annex VI of the regulation. Other targeted actions under the EGNSS Programmes that support the implementation and adoption of regulatory frameworks are those led by Galileo Fundamental Elements of H2020 project consortia. In this context, the fact of presenting what kind of conformance testing was facilitated for the eCall is found to be relevant and thus it is summarised here.

The test campaign was split in several phases, in the first part the analysis of the Annex VI of the eCall Commission Delegated Regulation was performed. The document has been used as baseline for the preparation of the scenarios used in the test campaign. The main tasks performed during the eCall activity were:

- Definition and implementation of the test scenarios, according to Annex VI of the Commission Delegated Regulation 2017/79;
- Evaluation of a number of close to market eCall test simulators to facilitate vendors' development, ensure consistency and share lessons learnt;
- Execution of the tests on each DUT;
- Test results analysis;

Preparation of proofreading of the implementation guidelines document [16];

- Generation of individual test report for both DUT manufacturers and test/simulator solutions, detailing the observed results and providing recommendations in view of compliance with the Annex VI of Commission Delegated Regulation 2017/79;

Aggregation of the results and generation of an eCall Conformance Testing Campaign Overall Assessment Report [17], [18].

The DUT performance were assessed with respect to the following key performance indicators (KPIs): usage of the SBAS corrections, positioning accuracy under static, dynamic and dynamic with shadow areas conditions, Cold Start Time-To-First-Fix (CSTTFF); re-acquisition time and receiver sensitivity in cold start mode.

JRC set up an ad-hoc test-bed designed to assess the performance of the eCall devices with respect to the technical requirements for compatibility with the positioning services provided by Galileo and EGNOS. This test-bed was based on a GNSS simulator, which was configured to generate the Open Service signals of GPS L1, Galileo E1, and SBAS, in accordance with the specifications given in the eCall Guidelines Report and with Galileo and EGNOS control documents [19]. The tests are carried out in conducted mode without including the antenna in the measurement chain as shown in Figure 12.

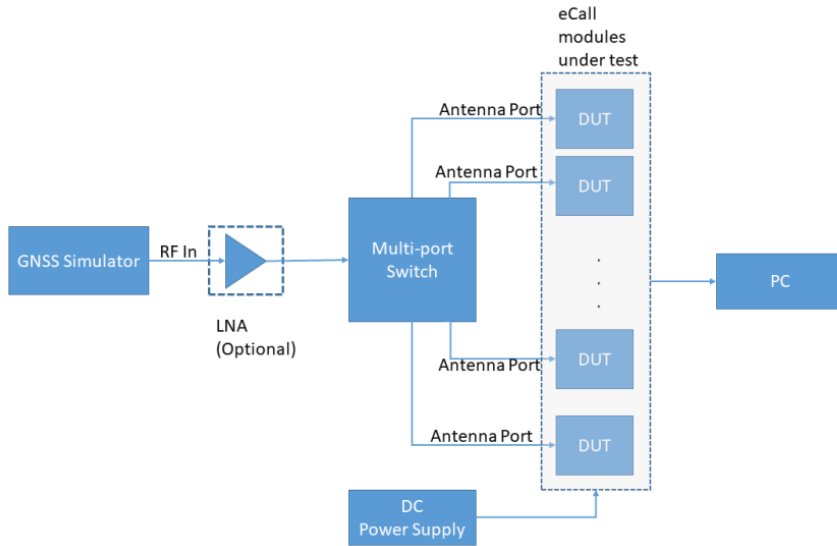


Figure 12. Schematic representation of the set-up developed for eCall conformance testing at the JRC.

The eCall test-bed was designed to be able to test multiple DUTs in a fully automated manner and, for that reason, two multi-port microwave electromechanical switches and a programmable multifunction switch driver have been added. This allowed automating long series of tests assessing the conformity of multiple devices sequentially.

All the analysis were based on the National Marine Electronics Association (NMEA) [20] messages output by the DUTs. A dedicated NMEA parser able to decode the most common NMEA messages was coded in the AWK programming language [21], and the collected results were analysed using in house developed Matlab scripts.

In all the scenarios used for testing the eCall device, requirements in terms of Position Dilution Of Precision (PDOP) were set in Annex VI of the Commission Delegated Regulation 2017/79. Specifically, it entails the selection of a set of 6 satellites per constellation giving a PDOP in the range between 2.0 and 2.5 during the entire duration of the scenario. In order to fulfil this requirement, an ad-hoc optimisation tool was developed at the JRC. This optimisation tool used an orbit propagator giving the precise location of the satellites in view from a given location on the ground at any given time. The orbit propagator ingests the satellite ephemeris data in the Two Lines Element (TLE) format was used together with an open-source implementation of the Standard General Perturbations Satellite Orbit Model 4 (SGP4) orbit propagator [22] coded in Python and a PDOP optimisation script in Matlab. This optimisation script provided the optimal set of satellites in view to meet the set PDOP requirements.

The flexibility of the GNSS simulator and the automation of the tests allowed to repeat the scenarios to have a statistically relevant number of samples to evaluate the CSTTFF in different signal power levels. Some sample results are presented in Figure 13. In the figure, the average, minimum and maximum CSTTFF values at the signal power levels of -130 dBm and -140 dBm , for all the DUTs are reported together with the thresholds (black dashed lines) set in the Regulation.

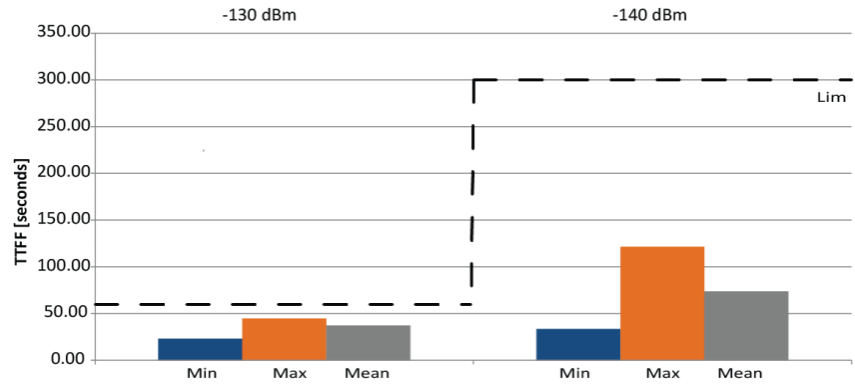


Figure 13. Barplot of the average, minimum and maximum CSTTFF values of the eCall devices measured at the signal power levels of -130 and -140 dBm.

For eCall modules, the dynamic tests are particularly relevant to verify positioning accuracy performance of the unit. One of the two dynamic scenarios considered had the vehicle moving along a pre-defined trajectory with an oval shape and specified ranges of speed and accelerations, in an urban-canyon with limited sky visibility conditions and repeated periods of total GNSS signals obscuration. The sketch of the simulated trajectory is shown in Figure 14. The trajectory integrates U-turns along a circular path with a certain radius and a turning acceleration, linear sectors with constant velocity, sectors with constant acceleration and deceleration, and it ends with a sudden deceleration of -20 m/s 2 that emulates an accident.

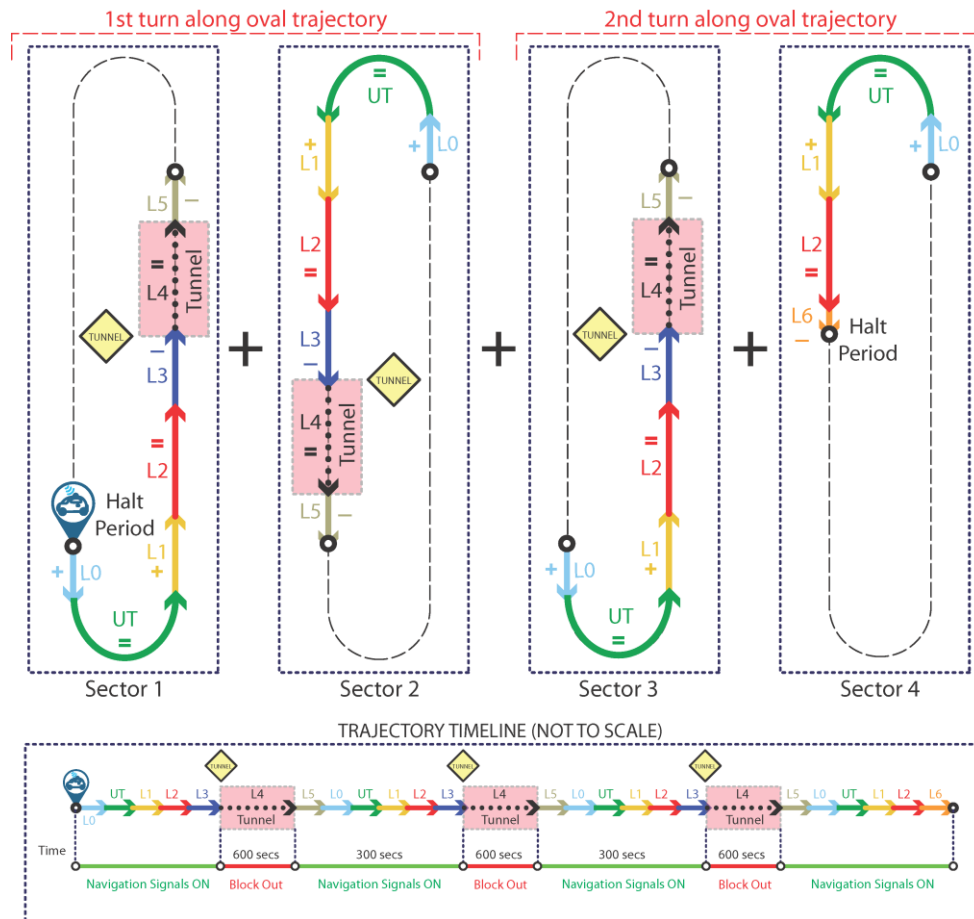


Figure 14. Sketch of simulated vehicle trajectory used in the dynamic scenario with limited sky visibility and repeated periods of GNSS signals obscuration for the eCall tests.

The performance of the devices was evaluated in dynamic scenarios with two satellite visibility conditions: in open-sky and in urban canyon. The latter was implemented using the antenna mask shown in Figure 15, where the signal strength of the satellites located within the light yellow coloured region suffer an extra attenuation of 40 dB.

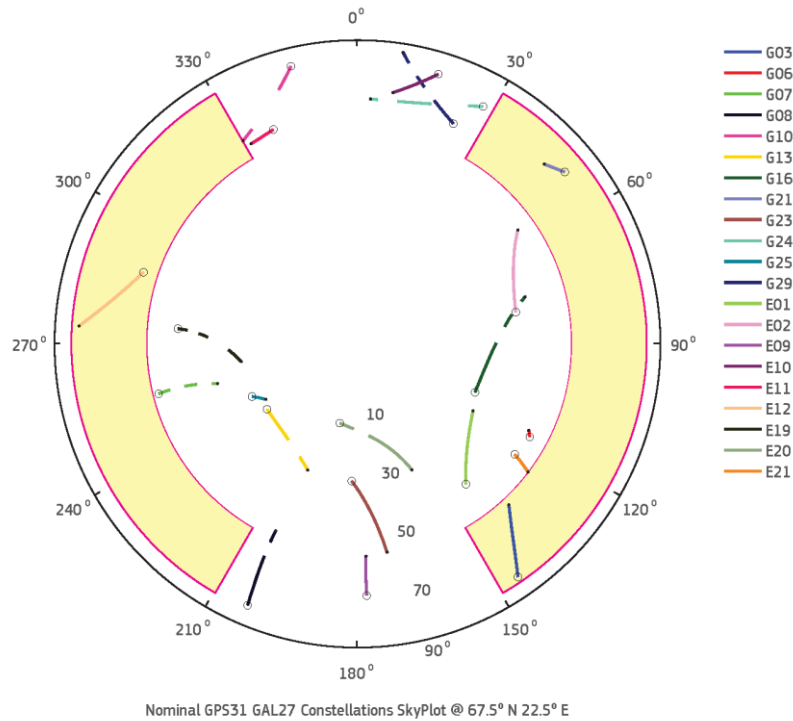


Figure 15. Skyplot showing the satellites in view for the second dynamic scenario with a limited sky view and the mask applied to the antenna pattern of the eCall device under test.

The positioning errors in the different scenarios are computed with respect to the reference solution provided by the GNSS simulator. The statistics of the horizontal positioning errors, with a 95% confidence level, for all the devices under test is shown in Figure 16 both in the dynamic clear sky and the dynamic urban scenarios. The bar-plots show the standard deviation, the maximum and minimum positioning errors, along with the error limit set in the eCall requirements.

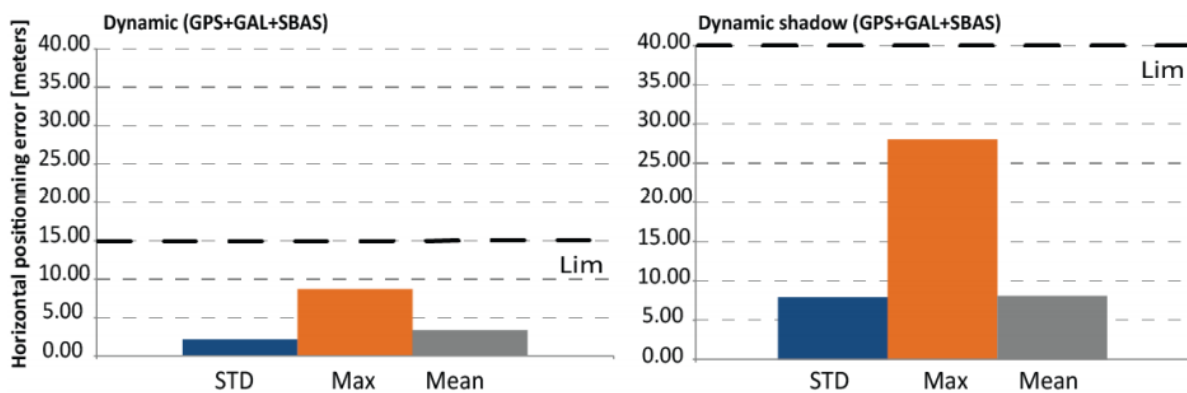


Figure 16. Horizontal positioning accuracy for eCall modules in dynamic and dynamic shadow mode for the combined configuration GPS+GAL+SBAS is shown in terms of STD, maximum and mean values. The limit fixed in the regulation is also indicated.

3.2.2 Performance assessment of Galileo-enabled ship-borne GNSS receivers

GNSS receivers today have indisputably become the main source of Position Velocity and Time (PVT) information in the maritime domain. The International Maritime Organisation (IMO) has recently adopted performance standards for multi-system ship-borne receivers, which highlights the importance of integrating the new GNSS systems, with their space-based and terrestrial-based augmentations. In addition, IMO has recognised Galileo as part of the World Wide Radio Navigation System [23]. In order to assess the correctness of the implementation of Galileo, and secondly, to identify potential performance improvements and non-compliances to the requirements set for Galileo in the Maritime Standard IEC 61108-3 [24], a test campaign has been carried out by the JRC [25]. The main phases of the activity were:

- Analysis of the available standards for maritime GNSS receivers, including tests and procedures.
- Familiarisation with the DUTs, logging capacity and connectivity requirements.
- Set-up design and implementation, including calibration activities.
- Tests execution.
- Data analysis and report generation including best practice and suggestion for receiver manufacturers and testing centres.

The test campaign was based on a set of 24 Test Cases (TCs) which can be classified in the following main categories:

- Position accuracy: the DUTs position solutions were assessed in both static and dynamic conditions and compared with the thresholds set in the standard.
- Timing: Time-To-First-Fix (TTFF) was analysed in cold and warm conditions and re-acquisition capability after a power interruption.
- Sensitivity: position and timing requirements were analysed in different Galileo signal power conditions.
- NMEA availability was verified in low and high speed conditions.
- Course Over Ground (COG) and Speed Over Ground (SOG) were assessed in different dynamic conditions.
- Coherency between quality flags and absence of GNSS signal was evaluated.
- Interference: position accuracy and availability, TTFF and re-acquisition time were assessed during continuous-wave, narrow/wide and pulsed interference.
- Receiver Autonomous Integrity Monitoring (RAIM)/Fault Detection and Exclusion (FDE): the capability to detect and exclude faulty satellites under pseudorange anomalous events were analysed.

Following the recommendations of the IEC Standard, the DUTs were intended as the ensemble of GNSS receiver and its antenna and, consequently, tests were performed in radiated mode in the EMSL. The set-up used in this campaign was that described in Section 3.1.3. A photograph of the seven ship-borne receivers and their antennas positioned on top of the measurement tower of the EMSL is shown in Figure 17. The movable platform was placed in front of the measurement tower and was used to hold an RF signal generator and a transmit antenna with its tripod. This test equipment was used to generate the interference signals specified in the IEC Standard 61108-3.

The sled B of the EMSL was positioned at the zenith, with the LHCP probe antenna broadcasting the RF signals from the GNSS simulator located behind the dom. The distance between the probe antenna and the antennas of the DUTs was about 9.5 m. It is worth mentioning that during this campaign, as specified in the IEC standard 61108-3, all the test scenarios assessed are single frequency E1 Galileo-only.

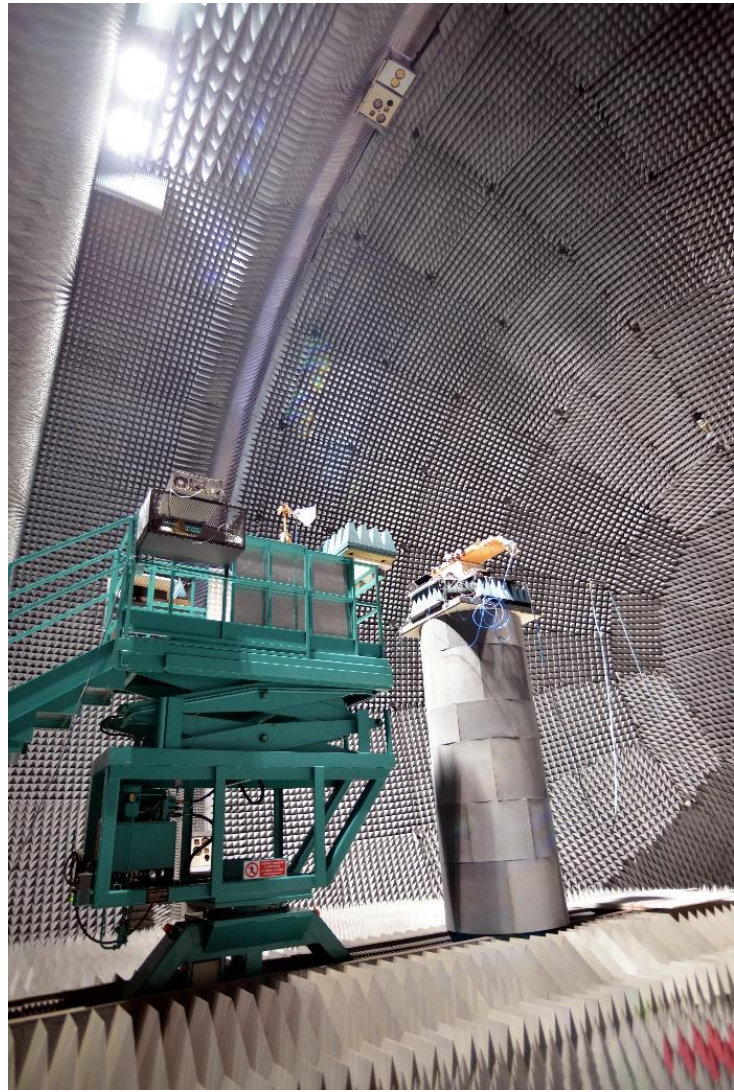


Figure 17. Photograph of the set-up used in the measurement campaign of the ship-borne receivers. The movable platform holds an RF signal generator and an antenna to generate RF interference signals.

The IEC Standard 61108-3 specifies GNSS signal power levels that would be measured with a 0 dBi antenna near the DUT. This means that the GNSS signal strengths have to be calibrated in advance. The power level of the GNSS simulator were adjusted such that the C/No measured with a reference GNSS receiver at the RF port of the front panel of the simulator were exactly the same as those measured with the same receiver and a 0 dBi RHCP antenna at the focus of the EMSL. In the radiated tests in the anechoic chamber, the high-power RF port of the GNSS simulator was used. The calibration of the power levels in the radiated tests was made as illustrated in Figure 18. The power loss of the programmable attenuator used in the radiated test was configured such that the observed C/No values measured with a reference receiver are the same as those in conducted mode using the calibrated RF output of the GNSS simulator. It must be noted that a 0 dBi RHCP antenna was not available and, instead, a standard gain horn of gain known was used. Further, an in-line low noise amplifier (LNA) of gain 25 dB was used both in the conducted and radiated tests. This was needed to raise the GNSS signal power levels and get them close with those that would be measured using an active GNSS antenna.

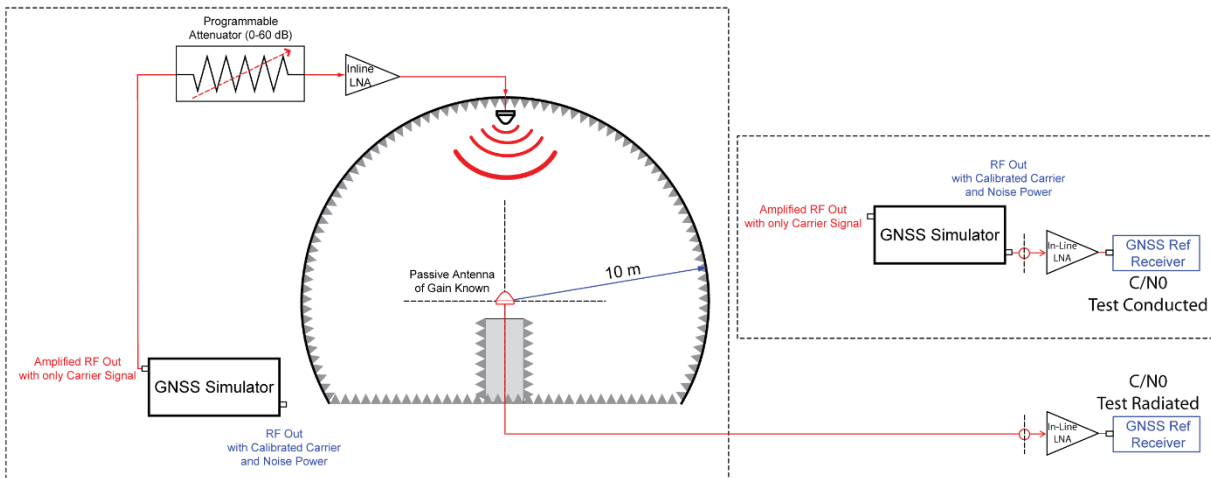


Figure 18. Sketch illustrating the calibration of the GNSS signal power levels in the radiated tests. Using the amplified RF output of the simulator and a programmable attenuator, C/N0 values observed with a reference receiver in the radiated tests (left) are fully aligned with those measured with the same receiver in conducted mode (right) using the calibrated RF output of the simulator.

The test scenarios with radio interference present were carried out using a programmable vector signal generator. This instrument can generate four classes of waveforms: continuous wave signals; frequency, phase and amplitude modulated signals; calibrated additive white Gaussian noise signals; and arbitrary digital waveforms with an instantaneous bandwidth up to 100 MHz. In order to verify that the power of the interference signal is compliant with the values reported in the standard, a calibration was performed. This calibration was made using a power meter and a reference horn antenna of known gain. This allowed to have signal power levels of the interference measured next to the antennas of the ship-borne receivers in line with the values specified in the standard. Two photographs with a close view of the set-up used with the programmable vector signal generator and a TX standard gain horn antenna on the movable platform of the EMSL are shown in Figure 19. The choice of having the interference signal generator and the TX antenna close to the measurement tower of the EMSL was made to limit the maximum power levels that had to be outputted by the signal generator. Having used a TX antenna at 10 m. distance would have required an RF high power amplifier able to output hundreds of Watts of RF power. This is due to the high propagation path losses from the TX antenna to the antenna of the ship-borne receivers under test.

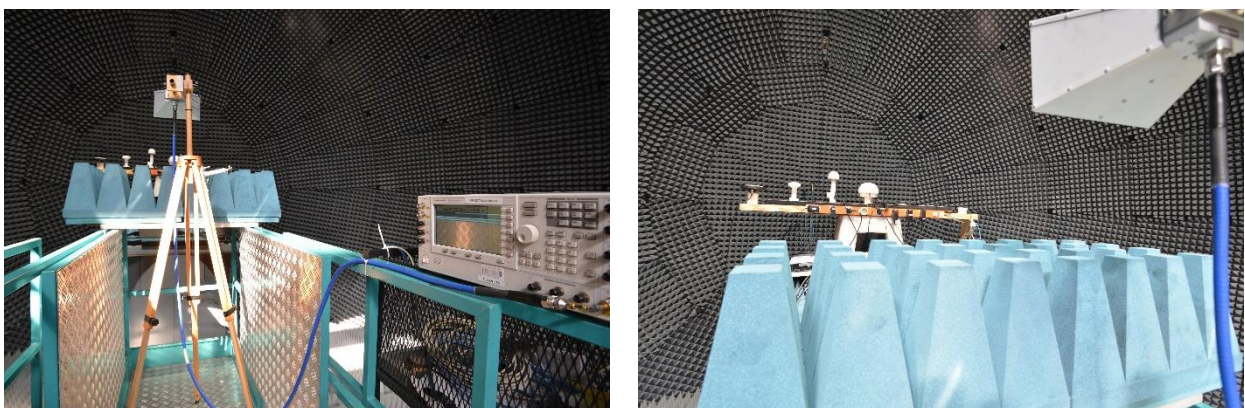


Figure 19. Two photographs with a close view of the set-up used with the programmable vector signal generator and a TX standard gain horn antenna on the movable platform of the EMSL.

An ad-hoc test suite was developed on a host laptop to automate the execution of the conformance tests specified in the standard. The suite was able to interface the DUTs via a virtual COM-USB RS232 and also over the network via a TCP socket. The control software was coded using PowerShell scripts that configured remotely the receivers and could also send

specific commands (e.g., a configuration sentence or a cold start command). Moreover, the test suite interfaced and operated remotely the GNSS simulator. The execution of a long series of test sessions logging the observation data from all the DUTs, going through the entire set of test scenarios, was possible. The latter is a very important point when comparing the performance of the DUTs under the presence of interference signals, as it guarantees that the test conditions for all devices are exactly the same.

Regarding the post-processing and analysis of the receiver logs, the NMEA format was used both for the logs of the receivers and the GNSS simulator. The NMEA log files were firstly parsed using an in-house software tool developed in C++. The datasets obtained were then formatted conveniently for a subsequent analysis using a suite of Matlab scripts, which was developed ad-hoc for this campaign.

For the sake of illustration, one example of the test scenarios that were assessed is given. Among the 24 test cases specified in the standard, there was a test to assess the RAIM/FDE capabilities of the DUTs. For this test case, an initial baseline static scenario had to be used. A second scenario introducing pseudorange ramps and satellite switch-off events, in accordance to the IEC standard specifications, was also created. This scenario starts with eight healthy satellites, after 25 minutes, a pseudorange ramp of one of the satellites was applied, with the pseudorange error gradually increasing up to 500 m. Right after, the error is kept constant for one minute, and then it is decreased down to 0 m. After the ramp, the satellite affected by the error is switched-off reducing the number of available satellites. In order to stress the RAIM/FDE algorithms implemented in the DUTs, this process is repeated with five satellites sequentially during the same test scenario. The pseudorange ramps together with the horizontal positioning errors observed by the DUTs are shown in Figure 20.

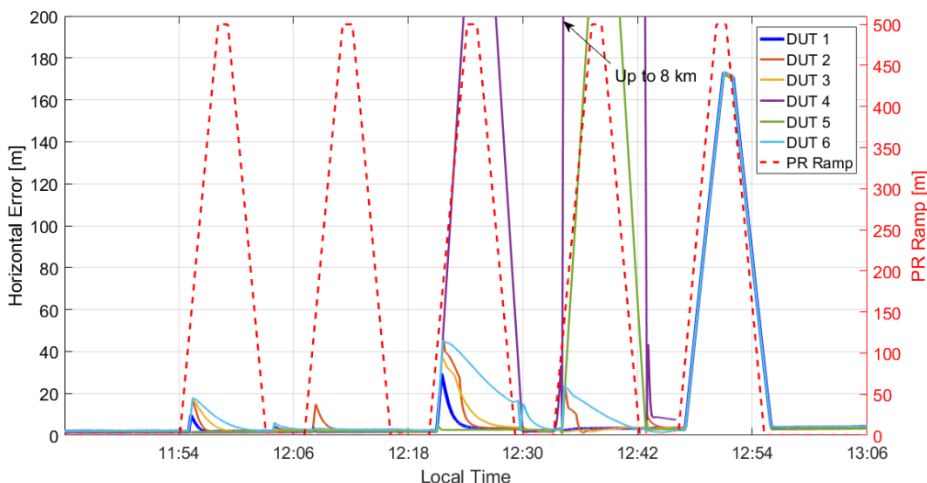


Figure 20. Pseudorange ramps and horizontal positioning error as a function of the time in the RAIM/FDE test case.

3.2.3 Performance assessment of smartphones exposing raw measurements

Location-based services (LBSs) is the market segment of Galileo with the largest number of users [26]. At the end of 2019, the number of Galileo-enabled smartphones was estimated to have surpassed 1 billion devices [27]. The development of LBS is driven by different needs, depending on the application: mobility, productivity, safety, etc. To satisfy these needs, the key requirements for GNSS are the TTFF, the positioning accuracy and PVT availability. Galileo satellites will further improve signal availability, thus enhancing continuity of service for LBS in urban and challenging environments. By contributing to multi-constellation solutions, Galileo can satisfy the need for higher accuracy and fast TTFF of such demanding applications as personal tracking.

Noting the strategic importance of LBS and the need to monitor the adoption of Galileo in the new smartphones that are released on the market, the JRC in close coordination with the GSA, has carried out a number of testing campaigns conducted in the over the Air (OTA) mode in a

shielded room using a GNSS simulator and a transmit antenna [28]. In addition to this, there have been H2020 projects aimed at promoting the adoption of Galileo and, more importantly, establish an EU-based, worldwide service to provide and/or enable location for LBSs and Machine-to-Machine (M2M) applications [29].

An interesting development that may enable higher accuracy for mass market devices is the new availability of raw measurements at the Operating System level, released in 2016 on smartphones running Android 7.0 (and higher) [30]. Until then raw measurements were exclusively accessible on high-end or professional GNSS receivers. This innovation was eagerly anticipated by the GNSS community and has triggered the development of numerous new LBS apps and services.

Future calls of R&D actions under the EGNSS Programmes are expected to target the development of new LBSs apps, services, or infrastructures. In the next sections, a description of two test campaigns, one with live SIS and a second one in the shielded room, is given to illustrate what are the testing capabilities available in this domain.

3.2.3.1 Smartphone testing using live signals in space

The test campaign on the smartphones using the live signal in space (SIS) was conducted as follows [31], [32]. The smartphones were placed inside a shielding box connected to a geodetic antenna placed on the rooftop of an office building. In this set-up, all the devices should determine a common position, the one of the rooftop antenna. The shielding box integrated a wideband antenna used to re-radiate GNSS signals inside. This type of set-up provides optimal visibility conditions for the data collection and allowed one to keep the smartphones in a controlled lab environment. Moreover, the position of the roof-top antenna was carefully surveyed: since the smartphone was deriving measurements related to the roof-top antenna, it was possible to assess position errors. Finally, the smartphones were powered through the USB connector integrated in the shielding box. Thus, allowing to perform long data collections without interruptions. The set-up for the static case is shown in Figure 21.

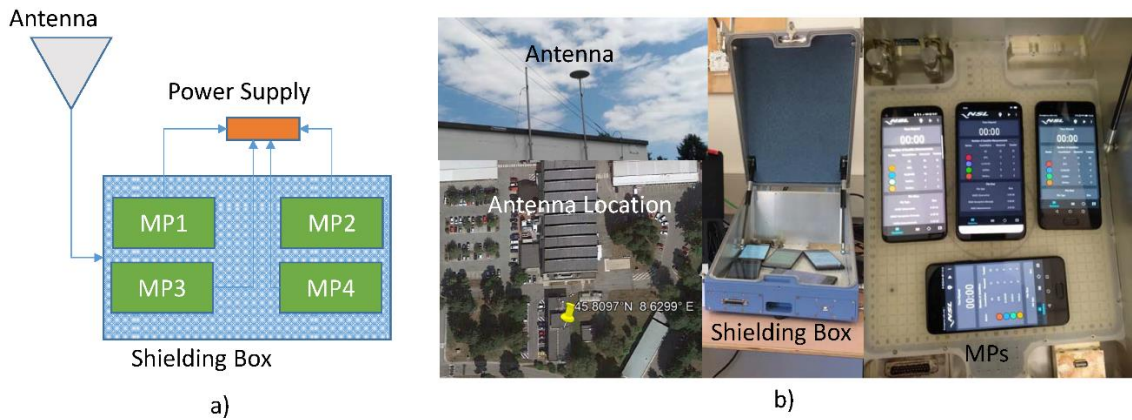


Figure 21. Experimental set-up adopted for the smartphone static test. a) Schematic representation of the test set-up. b) Views of the actual implementation of the set-up.

The smartphone data were collected and then analysed. Different level of analysis can be carried out depending on the information available. Measurement accuracy analysis could be performed using an ad-hoc in-house software developed. The suite integrates Receiver Independent Exchange (RINEX) file parsers and a specific navigation software for computing pseudorange and Doppler shift residual errors. Some sample results are shown in Figure 22, in which the obtained Cumulative Distribution Functions (CDFs) of the range and rate-rate errors are shown.

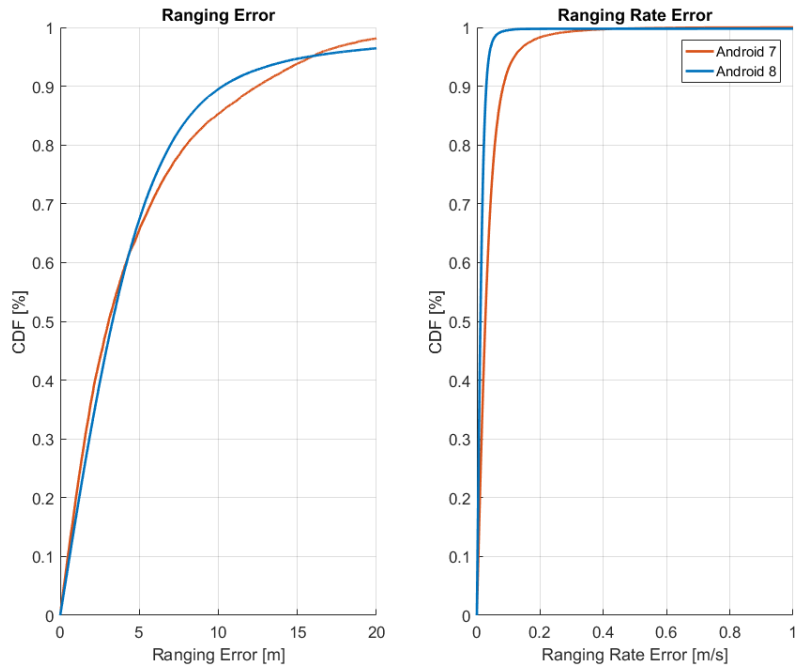


Figure 22. Cumulative Distribution Function of the Range and Range Rate error considering two smartphones equipped with different Android versions.

In addition, a customised navigation algorithm was developed for assessing the clock behaviour of Android devices exploiting raw GNSS measurements. The obtained Allan Deviations relative to the clock of an Android device using different strategies are shown in Figure 23.

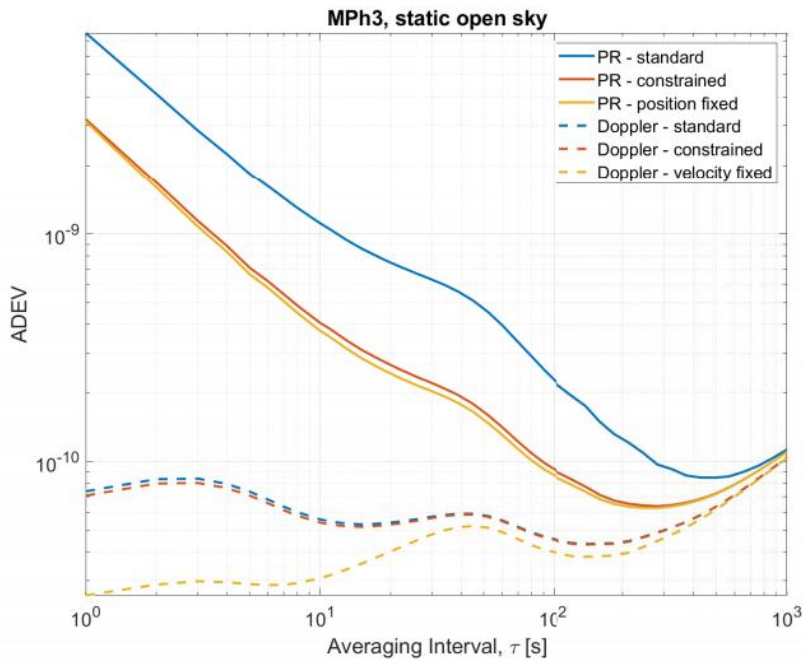


Figure 23. Frequency stability of an Android smartphone in open-sky conditions

An specific set-up for vehicular and pedestrian tests was also designed and implemented. Examples of the set-up prepared are shown in Figure 24 and in Figure 25 for pedestrian and vehicular tests, respectively. The vehicular set-up exploited the shielding box as described above. Here, the main difference is the use of a professional receiver for generating the reference trajectory.

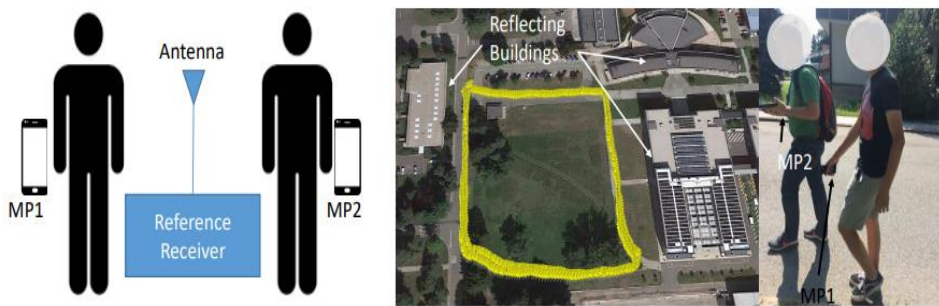


Figure 24. Pedestrian data collection set-up. On the left a schematic representation of the set-up. On the right side the trajectory and view of the actual implementation of the kinematic tests.

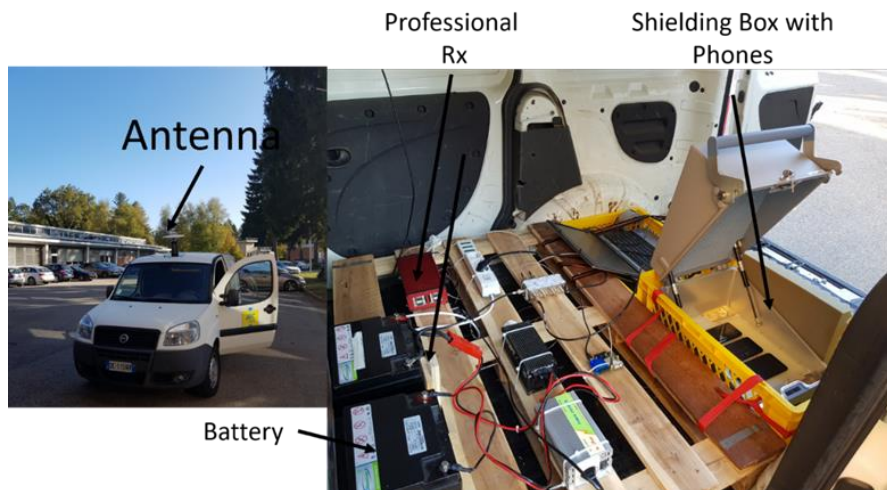


Figure 25. Photograph of the set-up used in the vehicular tests with the smartphones.

3.2.3.2 Smartphone testing using a GNSS simulator

The JRC laboratory is also able to test smartphone performance with simulated GNSS signals. A sketch of the set-up used for this test is depicted in Figure 26.

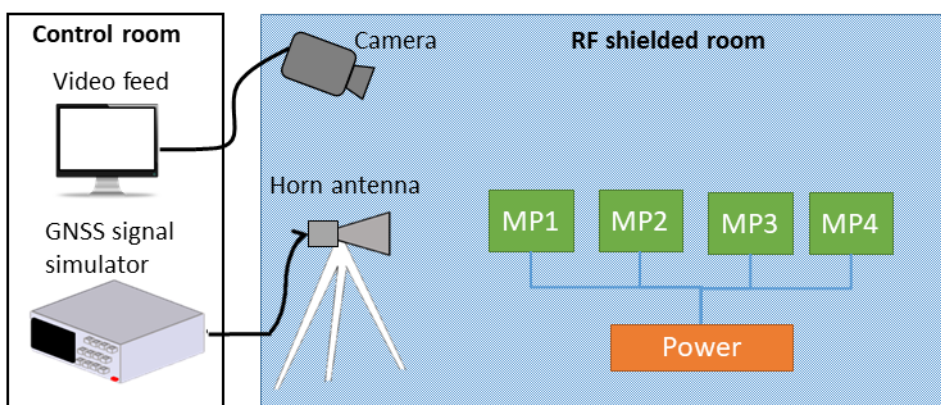


Figure 26. Schematic representation of the test set-up for smartphone testing using simulated GNSS signals.



Figure 27. Views of the actual set-up for smartphone testing using simulated GNSS signals, in the RF shielded room (left) and in the control room (right).

For this test, the devices were placed inside the RF shielded room, together with a standard gain horn antenna, as shown in Figure 27. The antenna radiates the GNSS signals generated by the simulator, located in the control room. Given the size of the room, a large number of devices can be tested simultaneously. The transmitted signal power can be calibrated using an approach similar to that used in the test campaign on the ship-borne receivers in the EMSL, presented in Section 3.2.2. A camera, installed in the shielded room, enables to remotely monitor the test. It can be used, for example, to control the correct logging of the data on the smartphone's screen. As for the live test, the collected data can then be analysed using the ad-hoc in-house software.

A suite of scenarios representative of diverse environments and dynamic conditions was created, and it is available for future testing campaigns. Testing using simulated GNSS signals enables to evaluate the performance of the smartphones under controlled conditions, which cannot be reproduced using live signals. For example, this set-up has been used to assess the performances of smartphones with Galileo only signals. In addition, the time of the scenario can be aligned with the current day of the testing to let the smartphones integrate live assisted-GNSS data.

3.3 Retrieval of reference trajectory solutions

The estimation of reference solutions is of paramount importance to assess systems and algorithms performance. JRC has supported several H2020 and Fundamental Element projects in the estimation of benchmark solutions for testing activities.

The JRC laboratory is equipped with several high-grade systems suitable to provide reference solutions for different applications. Specifically, the JRC owns multiple high-end geodetic receivers and antennas, by different manufacturers, which can be used to set up Real Time Kinematic (RTK) reference stations, able to transmit RTK corrections for providing high accuracy solutions in real time, or to log reference data to be used for Post Processing Kinematic (PPK) purposes.

The JRC laboratory has also at disposal a high-grade platform combining GNSS and an Inertial Measurement Unit (IMU) especially suitable to provide reference solutions for dynamic tests also in the presence of short GNSS outages.

In addition, JRC experts can assist in estimating reference solution also in environments where the GNSS signal reception is challenging using the total station available in the JRC laboratory.

Finally, the JRC acquired vast experience in the estimation of reference solutions obtained by post-processing GNSS and, when available, also IMU data.

This section provides some sample test cases to showcase the above capabilities.

3.3.1 GNSS/IMU based reference solution: an agriculture case study

As illustrative case, in the following the support activity given in the frame of the Field Aware Navigation and Timing Authentication Sensor for Timing Infrastructure and Centimeter level positioning (FANTASTIC) Fundamental Element project is detailed [33].

One of the goals of the project was to develop high accuracy solutions for agriculture applications. Several dynamic tests were performed to assess the performance of the GNSS geodetic antennas and receivers developed during the project.

The JRC supported the testing activity by providing a Synchronous Position, Attitude and Navigation (SPAN)-CPT system by Novatel [34], used as benchmark during the dynamic tests. The system, shown in Figure 28, includes a high performing Micro Electro Mechanical System (MEMS) IMU to deliver high accuracy navigation solutions exploiting an integrated solution. SPAN-CPT tightly couples GNSS positioning and IMU gyro and accelerometer measurements. The system can be configured to receive RTK corrections reaching centimetre accuracy under nominal conditions. Moreover, the IMU allows to bridge temporary GNSS outages of up to 60 seconds in duration.



Figure 28. Novatel SPAN-CPT system of the reference navigation system available at the JRC.

During the project, dynamic tests were performed using a cart whose sketch is provided on the left side of Figure 29. The cart carried the receivers developed in the frame of the project, indicated with the label FANTASTIC, and other receivers and systems used for comparison purposes. The SPAN-CPT system has been placed on the top of the cart in proximity of the antenna to reduce the level arm between the GNSS antenna and the IMU. A picture of the real cart is provided in the right side of Figure 29.

For the majority of these tests, the SPAN-CPT was configured to receive RTK corrections from a nearby reference station.

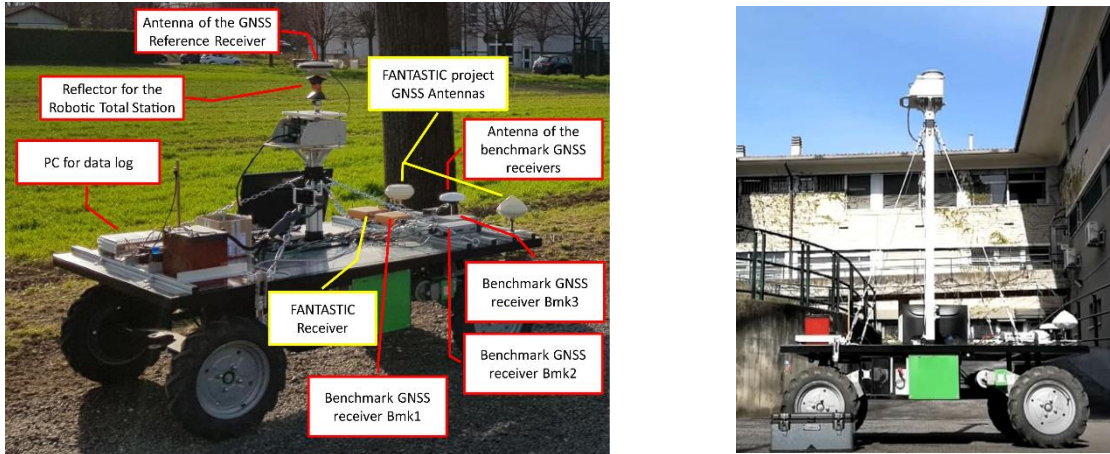


Figure 29. (Left side) Experimental set-up of the cart used for the dynamic test in the frame of the FANTASTIC project [35]; (Right Side) Picture of the cart used for the dynamic tests carrying the SPAN-CPT system on the top (Extracted from FANTASTIC White Paper [36]).

The data logged by the SPAN-CPT were also post-processed along with the base data, to obtain a PPK reference solution combining GNSS and IMU data through the Novatel Inertial Explorer software. This tool allows processing data from any receiver in PPK or in Precise Point Positioning (PPP) mode, providing high accurate solutions suitable to be used as reference. The tool allows also post processing GNSS and IMU data system by giving the freedom to combine them in a tightly or loosely coupled mode.

In the frame of the FANTASTIC project, the JRC provided reference solutions for several dynamic tests. In Figure 30 the cart used for the dynamic tests is shown while performing a data collection in a vineyard. In Figure 31, the reference trajectory obtained by post processing SPAN-CPT data set in PPK mode and combining the GNSS and IMU data from the SPAN-CPT using a tightly coupled approach is provided.



Figure 30. Cart carrying the devices under test during a dynamic data collection in a vineyard [35].

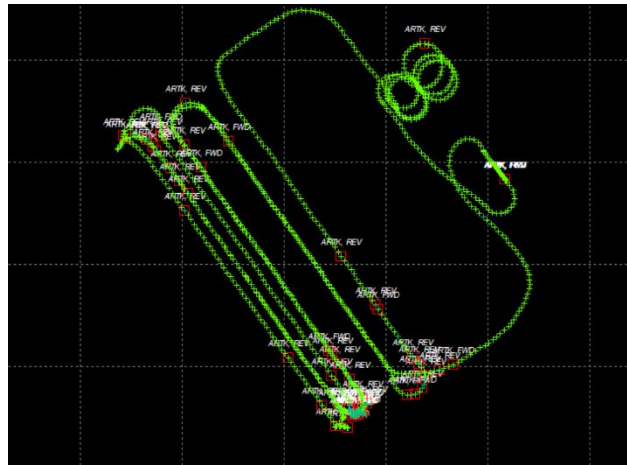


Figure 31. Reference trajectory obtained by post processing the SPAN-CPT and the reference station data.

The reference trajectory, is based on a fixed ambiguity solution for all the duration of the test, has been used by the consortium to assess the accuracy of all the DUTs, as shown from the plot in Figure 32. The latter reports the CDF of the horizontal position error, computed with respect to the SPAN-CPT reference solution, for the receiver developed in the frame of the project and all the other receivers used as benchmark.

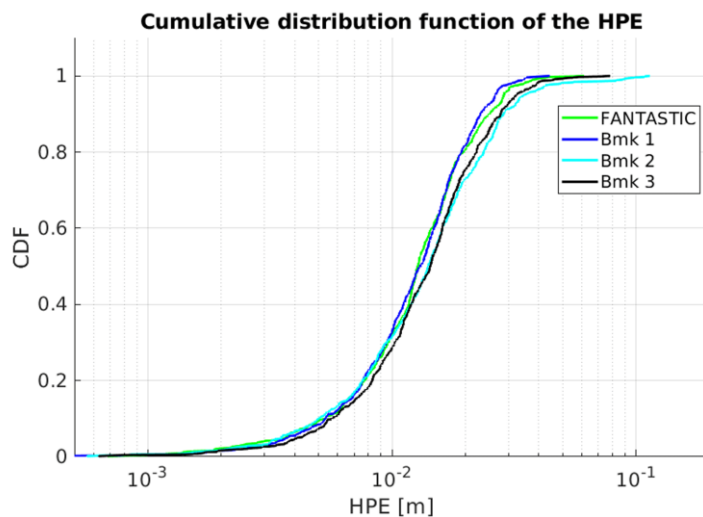


Figure 32. CDF of the horizontal position errors estimated for different devices under test and using the provided post-processed SPAN-CPT trajectory as reference [35].

3.3.2 GNSS based reference solution: a drone case study

The JRC supported the test activities performed in the frame of the Galileo-EGNOS as an Asset for UTM Safety and Security (GAUSS) H2020 Project [37].

The project had the objective to develop high performance positioning systems for drones. For this purpose, several flight tests were performed with different types of drones. The JRC assisted in setting up the reference station used to assess the GNSS solutions of the DUT carried on board of the drones.

In Figure 33 (left side), the RTK base station which was set-up at the ATLAS (Air Traffic Laboratory for Advanced Systems) facility is shown [38]. The tests were performed in Jaen, Spain in July 2020. A high grade GNSS reference receiver and antenna, provided by the JRC,

logged 5Hz reference data during flight tests performed with different drones. The Tucan drone, one of the drones used in the testing activities, is shown in the right side of Figure 33.



Figure 33. (Left Side) High-end geodetic antenna placed under open sky at the ATLAS facility, connected to a high geodetic receiver to serve as reference station during flight tests with drones (Right Side) Tucan drone used in the frame of the GAUSS Project (images courtesy of the GAUSS project).

Reference trajectory solutions were also computed by the JRC in the frame of the GAUSS project. The data from the rover receivers on-board the drones and from the base station were post processed in PPK mode. JRC is able to provide PPK and also PPP solutions, for this purpose, a commercial software, Inertial Explorer, by Novatel is exploited. The software uses the RINEX files of the base and the rover to estimate the PPK solution. If the data from the base station are not available, the software can download the data from the nearest publicly available reference stations. Moreover, from the RINEX file of the rover, the software can also provide a post processed PPP solution after downloading clock and orbit corrections. Built-in ionospheric processing improves accuracies for dual-frequency users. Figure 34 shows a sample reference trajectory estimated for one of the test flights performed by the above drone.



Figure 34. Reference trajectory computed for one of the flight performed by the Tucan drone with Novatel Inertial Explorer.

For some of the test flights, the computed PPK reference trajectories were compared with the one obtained from a laser ranging system owned by the consortium. The consistency between both solutions further validated the quality of the reference trajectory obtained. These reference trajectories were exploited by the consortium to assess the benefit of using Galileo and EGNOS to support drone operations (e.g. for navigation, detect and avoid, tracking etc.).

3.3.3 Total station based surveying: a 5G case study

To determine reference solutions in GNSS challenging environments, a total station can be used. This device allows to determine the position of a target using angle and distance measurements. The absolute position of the target can be obtained integrating GNSS positioning information. This approach was adopted to support a 5G measurement campaign carried on the JRC Ispra campus. During the campaign, 5G measurements were performed with respect to a reference point, where the 5G transmitter was located. The measurements were taken in a challenging environment for 5G signals, due to the presence of nearby buildings and trees. Unfortunately, this type of environment is also very challenging for GNSS signals, and prevented the straightforward use of a standalone GNSS receivers to determine the location of the points of measurements. As a solution, the points were surveyed using a total station, as shown in Figure 35. The total station measures vertical and horizontal angles as well as of the slope distance from the instrument to a given point. To coordinate the measurements, the station was set over a known point and its orientation was fixed using an additional known point (back sight). These reference points were selected in open-sky areas and their coordinates were determined beforehand using GNSS data processed in PPK mode. Using these points to set up the total station and the back sight, it was then possible to coordinate the points of measurements, even under dense tree coverage as illustrated in Figure 36.



Figure 35. Surveying of the measurement points using a GNSS receiver (left) and the total station (right).



Figure 36: Survey results for the test carried out with the total station in the JRC Campus.

3.4 RTK/PPP high accuracy positioning

High accuracy positioning refers to augmentation based techniques, such as real-time kinematics RTK and PPP, achieving position accuracies in the decimetre/centimetre order.

RTK is based on the presence of a nearby surveyed base station (or a network of stations in the case of Network-RTK) which allows cancelling out the common GNSS error through differential processing. PPP exploits GNSS corrections generated by a worldwide network of stations to obtain high accuracies without the need of a nearby base station. In addition to these traditional approaches, Galileo will make possible to achieve decimetre position accuracy through its High Accuracy Service (HAS). This service will transmit PPP corrections through the data component of Galileo E6 signal (E6-B), without the need of an external correction provider.

JRC has been performing and facilitating testing activities in the frame of several internal research activities, H2020 and Galileo Fundamental Elements R&D projects that required high accuracy positioning for different applications (e.g., agriculture, drones autonomous driving). Moreover, JRC supported the definition of the Galileo HAS carrying out numerous tests and analysis using both simulated and live signals.

A summary of the key JRC assets for high accuracy positioning is provided next.

3.4.1 RTK processing with high-end base and rover receivers.

The JRC laboratory has at a disposal four multi-channel high-grade GNSS receivers, from some of the main brands on the market, suitable to be used as base stations for RTK baselines. The above receivers allow streaming GNSS differential corrections over the Internet or via radio modem. These receivers can be used in conjunction with one of the five multi-band high-geodetic antennas, from different brands, available at JRC.

Currently, a fixed base station streaming RTK corrections has been set up in the JRC laboratory. For this purpose, one of the geodetic antennas, shown in Figure 37 has been permanently placed on the roof of the laboratory under open sky conditions. The antenna has been connected to one of the mentioned high-grade receivers which streams RTK corrections via radio modem. Moreover, JRC has at a disposal several antennas and receiver of medium grade, from multiple brands, that can be used as rover for RTK baselines.

JRC can support data collections of live signals in static and dynamic conditions. An example of rover antenna placed inside the JRC campus for a static RTK test is shown in Figure 38. The antenna is connected to a rover type receiver with an RTK engine capable to process the corrections provided by the base in the JRC laboratory.

For the dynamic tests, a van has been equipped to be able to easily conduct the tests with multiple receivers at the same time. In Figure 39, the external view of the van with the antenna mounted on the roof is shown. The antenna can be easily connected via a GNSS splitter to more rover receivers in parallel for comparison purposes.



Figure 37: Multi-frequency high-grade GNSS geodetic antenna placed on the roof of the JRC laboratory. A geodetic receiver using this antenna is the source of the RTK corrections.



Figure 38: Multi-frequency antenna connected to a high grade mid-grade receiver that was used as the RTK rover.



Figure 39: JRC van equipped with an antenna on the roof and receivers acting as moving rover for RTK.

3.4.2 RTK/PPP post-processing

In addition to the possibility to stream RTK corrections in real time, JRC can provide both PPK and PPP solutions. For this purpose, a commercial software, Inertial Explorer, by Novatel is exploited. As sample case in the following the support activity given in the frame of the FANTASTIC Fundamental project is shown. One of the goals of the project was to propose innovative solution to enhance the reliability of RTK solution.

The cart, carrying the receivers and antennas developed in the frame of the project, shown in Figure 40, was used to perform dynamic tests.

In Figure 41, an example of PPK solution obtained from the base and the rover RINEX files in case of a dynamic test is shown. In this case the processing provides solutions with fixed ambiguity for all the duration of the data collection.



Figure 40. Robotic cart used for the dynamic tests of the Fantastic Project (photograph taken during a demo organised at the occasion of a project review meeting on 30/10/2018, in Torino).

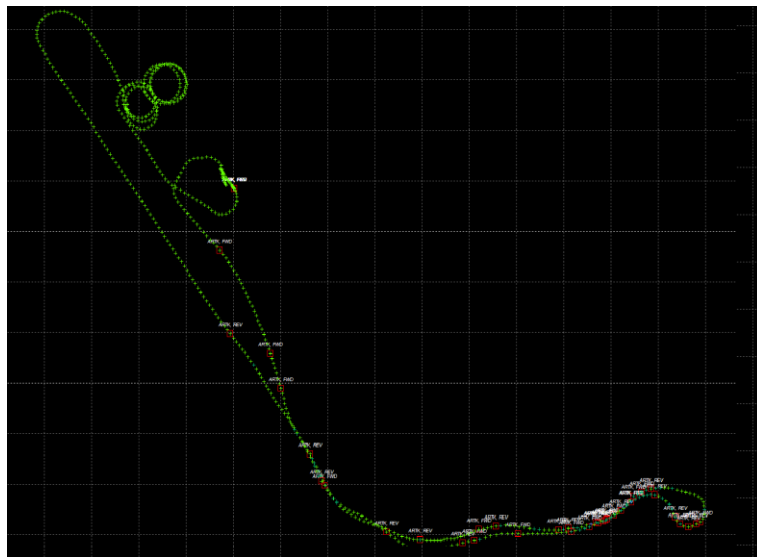


Figure 41. Example PPK solution for a dynamic test carried out in the frame of the FANTASTIC Project.

3.4.3 Simulation of Galileo E6 signal and navigation message

The EC has established that the Galileo will provide a free HAS enabling decimetre-level positioning through the provision of PPP corrections. These corrections will be transmitted through the E6-B data component of the Galileo E6 signal while the E6-C component will be encrypted and dedicated to the Commercial Authentication Service (CAS) [39], [40]. The capability to simulate Galileo E6 signals is a fundamental asset to carry out repeatable tests in a controlled environment. JRC offers the possibility to simulate Galileo E6 signals using a multi

constellation signal simulator. The simulator enables the encryption of the data or pilot component of the E6 signal so to enable the separated testing of the E6-B and E6-C data component.

Moreover, there is the possibility to upload the navigation message from an external file to provide maximum flexibility for testing purposes. In Figure 42, the simulator setting options for the Galileo signals, included the ones for the Galileo E6 signals are shown. It is important to note the tick boxes that activate the separate encryption of the data or pilot component of the E6 signals.

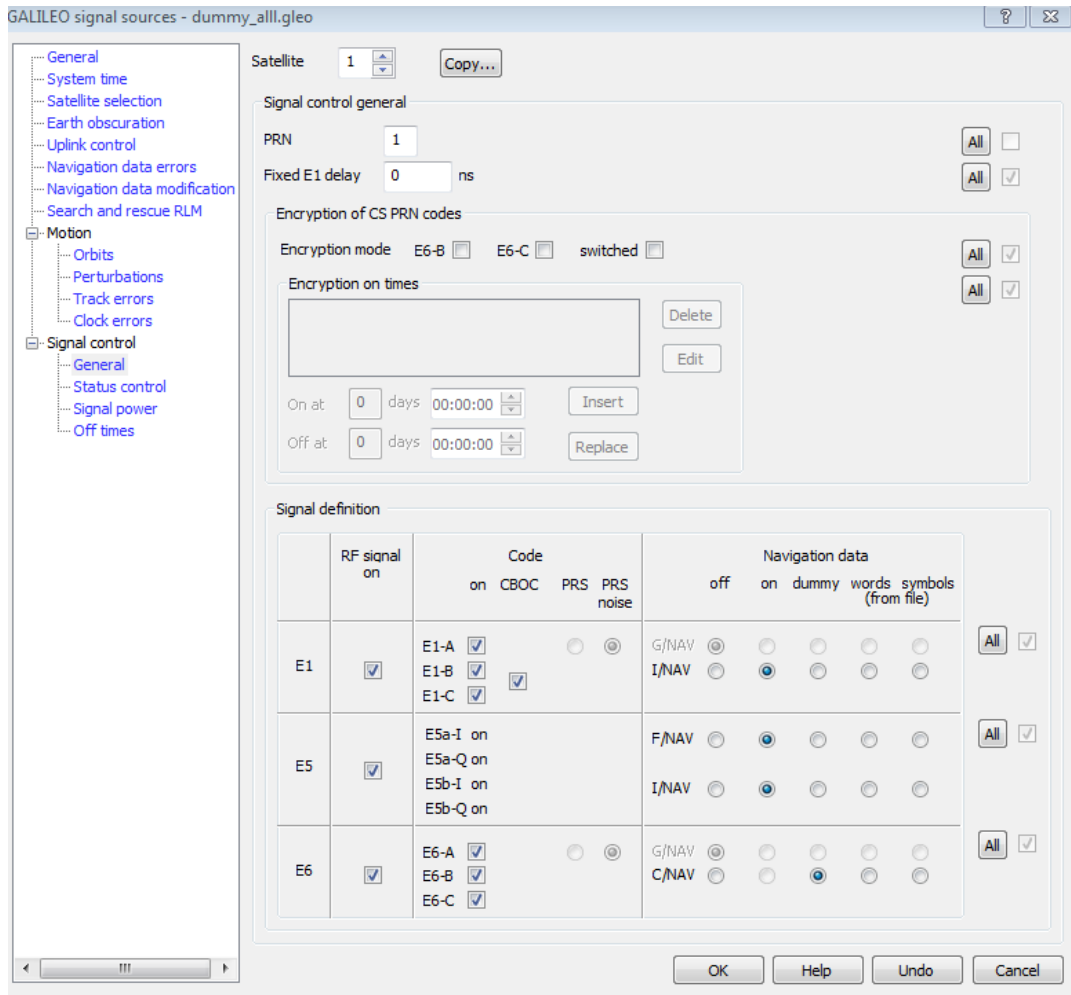


Figure 42. Setting for the definition of the Galileo signals in the GNSS simulator.

This simulator capability was exploited to study the demodulation performance for a wide range of Carrier-to-Noise Power Spectral density ratio (C/N0) conditions. The simulator can generate all Galileo signals in all Galileo frequency bands. A scenario with static, open-sky conditions and with the C/N0 of all signals progressively decreasing was created. This test was performed to assess the tracking limit of the different signals. In Figure 43, the C/N0 values obtained from the receiver for the above scenarios are shown.

Moreover, the simulator was configured to transmit a dummy message on Galileo E6 and on all the Galileo signals. In this way it was possible to estimate the Bit Error Rate (BER) experienced by the receiver for different signal power levels, as shown in Figure 44. Indeed, since the message is known, the number of erroneous bits extracted by the receiver have been directly evaluated.

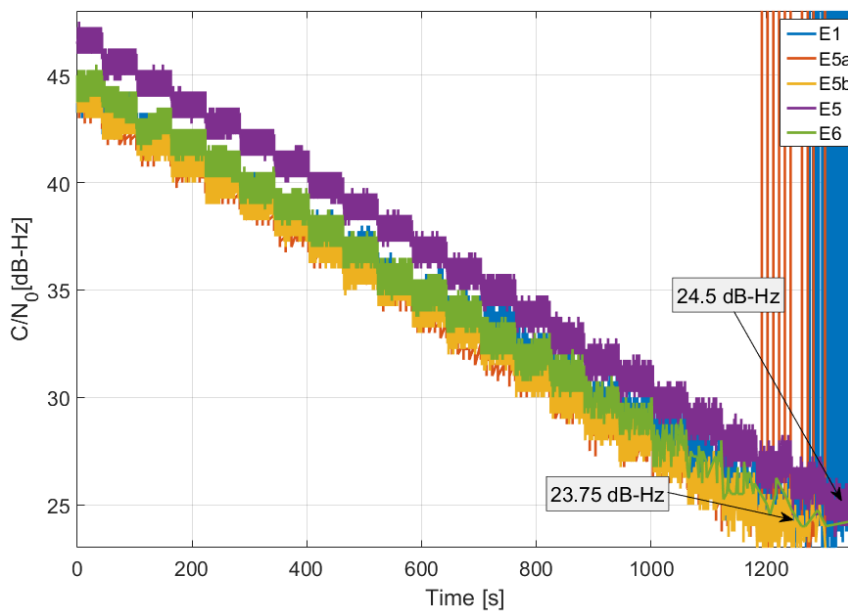


Figure 43: Loss of lock analysis for the different Galileo modulations analysed during the test with simulated signals.

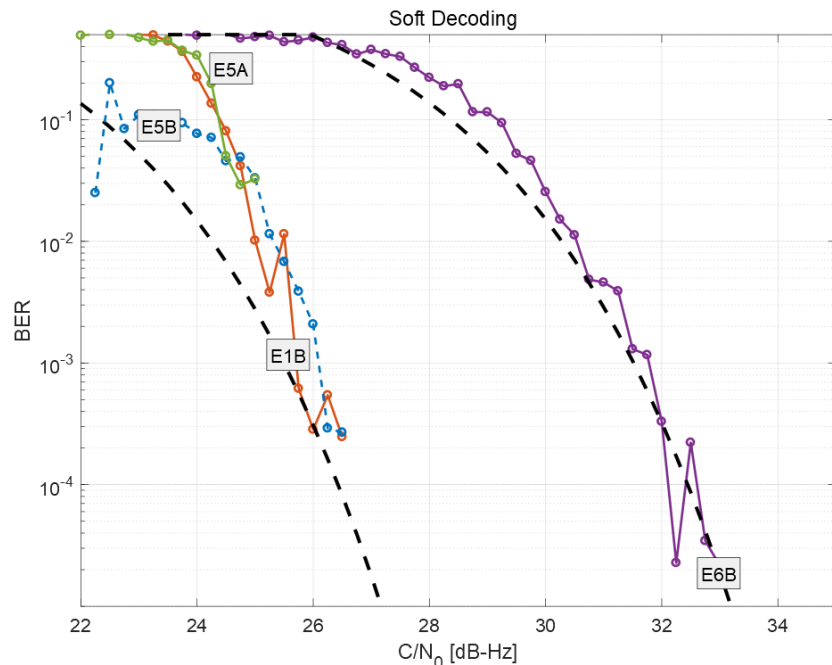


Figure 44: BER as a function of the C/N_0 extracted from a commercial receiver for all simulated Galileo signals including the Galileo E6 signal.

3.4.4 Galileo E6 signal reception quality analysis

In order to collect live E6 signals JRC can make available E6 capable antennas of high geodetic, rover and low-grade type. Moreover, currently in the JRC lab there are six receivers able to track the E6 signal. Four of these receivers allow to select to track only the data component, only the pilot component or both the components of the E6 signals. The receivers can also provide the decoded navigation message allowing to assess the demodulation capabilities. Apart from the commercial receivers the JRC can also offer GNSS front-ends able to collect Intermediate

Frequency (IF) data in the Galileo E6 band that can be then processed by any E6 capable Software Defined Receiver (SDR). The experimental set-up and the environment of one of the dynamic tests performed to assess the performance of E6 capable receivers and algorithms is shown in Figure 45. As sample case, one of the analysis performed with the data collected is shown in Figure 46 where the C/N₀ values extracted from the receiver and from the SDR implementing a Kalman Filter based tracking loop with 20 ms integration are compared [41]-[43].



Figure 45: Views of the experimental setup used for the dynamic test: (upper left side) Internal view of the van with the USRP 2, connected to an external rubidium clock, and the COTS receiver; (upper right side) External view of the van with the high geodetic antenna mounted on the roof; (lower left and right sides) Views of the environment selected for the dynamic test. The path is characterised by the presence of tall trees with rich foliage and sporadic buildings.

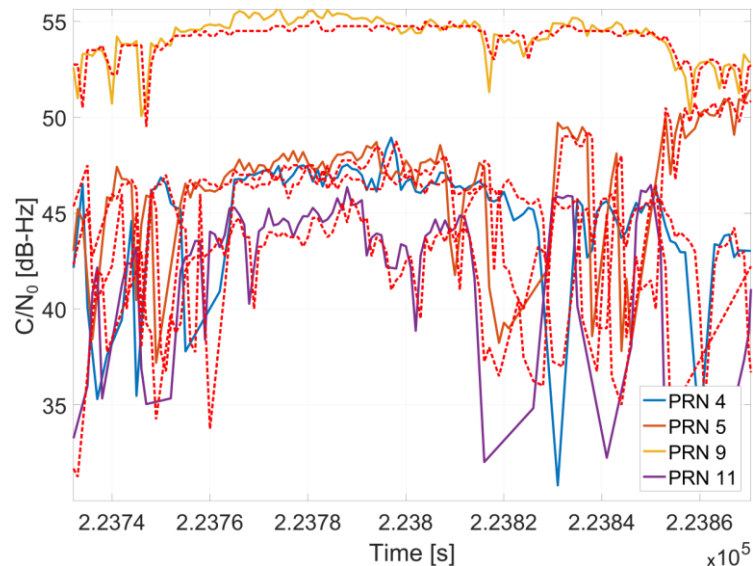


Figure 46: C/N₀ time series obtained from the COTS receiver (dashed red lines) and data-only KF tracking with 20 ms integration time (continuous line) for the dynamic test.

3.5 Testing of GNSS timing receivers

GNSS is currently widely used as a backbone for timing and synchronisation purposes across various user-segments, including critical networked infrastructures as telecommunications, energy distribution, and finance. For obvious reasons, timing and synchronisation is considered a highly strategic market-segment for the EU GNSS Programmes [26]. Consequently, the EU GNSS Programmes have a dedicated stream of R&D Actions aimed at supporting the development of Galileo-enabled GNSS timing receivers. One of the specific objectives of these projects is to promote the adoption of Galileo differentiators that can help increase the robustness and reliability of critical networked infrastructures, as for instance, the Galileo OSNMA [44], [45]. Concurrently with these projects, there is a separate stream of H2020 Mission and Services (MAS) R&D actions that are aimed at defining a robust and reliable Galileo and EGNOS timing service [46]–[49], with the associated specification of the performance indicators and required standards.

This section gives an outline of the GNSS testing capabilities for timing receivers currently available at the JRC.

3.5.1 Local oscillator characterisation

The local clock is a fundamental element of GNSS receivers and its performance has a large impact on the quality of the timing service provided. Consequently, the characterisation of the performance of the local oscillator is deemed important. A possible metric to use in this characterisation is based on the receiver clock bias and drift. JRC has developed an ad-hoc software suite for computing clock parameters starting from raw GNSS observables. Long data collections have been performed to evaluate clock stabilities. In Figure 47, a schematic representation of the methodology used for the characterisation of the local clock behaviour is shown. The diagram can be customised excluding the external clock or selecting a specific navigation engine.

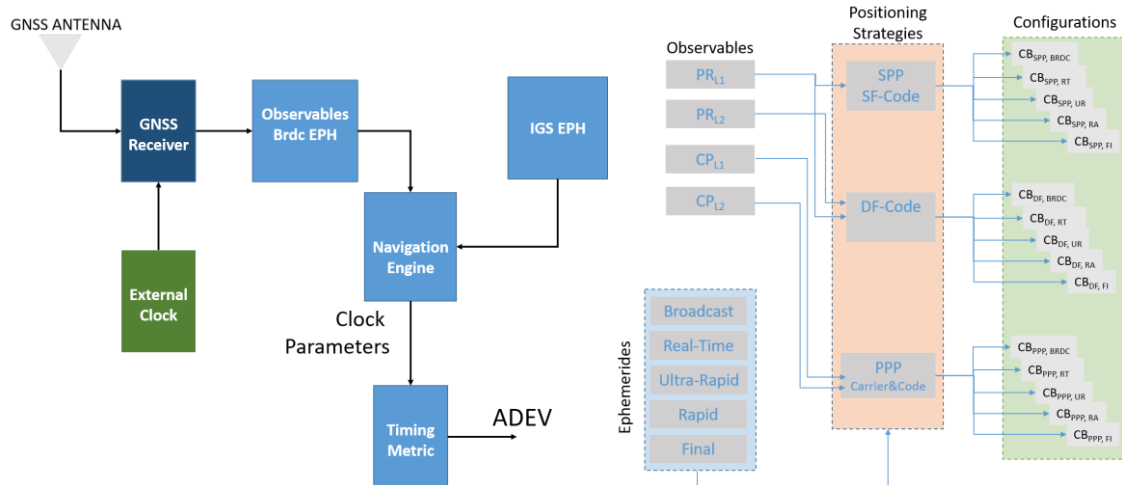


Figure 47. (On the right) Schematic representation of the process used for local clock characterisation. (On the left) Different navigation solution used for computing receiver clock bias.

An example of the set-up used to characterise the local clock of a GNSS receiver under test is shown in Figure 48. The developed set-up is highly flexible and allows to evaluate the impact of the different positioning strategies adopted for the clock bias and drift estimation. This is done simply by replacing the navigation engine with a specific navigation algorithm from single frequency single constellation SPP solution to the more complex multi-frequency PPP [50].

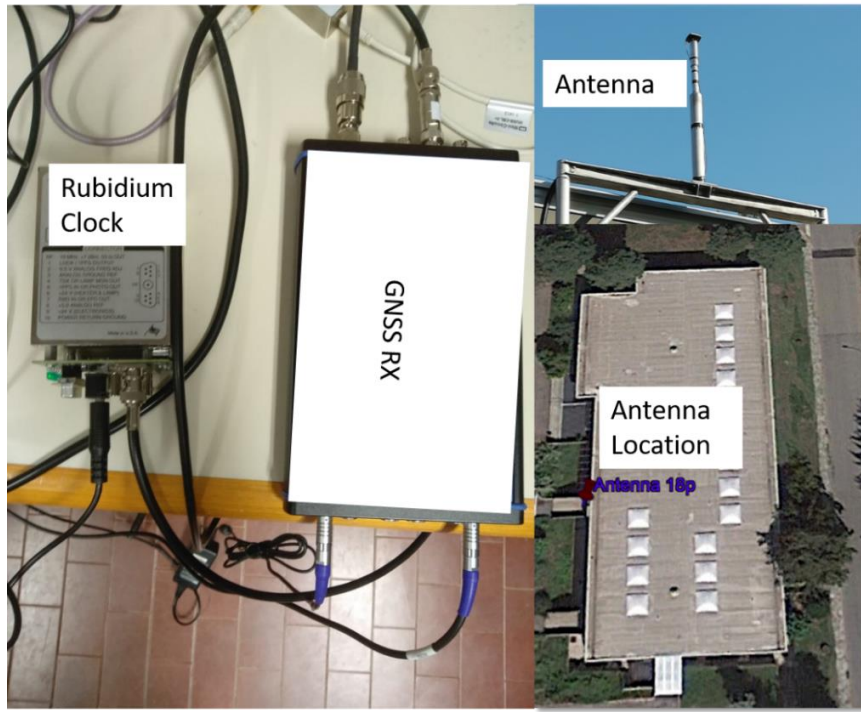


Figure 48. Set-up used for GNSS receiver local clock characterisation.

Noting the concern posed by GNSS jammers and the impact that they can have on the critical infrastructures relying on GNSS, specific set-ups have been developed to assess the impact of the RF interference (RFI) on the performance of GNSS timing receivers [51], [52]. Two different set-ups are shown in Figure 49. On the left side, a set-up developed to evaluate the impact of the mitigation techniques on GNSS timing capabilities. In this set-up, an RF signal combiner, an SDR front-end, and a customised Matlab software receiver were used. On the right side, a set-up developed in the anechoic chamber to characterise the performance of a GNSS timing receiver in radiated mode under the presence of RFI. In this case, both the GNSS signals from a rooftop antenna and the interference signal are broadcast inside the anechoic chamber.

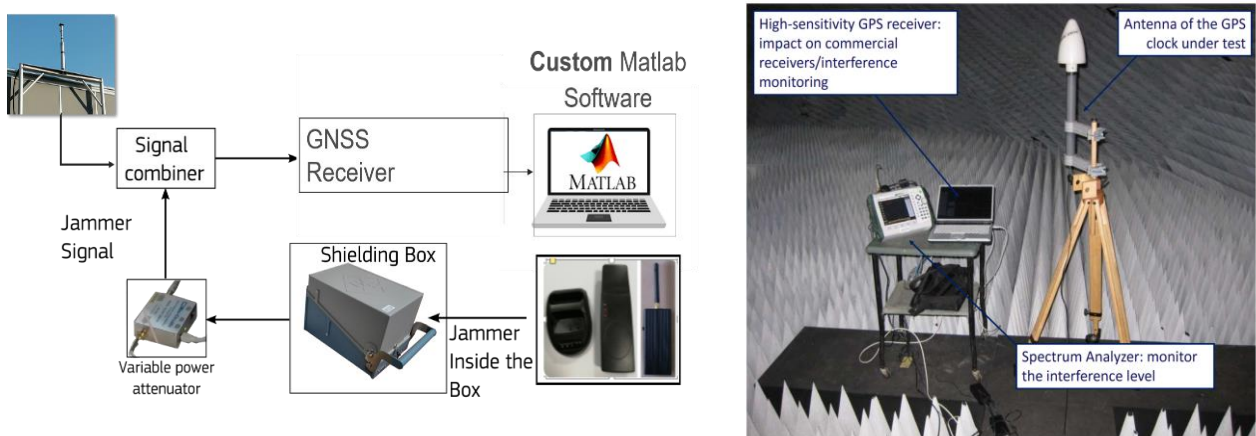


Figure 49. Set-up used for assessing the impact of RFI on GNSS timing. (On the right) Set-up used for evaluating the impact of jamming mitigation technique. (On the left) Set-up developed in the anechoic chamber to assess RFI impact on GPS timing receivers.

Using the latter set-up, a long series of tests, lasting up to 120 hours, with different types of interference signals and power levels, was completed. The characterisation of the GNSS timing receivers was done using a frequency counter and external Rubidium frequency standard. A wide

range of different KPIs measuring the effect of the interference in the short, mid, and long term stabilities of the GNSS timing receivers, could be assessed.

As an example, in Figure 50, the observed Allan deviation and Modified Allan deviations of the GNSS timing receivers measured are shown. On the left side, the results showing the performance of the various interference mitigation techniques using the first set-up. On the right side, the modified Allan deviations of one of the GNSS receivers under test for the interference test conditions assessed.

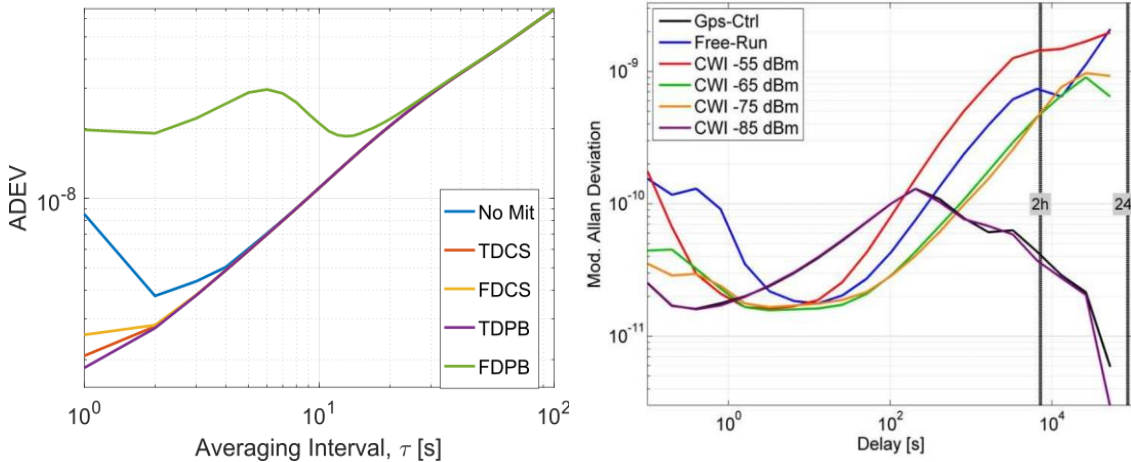


Figure 50. Sample results for local clock stability results using the two set-ups available at the JRC.

3.5.2 Pulse Per Second (PPS) signal analysis

One of the objectives of the FANTASTIC Project was that of showing the added-value of the OSNMA to enhance of robustness of GNSS timing receivers against spoofing attacks [33]. In June 2019, a live demonstration event was facilitated at the premises of the JRC. Two prototype receivers were made available by the Consortium, one of them with an OSNMA-enabled firmware, were used in a test where a GNSS simulator generated a combination of genuine and spoofed GNSS signals. During this demonstration, a multi-channel oscilloscope was used to monitor the PPS of the two GNSS receivers, one OSNMA-enabled and a second one without using OSNMA. A sketch of the set-up used in the demonstration is shown in Figure 51.

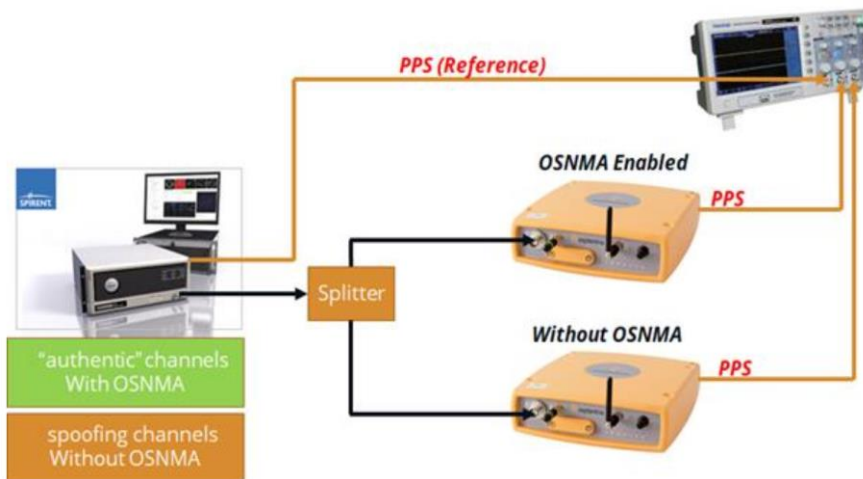


Figure 51. Test set-up used for monitoring PPS signal output. The GNSS simulator is used to generate both genuine and spoofed satellite signals during the test (taken from the Final Report of the FANTASTIC Project [33]).

The set-up includes the RFCS which generates the GNSS signals and also provides a reference PPS signal as an output. The PPS of the two receivers and that from the GNSS simulator are monitored with a multi-channel oscilloscope. A snapshot of the oscilloscope screen taken during the preparatory tests is shown in Figure 52.

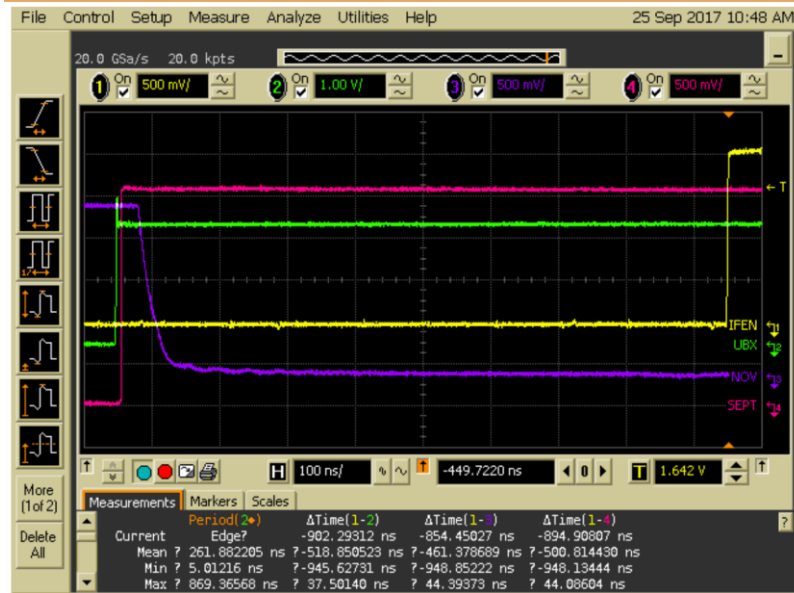


Figure 52 Snapshot of the multi-channel oscilloscope showing the true PPS (yellow) and PPS signals of other receivers under test (taken from the Final Report of the FANTASTIC Project [33]).

3.5.3 GNSS intersystem time bias evaluation

An additional element that is important when testing multi-constellation GNSS timing receivers is the GNSS inter-system bias. It is well known that the multi-constellation capability has the potential to extend GNSS usage to environments where single GNSS navigation is usually precluded. To adopt such technique, a user must be equipped with a multi-constellation receiver, the use of this device improves the performance of GNSS-based navigation in terms of accuracy and continuity, directly related to the enhanced number of measurements available but also for integrity. The main difference between the different GNSS is the adoption of different time scale; in addition, a multi-constellation receiver can introduce group delay differences or delays generated during the baseband and digital signal processing. The parameter including the system level effects and the receiver related ones is known as intersystem bias. JRC has developed a method to evaluate the stability of this parameter for different receivers using raw GNSS measurements as shown in Figure 53, where the GPS-Galileo case is considered [53]. Sample results for the GPS to Galileo inter-system bias are reported in Figure 54. In the upper part, the estimated inter-system bias time series is shown and it is compared with respect to the broadcast Galileo to GPS Time Offset (GGTO) values. This type of analyses allows to verify the presence of biases introduced by the receiver. In the lower part of Figure 54, the stability of the inter-system bias is shown.

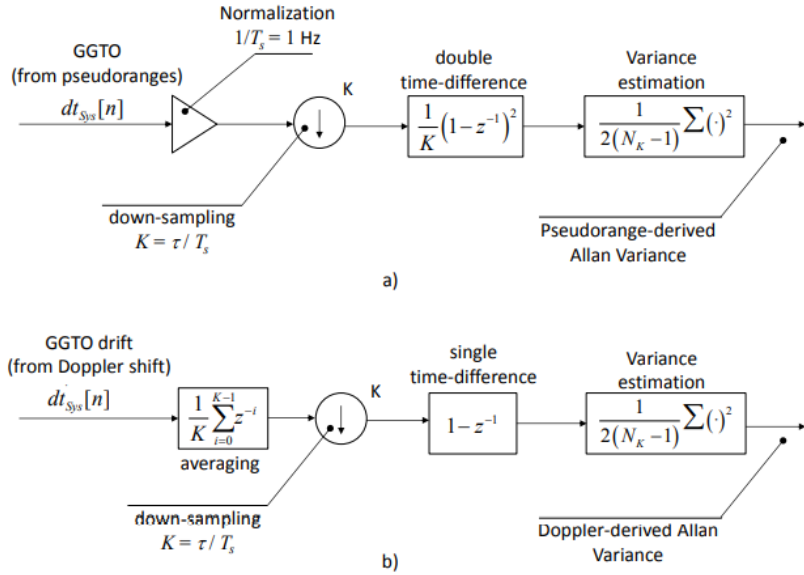


Figure 53. Evaluation of the Allan variance using GPS/Galileo inter-system bias and its drift estimates. a) Pseudorange-derived Allan variance. b) Doppler-derived Allan variance.

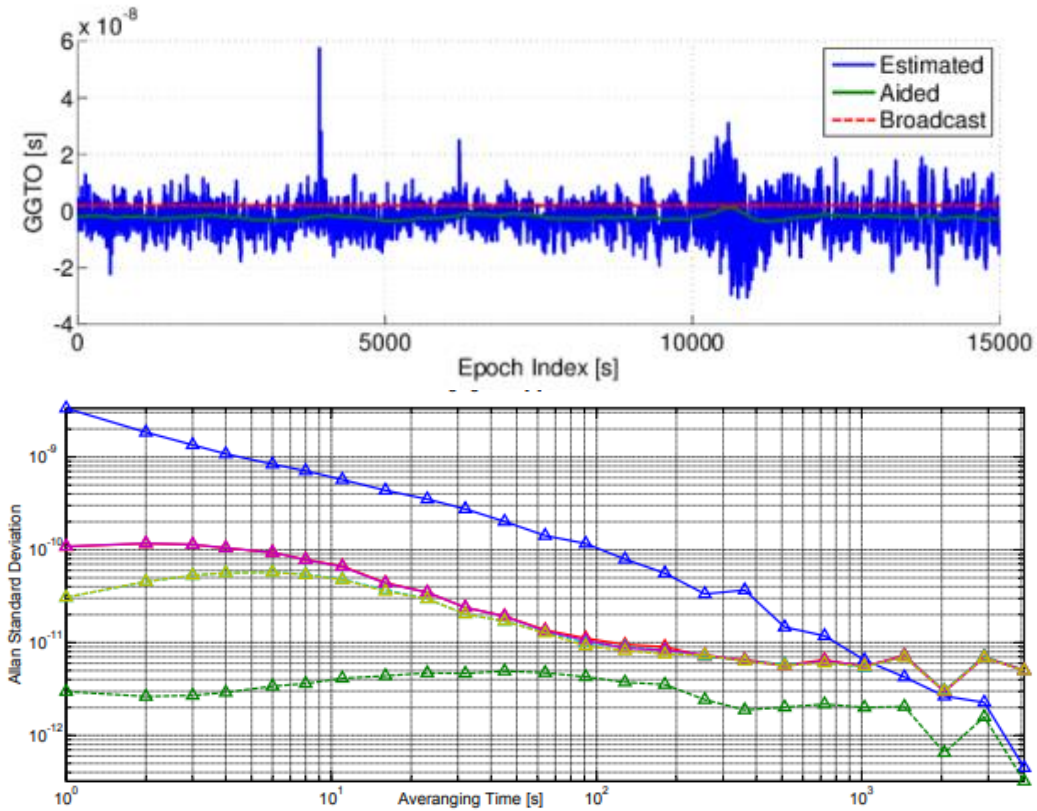


Figure 54. In the upper box: GPS to Galileo Inter-system bias time series obtained using a mass market receiver. In the lower plot: GPS-Galileo inter-system stability.

3.6 Laboratory testing with RFI and spoofing signals

It is well known that radio frequency interference (RFI) poses a serious threat to GNSS [54]–[56]. This is particularly true in case of liability critical and safety critical applications: in the former, the PVT information is directly related to legal and economic aspects while in the latter any malfunction of GNSS could have severe impacts on human life.

Noting the severe impact that RFI may have on the GNSS receiver performance, a stream of the R&D actions under the EU GNSS Programmes has addressed the need to develop technologies to monitor and detect GNSS jammers, particularly those used in cars or trucks [1], [57]. Additional R&D actions have been aimed at strengthening the robustness of the receivers using antenna systems with an enhanced resilience against jamming and spoofing in the road and maritime transport domains [3]–[5], [58].

In this section, a description of the key assets and relevant testing capabilities related to the assessment of the impact of the jamming and spoofing threats on GNSS receiver performance. Two recent testing campaigns conducted at the JRC are presented as illustrative examples.

3.6.1 Testing of GNSS receivers with RFI signals

One of the first testing campaigns with interference signals at the JRC was in radiated mode in the EMSL. This test campaign was conducted back in 2012, and was aimed at assessing the coexistence of a terrestrial mobile network in the USA (i.e., LightSquared). This terrestrial mobile network was subject of a compatibility study because it was proposed to be allocated in a band adjacent to GPS L1/GAL E1 [59], [60]. In this testing campaign, three Galileo-enabled COTS receivers were used and a quantitative assessment of the impact of the coexistence with this terrestrial network (i.e., with the LTE signals broadcast from nearby base stations) could be made. The metric used in that case was the loss of C/N₀ observed in relation to a baseline scenario with no signals from the terrestrial network present in the adjacent bands.

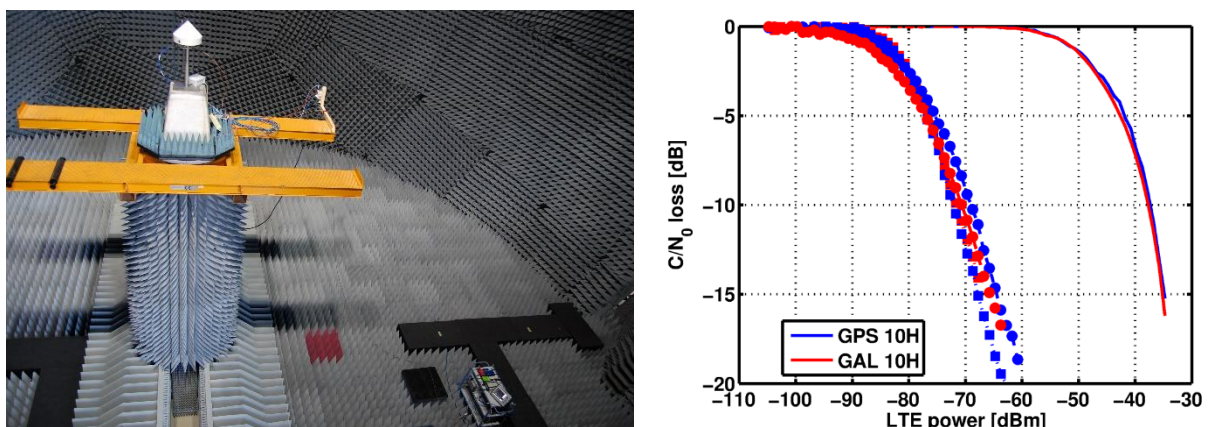


Figure 55. Photograph of the setup used in the EMSL for the compatibility assessment with LightSquared (left). Observed loss of C/N₀ versus power of the LTE signals with the three receivers tested and one of the proposed band allocations (right).

An important testing capability to highlighted here is that the laboratory at the JRC is equipped with state-of-the-art programmable RF vector signal generators. With these instruments, it is possible to generate a wide range of signal waveforms, signal modulations and pulsing schemes that might be needed in an interference or coexistence study. As an example, in the coexistence testing with LightSquared, a 3GPP FDD LTE waveform emulating the downlink from a LightSquared base station had to be generated and its power level ramped up in a controlled manner during the tests. Prior to these tests, a calibration of the power levels of both the GNSS simulator and the vector signal generator had to be completed. The former calibration was made following a test procedure equivalent to that used in the testing of the ship-borne GNSS receivers presented in Section 3.2.2. In this type of tests, the location where the radiated power levels are calibrated must be in the vicinity of the antenna of the receiver under test.

The test campaign reported in Section 3.2.2 included multiple radiated tests with RFI signals present and therefore, it is worth giving a more detailed description here. These tests were specified in the Maritime Standard IEC 61108-3 [24], which identifies specific performance requirements in terms of position accuracy and re-acquisition capability under narrow-band and wide-band interference, respectively.

As an example, one of the radiated tests with narrow-band interference required the generation of a pulsed continuous wave centred at 1575.42 MHz, a duty cycle of 10%, a pulse duration of 1 ms, and a peak carrier power of -20 dBm in the vicinity of the GNSS antenna. This pulsed RFI waveform was measured with a real time spectrum analyser inside the anechoic chamber, next to the measurement tower of the EMSL. A snapshot of this measurement is depicted in Figure 56, where the RFI signal power versus time, the power spectrum, and a spectrogram are shown.

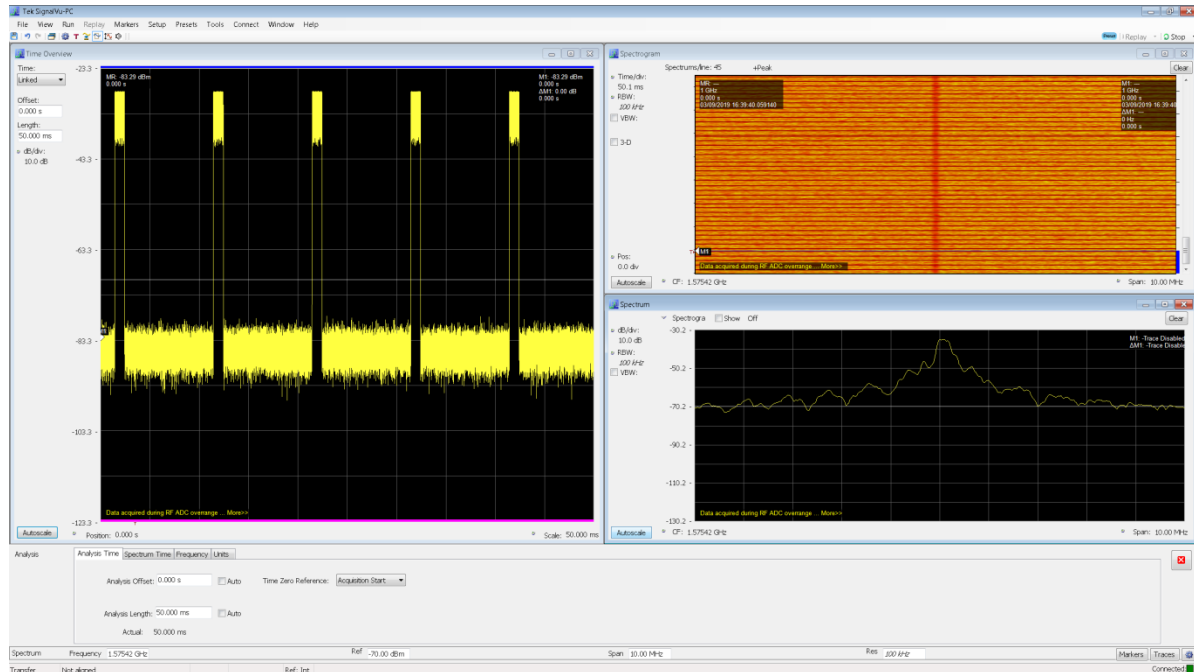


Figure 56. Snapshot of the real time spectrum analyser showing the narrow-band pulse interference signal, its power spectrum, power versus time, and power spectrogram.

The radiated tests with the wide-band interference in the standard were specified with a calibrated additive white Gaussian noise (AWGN) signal with instantaneous bandwidth of 1 MHz, centre frequency of 1575.42 MHz, and RMS power of -101 dBm in the vicinity of the GNSS antenna. In this test, the interference signal was not active permanently and had to be switched on and off following the timeline shown in .

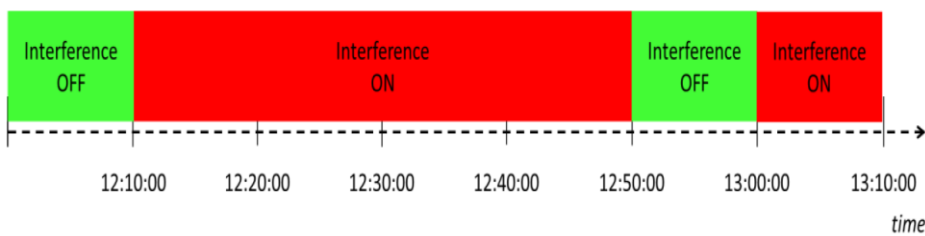


Figure 57. Timeline showing the time intervals where the wide-band interference signal was present.

The snapshot of the real time spectrum analyser got during the radiated test with the wide-band interference is depicted in Figure 58. As in the previous example, the power versus time, power spectrum and a spectrogram are shown.

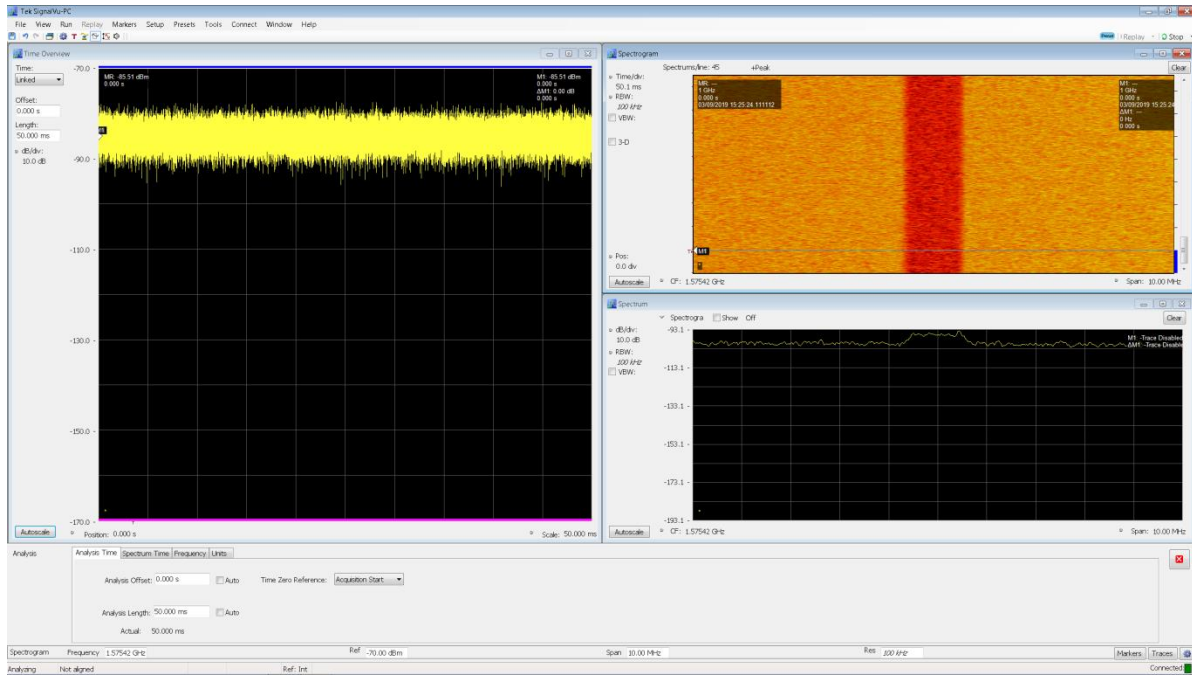


Figure 58. Snapshot of the real time spectrum analyser showing the wide-band AWGN signal, its power spectrum, power versus time, and power spectrogram.

A recent test campaign completed at the JRC was aimed at establishing a battery of automotive test scenarios generated with a GNSS simulator, with representative jamming and spoofing threats present [61]. This campaign was conducted to support the implementation of an EU regulatory framework for the Smart Tachograph (ST) [62], [63], which happens to be the first one mandating the adoption of the new OSNMA authentication service of Galileo.

For the jamming test scenarios, three RFI waveforms were selected based on what was observed during the extensive field monitoring made in the frame of the H2020 STRIKE3 Project [57]. Figure 59, Figure 60, and Figure 61 show the spectrograms and power spectral density of the three RFI waveforms selected for the ST test battery. These interference waveforms were programmed in Matlab and uploaded to the vector signal generator used in the test campaign.

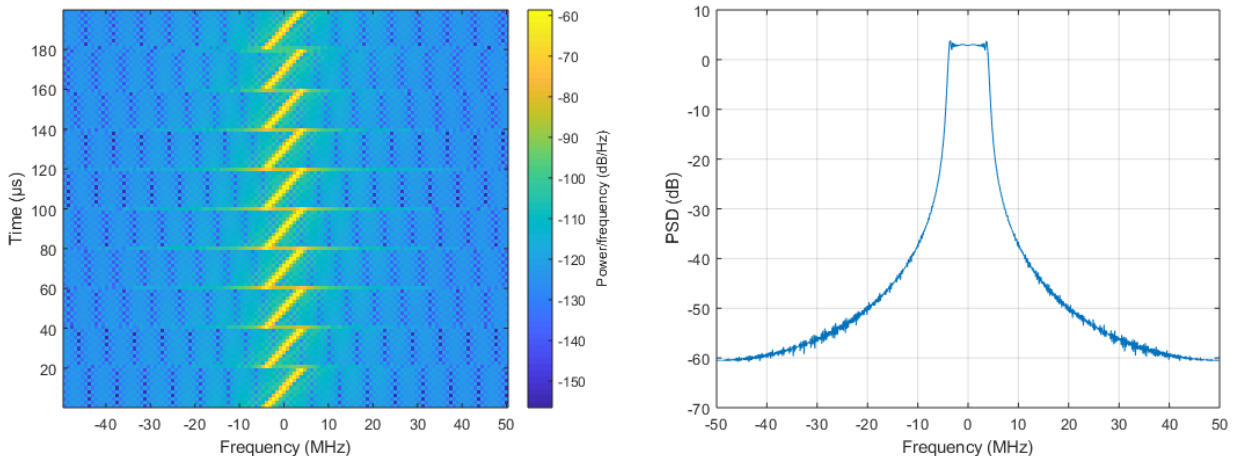


Figure 59. Spectrogram and power spectral density of a narrow-band sawtooth FM waveform, with a bandwidth of 10 MHz and a sweep time of 20 usec.

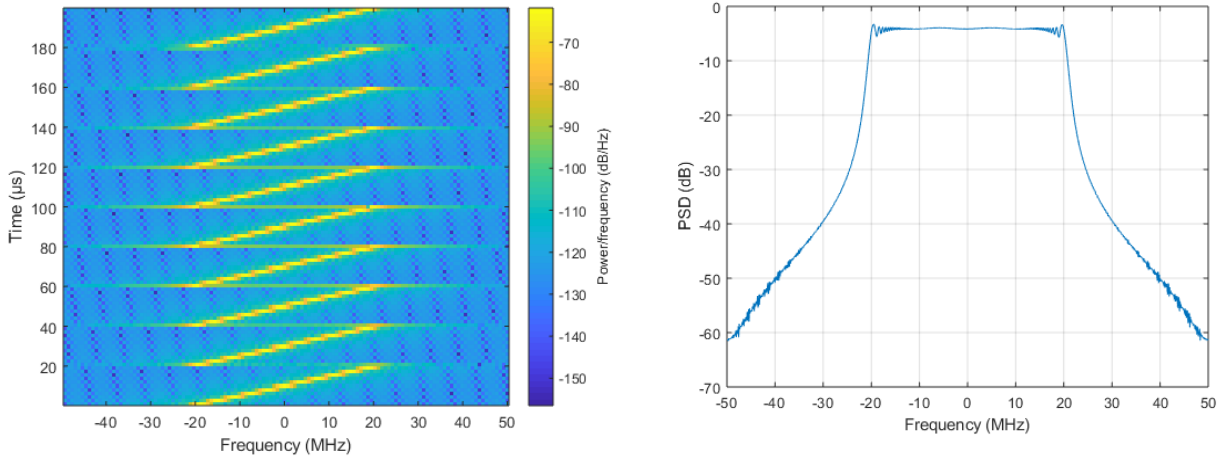


Figure 60. Spectrogram and power spectral density of a wide-band sawtooth FM waveform, with a bandwidth of 40 MHz and a sweep time of 20 usec.

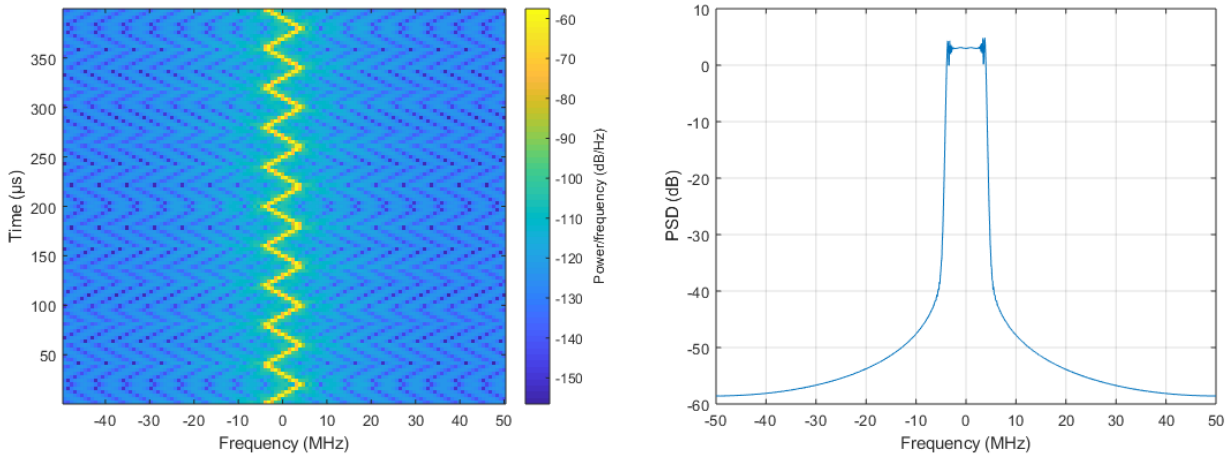


Figure 61. Spectrogram and power spectral density of a narrow-band triangular FM waveform, with a bandwidth of 10 MHz and a sweep time of 20 usec.

3.6.2 Testing of GNSS receivers with spoofing signals

In the last few years, the JRC has extended its portfolio of testing capabilities to cover the facilitation of both conducted and radiated tests with spoofing signals. The implementation of the spoofing attacks can be made using two different platforms. The first platform is based on the SIMSAFE add-on of the Spirent GSS9000 Simulator [13], which has been developed by Qascom. This add-on allows the integration of spoofing attacks on any given scenario created with the GNSS simulator. This tool allows the generation of a wide range of spoofing attacks, from the simplest loosely synchronised attack up to sophisticated multi-channel tightly synchronised attacks. The second platform that can be made available is based on the use of a GNSS simulator and a record and replay SDR device (see Section 3.7 for a more detailed description). With this platform, pairs of IF datasets are recorded separately, one with a baseline scenario clean and a second one with only the spoofing signals, and are combined off-line using an ad-hoc software tool. The latter platform was used to create the battery of automotive test scenarios with representative jamming and spoofing threats [61]. This test campaign was conducted to support the implementation of the EU Regulatory Framework of the Smart Tachograph (ST) [62], [63] and consequently, the baseline scenarios were created with the OSNMA authentication enabled on the GNSS simulator. For the sake of illustrating the testing capabilities to implement spoofing attacks, a description of the methodology and some example results are given next.

The methodology used to create the IF datasets with one of the selected spoofing threats for the ST test battery [61] is illustrated in the flowchart of Figure 62. A second flowchart, with photographs of the test equipment used to create the test battery with the jamming and spoofing threats, is shown in Figure 63. Lastly, a snapshot of the GUI of the software tool developed to merge two separate IF datasets and apply a time-dependent power weighting to one of them is depicted in Figure 64.

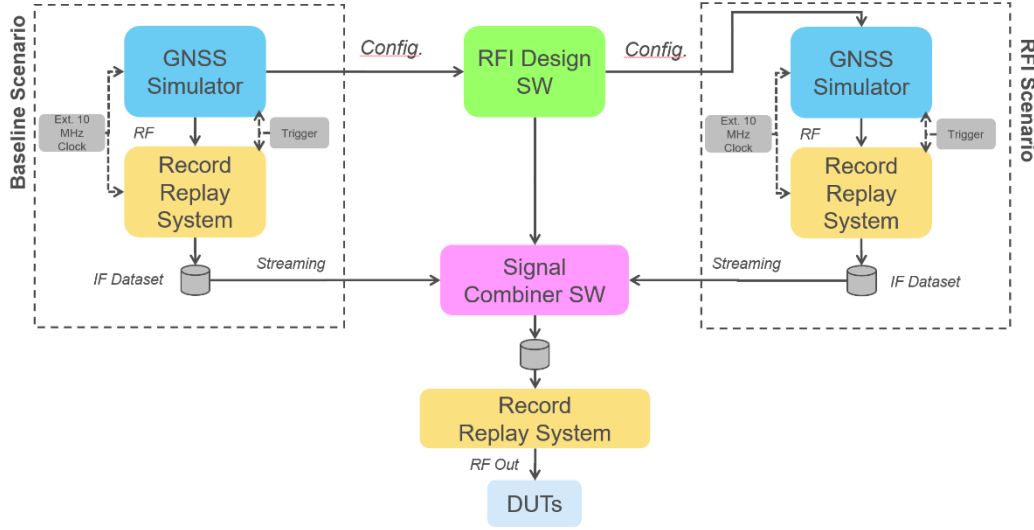


Figure 62. Flowchart diagram illustrating the methodology used to create the IF datasets with the spoofing threats for the ST test battery.

The main processing steps required to produce an IF dataset can be summarised as follows:

- 1) **Configure vehicle trajectory:** position, speed and orientation of the truck are simulated by means of a dedicated tool able to create trajectories with realistic kinematics of the vehicle.
- 2) **Configure and record baseline scenario:** the GNSS simulator is configured to generate GPS L1 and Galileo E1 signals with the truck trajectory defined in the previous step. A land mobile multipath model simulating a highway environment is activated in this case. The simulated signal is recorded in I/Q samples format file using the SDR device. Both the GNSS simulator and the SDR device must share a common clock (i.e., 10 MHz reference) and trigger pulse.
- 3) **Configure and record spoofing scenario:** the NMEA messages generated by the simulator are used in input at the RFI design software. This tool is aimed at generating all the following elements of the spoofing scenario:
 - the location or trajectory of the spoofer;
 - the specification of the pseudorange ramps and times when they are activated in the scenario. The pseudorange ramps are applied to simulate the variation of signal time-delay between the victim receiver and the spoofer.
 - the gain mask describing the relative gain between the nominal and threat signal as a function of time, which is applied when the two IF datasets are merged.

The simulated signal is recorded in I/Q samples format file using the SDR device, sharing a common clock and trigger pulse as in the previous recording.

- 4) **Merging of the baseline and spoofing IF datasets:** the two IF datasets are merged in post-processing applying the relative gain mask set in previous step.
- 5) **Playback of the IF combined scenario:** the combined IF dataset is played with an SDR device. The output RF signal is fed to the GNSS receiver under test.

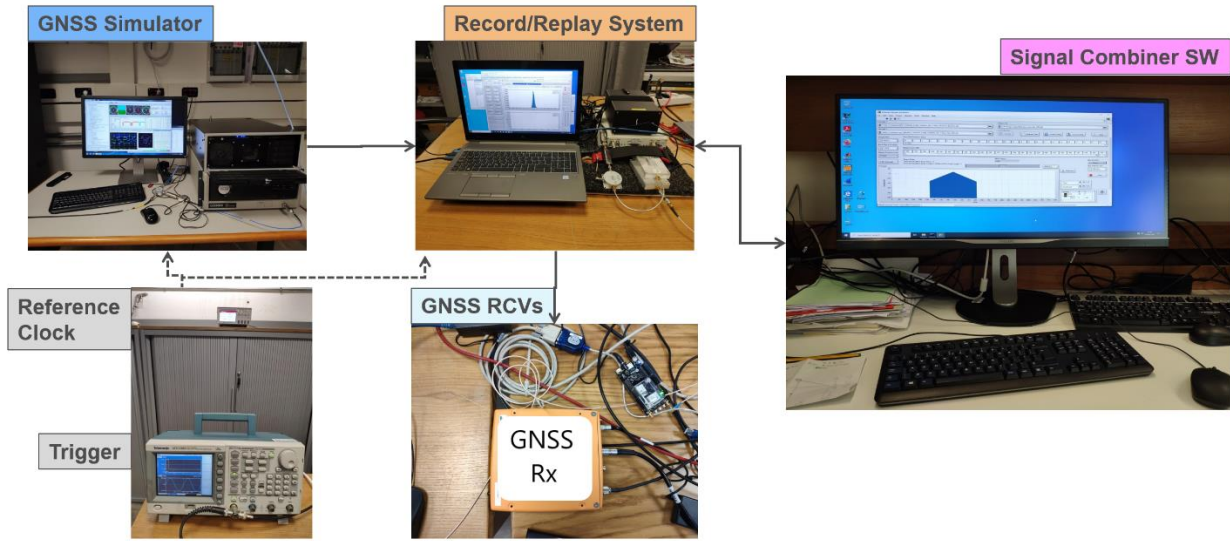


Figure 63. Photographs of the test equipment used to create the battery of test scenarios with jamming and spoofing threats.

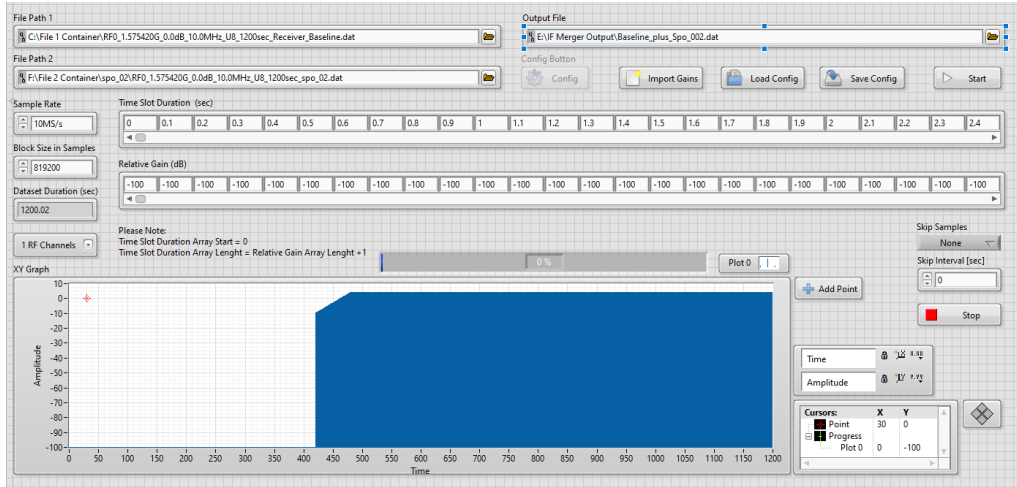


Figure 64. GUI of the software tool used to merge the two IF datasets, weighting the relative power level of one of them in accordance with a pre-defined profile.

For the sake of illustration and just to give an outline of the type of scenarios present in the ST test battery, the threats considered be classified and briefly described as follows:

1) Unintentional threats:

- **GNSS-Repeaters**: under this category, the battery includes two scenarios with a GNSS repeater present, respectively, at a minimum range distance of 30 m and 3 km. A typical example is the case of signal spill-over from a malfunctioning or misplaced repeater in an airport hangar close to a road or highway. The GNSS receiver in the Smart Tachograph on-board the truck is exposed to the line-of-sight signals broadcast by the satellites and those re-radiated from the repeater.

2) Intentional threats:

- **Collateral attack**: under this category, the spoofers targets another vehicle, but it is also reaching collaterally the GNSS receiver in the TS on-board the truck. the battery includes the following variants:
 - **Collateral Spoofing - simulator**: The spoofers transmits GNSS-like signals containing incorrect or invalid navigation message and the ranging

information among channels have been aligned in order to force the receiver to estimate a different PVT solution. A characteristic of this collateral attack is that its effect on the non-intended receiver is time limited.

- **Collateral Spoofing – re-radiator:** it can be considered as intermediatespooferto transmit a GNSS-like signal based on real time reception of actual GNSS signals. It mainly intervenes in the ranging information to mimic the PVT estimation. Being a collateral attack, the transmitted signals may be self-coherent, but they would not be coherent with the vehicle's dynamics and the signals tracked by the GNSS receiver in the ST.
- **Targeted spoofing attack – simulator:** this is the case of a spooferto located in the passenger seat of the ST hosting vehicle and under direct control of the driver. The counterfeit signal is self-coherent and coherent with the dynamics and signals tracked by the ST receiver.
- **Targeted spoofing attack – re-radiator:** as above, this case is similar to the corresponding collateral spoofing attack, but whose intended purpose is to deceive the ST receivers. It represents the most advanced attack and it can combine the full reproducibility of navigation messages (OSNMA included).

The bit depth used to record and playback of ST IF datasets was 8 bit for the spoofing scenarios, and 16 bit for an additional set of scenarios with jamming signals. The duration of the scenarios was 20 min, except for two scenarios lasting, respectively, 10 and 60 min. The sampling rate was in all cases 10 MSamples/sec. The current number of scenarios in the test battery is 11 and the data volume associated is above 350 GByte of data.

As an example, a sketch illustrating the test case of the targeted spoofing attack with a GNSS simulator aboard the truck hosting the ST, and the observed genuine and spoofed trajectories and velocity profiles are shown in Figure 65. Here, the effect of the spoofing attack (i.e., the trajectory of the spoofer diverges from the one actually followed by the truck) can be noticed at minute 8 from the start of the test.

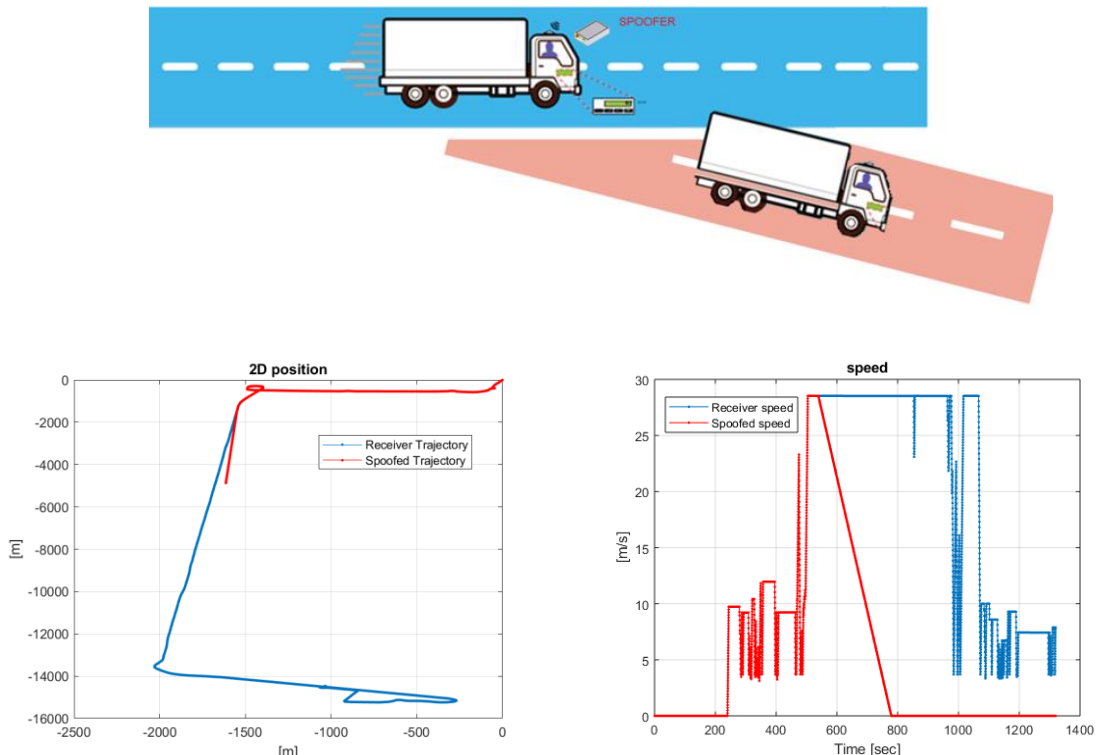


Figure 65. Sketch of the targeted spoofing attack with the GNSS simulator on board the truck (top); 2D genuine and counterfeit trajectories (bottom left) and speed profiles (bottom right) corresponding to the same test case.

3.7 GNSS signal record & replay testing

This section gives a description of the testing capabilities regarding the record and playback of the GNSS signals, outlining the specific functionalities and the test equipment that can be made available to the project consortia coming to the JRC.

In recent years, GNSS record and playback systems have become a standard piece of test equipment in many laboratories due to their flexibility, compactness, and affordability. These devices allow to record GNSS signals for a time that is just limited by the available storage capacity. These recorded scenarios can be played by the same device or by other GNSS playback devices, provided an inter-changeable data format was used. The latter is a very important point as it allows the sharing of pre-recorded reference datasets with interested users.

The record and replay system that can be made available at the JRC is based on an SDR-based platform [64], the Universal Software Radio Peripheral (USRP) NI 2944R [65]. This device integrates two RF daughterboards that can record and playback RF signals with a centre frequency up to 6 GHz and an instantaneous bandwidth of 120 MHz. This USRP device is interfaced with a host PC using a Peripheral Component Interconnect (PCI) express card and a PCI-to-Thunderbolt 3 adapter. This fast interface allows a continuous record/playback of an IF data stream to/from the host PC at a maximum rate of 100 MSamples/sec. A reliable streaming at high sampling rates, though, requires the use of either a solid state drive (SSD) or a NAS device attached to the host PC. A control software tool on the host PC and an ad-hoc firmware on the FPGA in the USRP device developed in-house are used. This record and replay system was used both with in a static location connected to a roof-top GNSS antenna and, interestingly, on a van to conduct recordings of GNSS signals while driving. Two photographs of the set-up used in these automotive tests is shown in Figure 67.



Figure 66. Photographs of the JRC's van with the record and replay system used in the OSNMA test drives: outer (left) and inside (right) views of the van, showing the laptop, USRP device, rubidium clock, and PCI-to-Thunderbolt 3 adapter.

Two important features of the record and replay system used at JRC that is worth mentioning are as follows:

- 1) Configurable bit depth: the USRP system records and plays back RF signals as interleaved I/Q samples at a zero IF and with a programmable bit depth (i.e., 1, 2, 4, 8, and 16 bits). The choice of the bit depth is the result of a trade-off between the degradation of signal-to-noise ratio and the dynamic of the sampled RF signals. In the case of GNSS testing in the absence of interference signals, 1 or 2 quantisation bits are normally sufficient to record and play back a GNSS signal with a negligible loss of information.
- 2) GNSS repeater with time delay adjustable on the fly: an interesting functionality of the record and replay system of the JRC is that it can be used as a GNSS repeater with a

time delay that can be changed in real time. The current range of time delays that can be set is from 5 ms to a maximum of about 60 sec. This functionality was added to assess the performance of an OSNMA-enabled test receiver, and more specifically, to verify that the receiver meets a requirement on the loose time synchronisation. A block diagram illustrating the functionality of the variable time-delay in the record and replay system of the JRC is show in Figure 67.

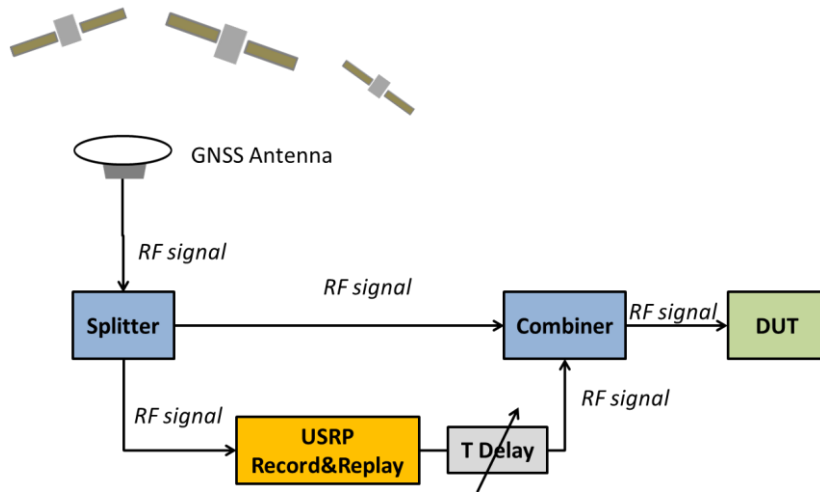


Figure 67. Block diagram of the record and replay system in the configuration to function as a GNSS repeater with an adjustable time delay.

3.8 Testing of OSNMA-enabled receivers

The Galileo Open Service Navigation Message Authentication (OSNMA) is a new feature of Galileo OS that provides means to authenticate navigation data through information transmitted in the SIS, as part of the E1B I/NAV message. Starting in 2013, the definition and implementation of this new service at system level have been supported by a series of H2020 Mission And Services (MAS) R&D Actions and internal studies under the EU GNSS Programmes [7], [66]–[68]. The GNSS laboratory of the JRC supported these projects, facilitating extensive testing and validation activities. In preparation of the foreseen entry-in-service of the OSNMA, the JRC also supported the adoption of the service by users, facilitating testing and demonstration activities of H2020 and Galileo Fundamental Elements Projects with a focus on GNSS user-segments or use cases (e.g., smart tachograph, timing receivers, drones, maritime, etc). Through these support activities, JRC has acquired a significant know-how on the OSNMA protocol, as well as several key testing assets, delivered by the supported projects or procured separately. These capabilities were exploited during the OSNMA internal live test phase, which took place between November 2020 and April 2021. Within this test phase, JRC contributed to the service validation and to the assessment of the user segment readiness, analysing over 100 days of recorded OSNMA data.

The following sections provide a description of the key assets and relevant testing capabilities that are available at the JRC to support future OSNMA-related R&D actions under the EU GNSS Programmes.

3.8.1 Generation of the Galileo OSNMA data stream

To support the adoption of OSNMA by the user community, thorough testing of OSNMA-enabled receivers is required. This testing shall cover two aspects:

- Ensure the correct implementation of the protocol through functional testing, aiming at verifying the cryptographic processing capabilities of the receiver, both during nominal operations and during renewal and revocation operations.
- Assess the performance of the receiver under different testing conditions (e.g. visibility, dynamic conditions). This assessment is carried out using traditional OS key performance indicators as well as specific OSNMA indicators, such as the authentication failure rate, time to first authenticated fix and OSNMA PVT accuracy.

In order to support these two activities, a testing signal with OSNMA data is needed. Considering that OSNMA is not yet publicly available, this signal can be obtained through simulation or through recording of the SIS during the testing phase.

In fact, during the OSNMA internal test phase, JRC recorded RF signal snapshots from the live signal. These recordings cover various OSNMA configurations and include renewal and revocation operations. They were retrieved both in static and dynamic conditions, including various environments for the dynamic samples (e.g. sub-urban, urban). These RF samples can be replayed to the receiver under test using an SDR system.

In addition, the E1B I/NAV data stream has been continuously recorded over the full duration of the internal test phase. This data can in turn be provided to a GNSS simulator in order to generate signals including OSNMA. This approach exploits the capacity of the simulator to accept user-defined I/NAV stream and can also be used with simulated OSNMA data. The RF signal generated in this way can also be recorded by an SDR system for future analysis or re-transmission.

The combination of real data and simulation capabilities represents a versatile solution to generate the most relevant aspects of the OSNMA protocol while covering as well specific conditions and corner cases.

3.8.2 OSNMA-enabled receivers

3.8.2.1 Hardware OSNMA-enabled receiver

To assess the performances of the OSNMA enabled devices, a reference receiver is required, to act as a control. This is of particular importance for OSNMA, as the service is still in its early

stages. The receiver used to this end is an OSNMA-enabled GNSS receiver from Septentrio [69]. The receiver has a specific firmware and represents a highly reliable HW solution, compliant with the OSNMA protocol specifications.

3.8.2.2 OSNMA-enabled software receiver

In addition to the hardware receiver, a fully OSNMA-enabled software GNSS receiver is also available. The NGene2 receiver, developed by the LINKS Foundation, is a real-time GPS/EGNOS/Galileo L1/E1 single frequency receiver, which can be executed by standard PCs running a Linux operating system. The software implementation offers more flexibility than a typical receiver, providing more detailed information on the different processing stages and, in particular, on the different verifications carried out in the frame of the OSNMA protocol.

In addition to its real-time capabilities, the receiver is also able to process sampled signal in post-processing mode. It can also directly process navigation data (by-passing the acquisition and tracking loops), enabling to run analysis at a higher speed. Figure 68 shows the interface of the NGene2 receiver.

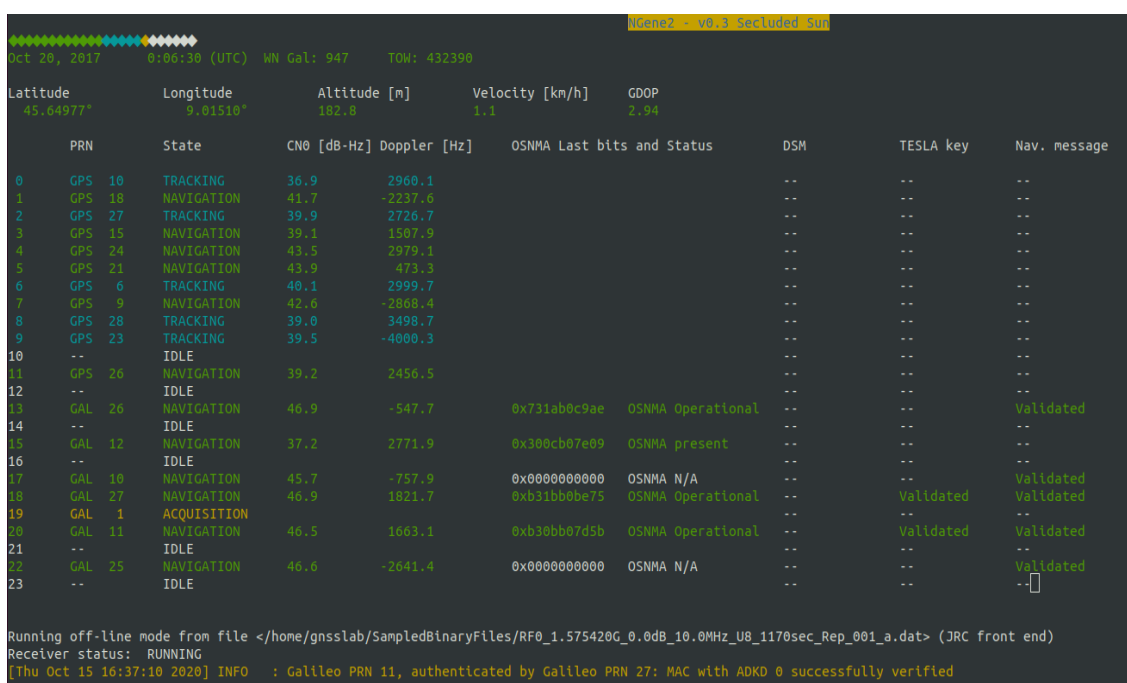


Figure 68. GUI of the OSNMA-enabled SW Receiver.

3.8.3 Post processing tools

3.8.3.1 Analysis of receiver OSNMA related outputs

In order to support manufacturers in testing their receivers' compliance to the OSNMA protocol and assessing their performances, the JRC developed a software library for the parsing of proprietary Septentrio and NGene2 logs files. The library also supports a detailed analysis of the OSNMA data retrieved by receiver and of the operations it carries out as part of the protocol. In particular, it is possible to analyse the following aspects:

- Percentage of received digital signature messages (DSM);
- Detailed information on the retrieved public key and TESLA chain parameters;
- Results of the public key and TESLA chain root key verification processes;
- Detailed information on the navigation data being authenticated;
- Results of the tag verifications and of the navigation data authentication.

The following figures are extracted for the report generated by the analysis of the reference HW receiver in a nominal OSNMA scenario, they are selected for illustrative purpose.

Figure 69 shows some of the parameters of the TESLA chain retrieved in the associated DSM.

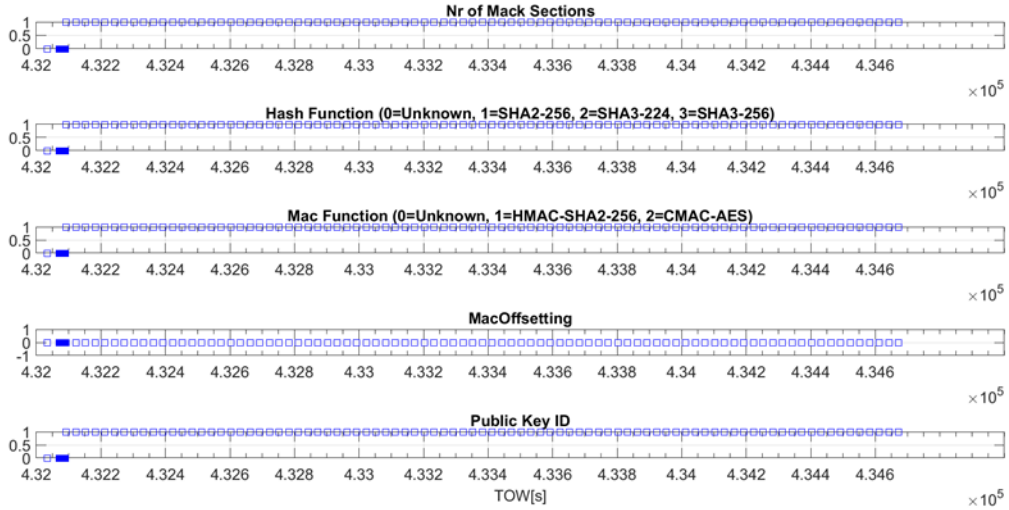


Figure 69. TESLA chain parameters, including number of MACK sections (NMACK), Hash function (HF), MAC function (MF), MACK Offset (MO) and public key ID (PKID).

Figure 70 shows the status of the transmitted tags for a given satellite. The green markers show successfully authenticated tags while in yellow ones correspond to tags that are not yet verified, due to lack of the corresponding navigation data to authenticate.

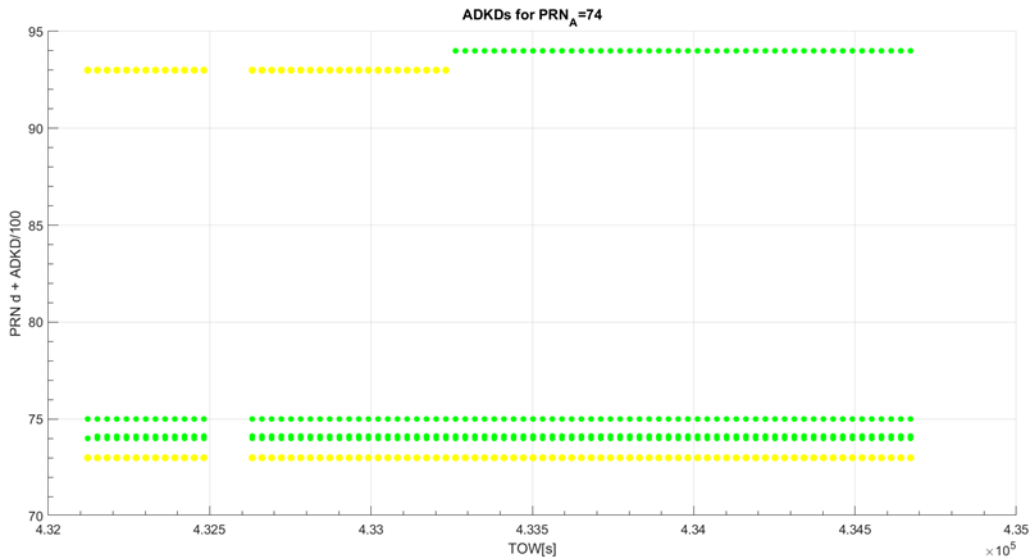


Figure 70. ADKD status for Galileo SVID14.

3.8.3.2 Broadcast OSNMA field analysis

The JRC has developed a post-processing software suite able to parse the Galileo I/NAV stream logged in SBF format. The parsed data is then analysed to retrieve the relevant OSNMA-related information broadcast in the SIS. The analysis represents a useful mean to check the actual broadcasted OSNMA configuration and to complement the verification of the receiver's compliance to the OSNMA protocol.

3.8.4 Modular set-up for OSNMA testing

In conclusion, the JRC can support users in the adoption of the novel OSNMA service by offering testing capabilities that cover both:

- the generation of the OSNMA data in various conditions (w.r.t. the OSNMA protocol operations and the receiver reception conditions);
- the verification of the correct processing of the received data by the tested receiver.

These capabilities, described in detail in the previous sections, can be fully exploited using the developed high flexible and modular testing set-up, described in Figure 71.

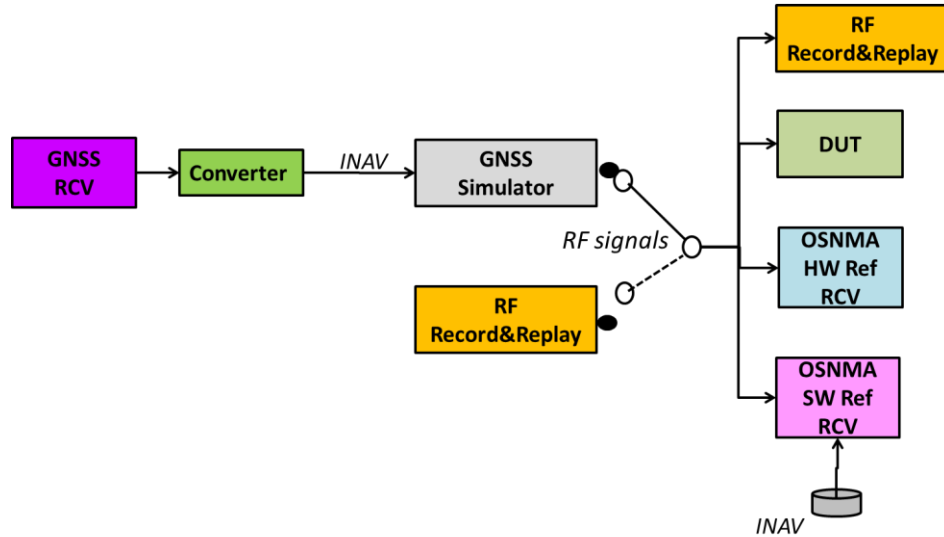


Figure 71. OSNMA testing capabilities.

In summary, the device under test can be assessed either:

- by replaying RF samples recorded during the OSNMA internal test phase;
- by using a GNSS simulator configured to use E1B I/NAV data containing OSNMA.

The performance assessment of the DUT can then be carried out using OSNMA reference receivers as a baseline for comparison. Additional software tools developed at JRC can also be exploited to perform a detailed analysis of the behaviours observed.

3.9 JRC Living Labs

The JRC Ispra Campus provides an ideal ground for on-site testing campaigns as it offers:

- Smart city infrastructure including smart grids, smart homes and smart mobility;
- Varied topography urban, semi-urban, rural and woodland areas.
- Ability to deploy specific testing scenarios.

Through the Living Labs initiative [70], the JRC is opening its research sites to put new technologies and applications into practice, in real-life and control environments.

In the specific case of the Ispra Site, the JRC offers living labs test environment spread over the 170 ha campus that includes:

- Over 100 buildings, one to five-floor structures and 36 km of roads. Site is utilised by 2,250 staff daily. It has independent logistical services necessary to run a small town, including energy generation and water provision. This enables smart city testing with interconnected infrastructures and interlinked facilities for smart grids, smart homes, smart mobility and advanced communication testing. Additionally, this infrastructure, modelled on smart city/campus concept, embeds sensors and devices that take constant readings of variables such as traffic flow, energy consumption, air quality and similar. The campus composition is shown in Figure 72.



Figure 72. Satellite high-resolution image of the campus of JRC Ispra Site (source: Google Earth).

- Urban, flat semi-urban, rural and woodland areas with varied topography, allowing for the varied testing campaigns, as shown in Figure 73.

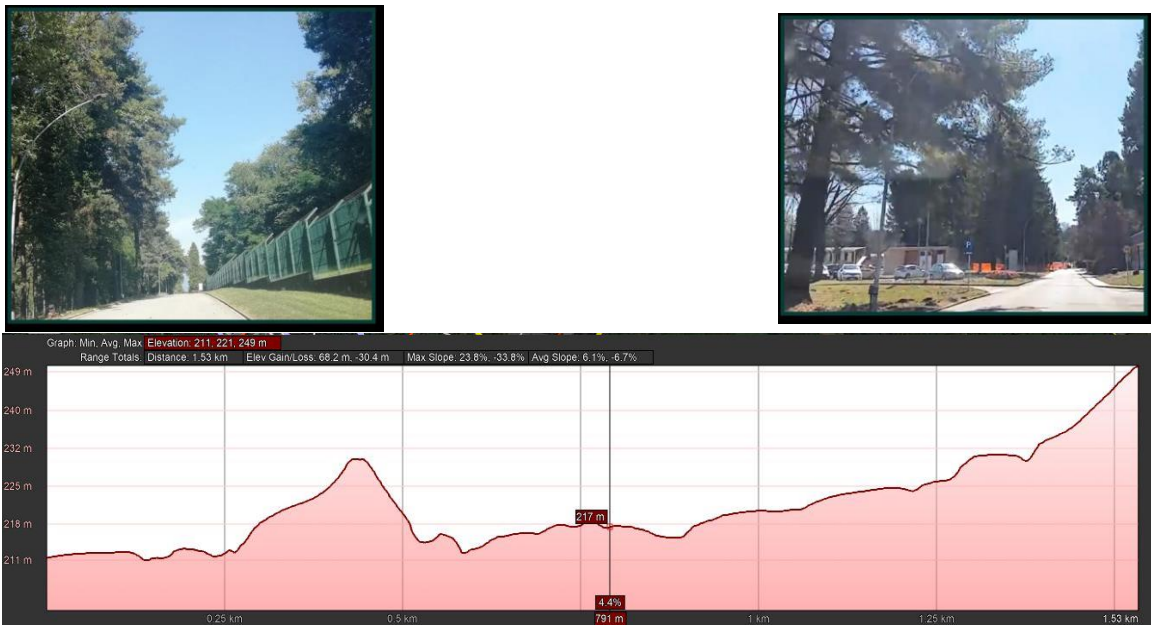


Figure 73. Examples of the test environments available on the JRC Ispra Campus.

- A flight zone up to 600 m is shown in Figure 74; the flight zone is under the control of the JRC Ispra Site Manager, and can be used for drone testing, as described in the following test case.

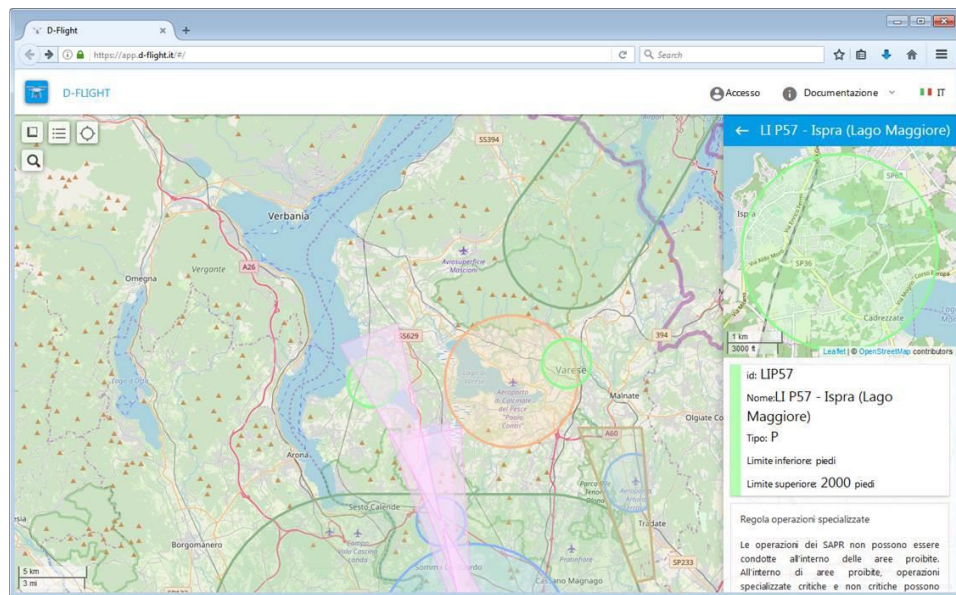


Figure 74. Representation of the LI P57 "No Fly Zone" on the ENAV aeronautical map. This spatial area is under the control of JRC Ispra Site Manager.

3.9.1 SARA drone flight trials in the JRC Campus

As part of the Living Labs initiative, a flight trial was carried out by the Search and Rescue Aid (SARA) project consortium at JRC Ispra. Following the preparation of a test plan and its approval by the site management, several flights were carried out. In particular, two drones with different configurations were used to collect GNSS data, which was then post-processed by JRC in PPK mode using as a base a receiver installed on the campus. In addition to collecting GNSS data, the drones were used to record videos of the traffic on a portion of the campus road, to investigate the potential of drones in traffic monitoring. Some activities related to the SARA project are shown in Figure 75.



Figure 75. Tethered drone used in the flight trial (top-left), drone flying on the campus (top-right) and view from the on-board camera used for traffic monitoring (bottom). All photographs taken during the demonstration of the SARA Project in the campus of the JRC Ispra Site, on 1/10/2020.

3.9.2 Testing of an indoor navigation app on a smartphone

Seamless and continuous navigation is more and more a requirement for different applications and one of the most challenging environment for navigation is indoor. Indoor navigation is a challenging task which involves the solution of several problems such as signal attenuation, fading and measurements biases due to multipath propagation. Different solutions are currently available for indoor navigation exploiting WiFi signals, fingerprinting, IMU and map constraints. Testing the solutions for indoor navigation is an even more challenging task, JRC has developed a testing environment in an office building to evaluate the performance of navigation systems in indoor environments. Two type of tests can been performed: a repeatability test and an accuracy test. In the first case, a trajectory is repeated for several times in order to verify the consistency of the solutions obtained in the different laps. An example of such test is reported in Figure 76, during the test the user performed several loops around a large table present in a meeting room trying to always repeat the same trajectory. The quality of the navigation solution is assessed by comparing the different trajectories estimated for the different loops. A high consistency level of the navigation solution indicates the good performance of the system.

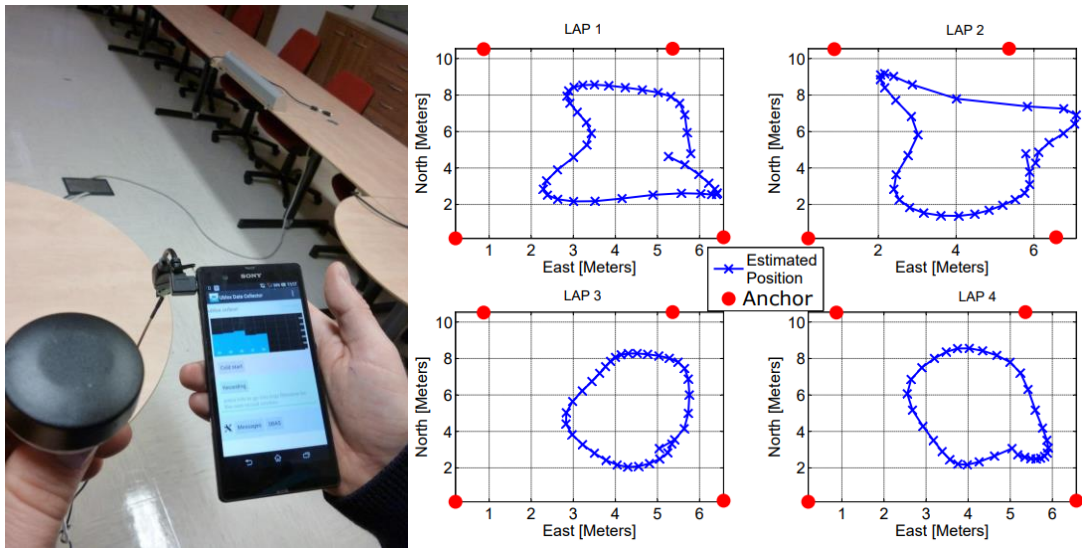


Figure 76. Example of repeatability test. On the left side the navigation device under test. On the right side, the reconstruction of the four laps performed by the user.

The accuracy evaluation is performed using a set of control points in a corridor. The coordinates of the control points are estimated using a total station. The example of the control points is shown in Figure 77. Using this test environment is possible to evaluate the trajectory of a user along the corridor. The corridor is characterised by a displacement of about 25 meters in the North-South direction and only 5 meters in the East-West direction.



Figure 77. Example of indoor accuracy test. On the left side the navigation device under test. On the right side, the displacement of the control points.

Using this approach, the user moves along the trajectory defined by the control points: the user can be also static on each control point for a specific time interval. In Figure 78, an example of the results obtained using the testing capacity presented. During the considered test, the user moved along the trajectory defined by the control points: the user was static on each control point for about 20 seconds. The test allowed to identify an anomalous behaviour of the navigation device in the correspondence of the control point number 7.

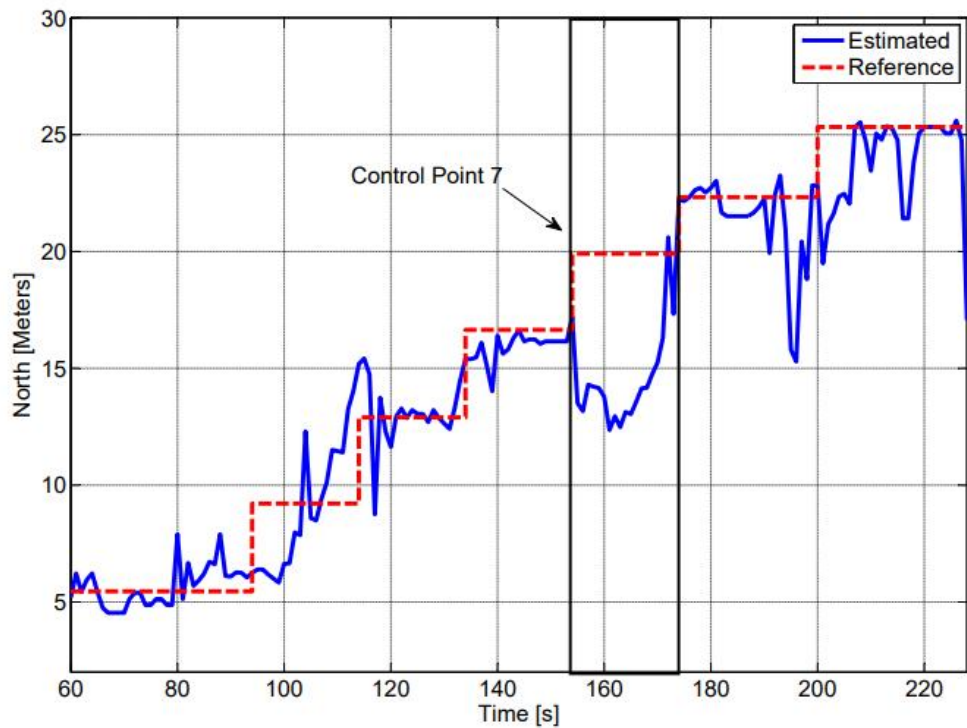


Figure 78. North coordinate evolution as a function of time. The red dotted line indicates the position of the control points.

3.10 Future updates on the inventory of GNSS testing capabilities

In the coming years, the inventory subject of this report will be subject to updates of existing capabilities and addition of new ones. This section presents a summary of the expected updates and additions, which are right now in preparation at the JRC.

The main expected updates and additions to this inventory can be summarised as follows:

1) Characterisation of the phase centre offset and phase centre variation of GNSS antennas:

This is a testing capability that is expected to be made available after the integration of a new pan-tilt antenna positioner FLIR D300-RF [71]. This positioner will be mounted on top of the measurement tower of the EMSL laboratory. The control software of the EMSL laboratory has already been upgraded to integrate the pan and tilt axes of the new positioner. This will allow the execution of automated tests to characterise the radiation pattern and the phase center variation of the antennas under test. A photograph of the pan-tilt positioner, which currently in it its final integration phase, is shown in Figure 79.

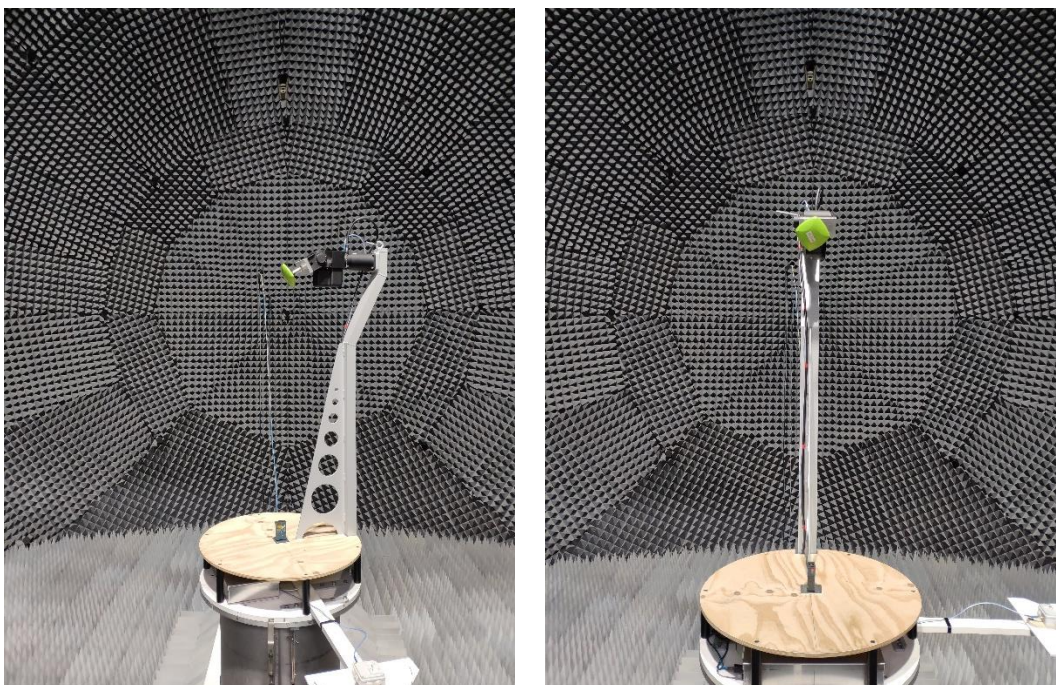


Figure 79. Photographs of the pan-tilt antenna positioner mounted on the measurement tower of the EMSL during one of the integration tests; (left) side and (right) front views of the pan-tilt antenna positioner.

This new antenna positioner will allow the characterisation of the phase centre variation as a function of the azimuth and elevation angles of the antenna under test. One interesting feature of the positioner is that integrates a pass-through RF rotary joint that exposes an RF connector next to the antenna under test. This pass-through connector allows a full 360 degrees rotation of the pan axis of the positioner without stressing mechanically the RF cable. Further, the pan-tilt positioner allows the mounting of an antenna under test on a circular ground plane, something that is potentially of interest to characterise both avionics and automotive antennas.

2) Galileo OSNMA testing aligned with the foreseen OSNMA ICD and Implementation Guidelines:

At the moment of completing this report, the foreseen OSNMA ICD and Implementation Guidelines have not yet been released. As soon as the specification of the authentication scheme gets closed, the testing capabilities reported in Section 3.8 of this inventory will be revisited and updated accordingly.

The same considerations apply to the facilitation of tests on receivers implementing the Galileo HAS and CAS services. Following the foreseen publication of the corresponding

ICD and Implementation Guidelines, an update of Section 3.4 of this inventory is foreseen, giving a description of the testing capabilities aligned to these two reference documents.

- 3) Testing of receivers integrating the Galileo I/NAV improvements:** following the recent release of the issue 2.0 of the Galileo Open Service ICD in January 2021 [19], which provides the specification of three new features to be introduced to the I/NAV message transmitted on the Galileo E1-B signal component, an update on the testing capabilities available at the JRC is foreseen. The GNSS simulation platform at the JRC will be updated to allow the testing of new receivers exploiting the new features introduced on the I/NAV message.
- 4) Testing of Galileo-enabled IOT devices and smartphones using assisted GNSS:** it is well known that GNSS assistance improves receivers performance by providing information, through an alternative communication channel, typically the mobile network, that the receiver would ordinarily have received from the satellites themselves. Normally, assistance data include ephemeris with satellite orbit and clock model data, which are derived from an estimated location and time [54], [72], [73]. The present GNSS simulation platform available at the JRC does not integrate a network emulator with the functionality of generating GNSS assistance data fully consistent with the scenario configured on the GNSS simulator. The addition of this testing capability is something currently under consideration.

References

- [1] 'Detection, Evaluation and Characterization of Threats to Road Applications', Feb. 21, 2013. <https://www.gsa.europa.eu/detection-evaluation-and-characterization-threats-road-applications> (accessed Apr. 06, 2021).
- [2] E. Domínguez *et al.*, 'Vehicular and Pedestrian GNSS Integrity Algorithms and Results for Urban and Road Environments Developed After an Extensive Real Data Collection Campaign', in *Proceedings of the 28th International Technical Meeting of the Satellite Division of The Institute of Navigation (ION GNSS+ 2015)*, Sep. 2015, pp. 553–568, Accessed: Mar. 30, 2021. [Online]. Available: <http://www.ion.org/publications/abstract.cfm?jp=p&articleID=13122>.
- [3] 'First Operational, Secured and Trusted galileO Receiver for ITS', May 13, 2015. <https://www.gsa.europa.eu/first-operational-secured-and-trusted-galileo-receiver-its> (accessed Apr. 15, 2021).
- [4] 'Trusted multi-application receiver for trucks | European Global Navigation Satellite Systems Agency'. <https://www.gsa.europa.eu/trusted-multi-application-receiver-trucks> (accessed Apr. 07, 2021).
- [5] 'Trusted Vessel Information from Trusted On-board Instrumentation | TRITON Project | FP7 | CORDIS | European Commission'. <https://cordis.europa.eu/project/id/312687> (accessed Apr. 07, 2021).
- [6] E. Göhler, I. Krol, M. Bodenbach, J. Winkel, G. Seco-Granados, and I. Fernandez-Hernandez, 'A Galileo E6-B/C Receiver: Signals, Prototype, Tests and Performance', Sep. 2016, pp. 486–496, doi: 10.33012/2016.14828.
- [7] European Commission, 'First Signal-In-Space tests of the Galileo Commercial Service Demonstrator', *Internal Market, Industry, Entrepreneurship and SMEs - European Commission*, Jun. 27, 2014. https://ec.europa.eu/growth/content/first-signal-space-tests-galileo-commercial-service-demonstrator-0_en (accessed Mar. 30, 2021).
- [8] A. J. Sieber, 'The European Microwave Signature Laboratory', *EARSel Adv. Remote Sens.*, vol. 2, no. 1, pp. 195–204, Jan. 1993.
- [9] J. M. Lopez-Sanchez and J. Fortuny-Guasch, '3-D radar imaging using range migration techniques', *IEEE Trans. Antennas Propag.*, vol. 48, no. 5, pp. 728–737, May 2000, doi: 10.1109/8.855491.
- [10] J. Fortuny-Guasch and J. M. Lopez-Sanchez, 'Extension of the 3-D range migration algorithm to cylindrical and spherical scanning geometries', *IEEE Trans. Antennas Propag.*, vol. 49, no. 10, pp. 1434–1444, Oct. 2001, doi: 10.1109/8.954932.
- [11] S. R. Cloude, J. Fortuny, J. M. Lopez-Sanchez, and A. J. Sieber, 'Wide-band polarimetric radar inversion studies for vegetation layers', *IEEE Trans. Geosci. Remote Sens.*, vol. 37, no. 5, pp. 2430–2441, Sep. 1999, doi: 10.1109/36.789640.
- [12] J. Fortuny, K. Boniface, C. Gioia, M. Susi, M. Paonni, and M. Sgammini, 'GNSS RF Signal Testing and Evaluation at the EC Joint Research Centre: An enabler of the Galileo market uptake', in *2019 European Microwave Conference in Central Europe (EuMCE)*, Prague, Czech Republic, May 2019, pp. 323–326.
- [13] 'GSS9000 Series GNSS Simulator - Spirent'. <https://www.spirent.com/products/gnss-simulator-gss9000> (accessed Mar. 26, 2021).
- [14] J. T. Curran, M. Bavaro, and J. Fortuny, 'Analog and Digital Nulling Techniques for Multi-Element Antennas in GNSS Receivers', in *Proceedings of the 28th International Technical Meeting of the Satellite Division of The Institute of Navigation (ION GNSS+ 2015)*, Sep. 2015, pp. 3249–3261.
- [15] *Commission Delegated Regulation (EU) 2017/79 of 12 September 2016 establishing detailed technical requirements and test procedures for the EC type-approval of motor*

vehicles with respect to their 112-based eCall in-vehicles systems, of 112-based eCall in-vehicle separate technical units and components and supplementing and amending Regulation (EU) 2015/758 of the European Parliament and of the Council with regard to the exemptions and applicable standards (Text with EEA relevance.), vol. 012. 2017.

- [16] 'GSA publishes eCall guidelines to facilitate GNSS compatibility tests', May 10, 2019. <https://www.gsa.europa.eu/newsroom/news/gsa-publishes-ecall-guidelines-facilitate-gnss-compatibility-tests> (accessed Mar. 30, 2021).
- [17] K. Boniface, C. Gioia, M. Susi, J. Fortuny-Guasch, and F. Sbardellati, 'Galileo and EGNOS Adoption in Automotive Emergency Call System (eCall)', in *Proceedings of the 32nd International Technical Meeting of the Satellite Division of The Institute of Navigation (ION GNSS+ 2019)*, Sep. 2019, pp. 1284–1294, doi: 10.33012/2019.17130.
- [18] 'GSA/JRC ECALL Conformance Testing Campaign: ECALL Devices Assessment Report'. Jan. 10, 2018, Accessed: Mar. 30, 2021. [Online]. Available: <https://www.gsa.europa.eu/sites/default/files/content/gsa-jrc-ecall-conformance-testing-campaign.pdf>.
- [19] 'Updated Galileo OS SIS ICD now available', Jan. 11, 2021. <https://www.gsa.europa.eu/newsroom/news/updated-galileo-os-sis-icd-now-available> (accessed Mar. 26, 2021).
- [20] 'National Marine Electronics Association - NMEA'. https://www.nmea.org/content/STANDARDS/NMEA_0183_Standard (accessed Mar. 30, 2021).
- [21] A. V. Aho, B. W. Kernighan, and P. J. Weinberger, *The AWK programming language*. Reading, Mass: Addison-Wesley Pub. Co, 1988.
- [22] D. Vallado and P. Crawford, 'SGP4 Orbit Determination', presented at the AIAA/AAS Astrodynamics Specialist Conference and Exhibit, Honolulu, Hawaii, Aug. 2008, doi: 10.2514/6.2008-6770.
- [23] 'Sub-Committee on Navigation, Communications, Search and Rescue (NCSR), 3rd session, 29 February-4 March'. <https://www.imo.org/en/MediaCentre/MeetingSummaries/Pages/NCSR,-3rd-session.aspx> (accessed Mar. 26, 2021).
- [24] 'Maritime navigation and radiocommunication equipment and systems - Global navigation satellite systems (GNSS) - Part 3: Galileo receiver equipment - Performance requirements, methods of testing and required test results'. International Electrotechnical Committee, Accessed: Mar. 26, 2021. [Online]. Available: <https://webstore.iec.ch/publication/4517>.
- [25] C. Gioia, L. Cucchi, J. Fortuny-Guasch, and M. L. Martinez, 'Galileo Adoption in Shipborne Equipment', Sep. 2020, pp. 884–895, doi: 10.33012/2020.17730.
- [26] 'GNSS Market Report Issue 6, October 2019', Oct. 11, 2019. <https://www.gsa.europa.eu/gnss-market-report-issue-6-october-2019> (accessed Mar. 26, 2021).
- [27] 'GSA celebrates 1 billion Galileo smartphone users', Sep. 09, 2019. <https://www.gsa.europa.eu/newsroom/news/gsa-celebrates-1-billion-galileo-smartphone-users> (accessed Mar. 26, 2021).
- [28] T. Jahn *et al.*, 'Assessment of GNSS Performance on Dual-Frequency Smartphones', Oct. 2019, doi: 10.33012/2019.16860.
- [29] 'European Location As A Service Targeting International Commerce', May 13, 2015. <https://www.gsa.europa.eu/european-location-service-targeting-international-commerce> (accessed Mar. 26, 2021).
- [30] 'Raw GNSS Measurements', *Android Developers*. <https://developer.android.com/guide/topics/sensors/gnss> (accessed Apr. 09, 2021).

- [31] C. Gioia, S. Damy, and D. Borio, 'Precise Time in your Pocket: Timing Performance of Android Phones', Feb. 2019, doi: 10.33012/2019.16749.
- [32] C. Gioia and D. Borio, 'Android positioning: from stand-alone to cooperative approaches', *Appl. Geomat.*, Sep. 2020, doi: 10.1007/s12518-020-00333-4.
- [33] 'Project FANTASTIC: Field Aware Navigation and Timing Authentication Sensor for Timing Infrastructure and Centimeter level positioning', *FANTASTIC Project*. <http://gnss-fantastic.eu/> (accessed Mar. 26, 2021).
- [34] 'SPAN GNSS Inertial Navigation Systems'. <https://novatel.com/products/span-gnss-inertial-navigation-systems> (accessed Mar. 26, 2021).
- [35] M. Pini, G. Marucco, G. Falco, M. Nicola, and W. De Wilde, 'Experimental Testbed and Methodology for the Assessment of RTK GNSS Receivers Used in Precision Agriculture', *IEEE Access*, vol. 8, pp. 14690–14703, 2020, doi: 10.1109/ACCESS.2020.2965741.
- [36] 'Newsletter', *FANTASTIC Project*. <http://gnss-fantastic.eu/newsletter/> (accessed Apr. 27, 2021).
- [37] 'Project GAUSS – Galileo-EGNOS as an Asset for UTM Safety and Security'. <https://projectgauss.eu/> (accessed Mar. 26, 2021).
- [38] 'ATLAS | Air Trafic Laboratory for Advanced unmanned Systems'. <http://atlascenter.aero/en> (accessed Apr. 09, 2021).
- [39] 'GSA publishes High Accuracy Service information update', Mar. 15, 2021. <https://www.gsa.europa.eu/newsroom/news/gsa-publishes-high-accuracy-service-information-update> (accessed Mar. 30, 2021).
- [40] 'Galileo's High Accuracy Service: Field Experimentation of Data Dissemination Schemes - Inside GNSS - Global Navigation Satellite Systems Engineering, Policy, and Design'. <https://insidegnss.com/galileos-high-accuracy-service-field-experimentation-of-data-dissemination-schemes/> (accessed Mar. 30, 2021).
- [41] M. Susi and D. Borio, 'Galileo E6-B Tracking with Non-coherent Integration and Kalman Filtering', Sep. 2019, pp. 3528–3542, doi: 10.33012/2019.16934.
- [42] M. Susi and D. Borio, 'Kalman filtering with noncoherent integrations for Galileo E6-B tracking', *NAVIGATION*, vol. 67, no. 3, pp. 601–618, 2020, doi: <https://doi.org/10.1002/navi.380>.
- [43] D. Borio and M. Susi, 'Non-Coherent Processing of Galileo E6b Signals', Sep. 2018, pp. 4258–4270, doi: 10.33012/2018.16085.
- [44] 'GEARS - Orolia - GSA - Timing receiver - Critical Infrastructure - Galileo'. <https://gears-gsa-project.eu/> (accessed Apr. 12, 2021).
- [45] 'News – GIANO Project'. <https://gianoproject.eu/news/> (accessed Apr. 12, 2021).
- [46] P. INGLING, 'EGALITE - EGNOS and Galileo Timing Service Extension and Consolidation', *Internal Market, Industry, Entrepreneurship and SMEs - European Commission*, Jul. 31, 2020. https://ec.europa.eu/growth/sectors/space/research/horizon-2020/egalite_en (accessed Apr. 12, 2021).
- [47] R. Píriz *et al.*, 'Safety Analysis for a New GNSS Timing Service via Galileo', Sep. 2019, pp. 3359–3376, doi: 10.33012/2019.17105.
- [48] M. Kirkko-Jaakkola *et al.*, 'Receiver-Level Robustness Concepts for EGNSS Timing Services', in *Proceedings of the 30th International Technical Meeting of the Satellite Division of The Institute of Navigation (ION GNSS+ 2017)*, Sep. 2017, pp. 3353–3367, doi: 10.33012/2017.15137.
- [49] P. INGLING, 'EGNSS Timing Services', *Internal Market, Industry, Entrepreneurship and SMEs - European Commission*, Jun. 04, 2018. https://ec.europa.eu/growth/sectors/space/research/horizon-2020/egnss-timing-services_en (accessed Apr. 12, 2021).

- [50] C. Gioia, D. Borio, E. Realini, A. Gatti, and G. Tagliaferro, 'From Single to Precise Point Positioning: The Impact on Time Retrieval', in *2020 IEEE/ION Position, Location and Navigation Symposium (PLANS)*, 2020, pp. 1104–1110, doi: 10.1109/PLANS46316.2020.9109981.
- [51] D. Borio and C. Gioia, 'GNSS interference mitigation: A measurement and position domain assessment', *NAVIGATION*, vol. 68, no. 1, pp. 93–114, Mar. 2021, doi: 10.1002/navi.391.
- [52] D. Borio and C. Gioia, 'Interference mitigation: impact on GNSS timing', *GPS Solut.*, vol. 25, no. 2, p. 37, Apr. 2021, doi: 10.1007/s10291-020-01075-x.
- [53] C. Gioia and D. Borio, 'A statistical characterization of the Galileo-to-GPS inter-system bias', *J. Geod.*, vol. 90, no. 11, pp. 1279–1291, Nov. 2016, doi: 10.1007/s00190-016-0925-6.
- [54] G. G. (Associate E. Y. Jade Morton Frank van Diggelen, James J. Spilker Jr., Bradford W. Parkinson (Editors), Sherman Lo, *Position, Navigation, and Timing Technologies in the 21st Century: Integrated Satellite Navigation, Sensor Systems, and Civil Applications*, Set. WILEY, 2021.
- [55] P. J. G. Teunissen and O. Montenbruck, Eds., *Springer Handbook of Global Navigation Satellite Systems*. Cham: Springer International Publishing, 2017.
- [56] F. Dovis, Ed., *GNSS interference, threats, and countermeasures*. Boston: Artech House, 2015.
- [57] 'STRIKE3 Project'. <http://gnss-strike3.eu/> (accessed Apr. 12, 2021).
- [58] 'Project GAMMA'. <https://www.projectgamma.eu/> (accessed Apr. 13, 2021).
- [59] C. O'Driscoll *et al.*, 'Compatibility Analysis Between LightSquared Signals and L1/E1 GNSS Reception', Apr. 2012, pp. 447–454, Accessed: Mar. 26, 2021. [Online]. Available: <http://www.ion.org/publications/abstract.cfm?jp=p&articleID=10113>.
- [60] M. Rao, C. O'Driscoll, D. Borio, and J. Fortuny, 'LightSquared effects on estimated C/N 0, pseudoranges and positions', *GPS Solut.*, vol. 18, no. 1, pp. 1–13, Jan. 2014, doi: 10.1007/s10291-012-0304-6.
- [61] L. Cucchi, J. Fortuny, G. Baldini, I. Fernandez-Hernandez, B. Martinez, and G. Vecchione, 'A GNSS Jamming/Spoofing Test Suite for Smart Tachograph Applications', Oct. 2020, doi: 10.33012/2020.17759.
- [62] *Commission Implementing Regulation (EU) 2016/799 of 18 March 2016 implementing Regulation (EU) No 165/2014 of the European Parliament and of the Council laying down the requirements for the construction, testing, installation, operation and repair of tachographs and their components (Text with EEA relevance) C/2016/1597* .
- [63] *Commission Implementing Regulation (EU) 2018/502 of 28 February 2018 amending Implementing Regulation (EU) 2016/799 laying down the requirements for the construction, testing, installation, operation and repair of tachographs and their components (Text with EEA relevance) C/2018/1116*, vol. 32018R0502. .
- [64] J. Mitola, *Software radio architecture: object-oriented approaches to wireless systems engineering*. New York: Wiley, 2000.
- [65] 'USRP-2944'. <https://www.ni.com/it-it/support/model.usrp-2944.html> (accessed Apr. 20, 2021).
- [66] D. Calle, S. Cancela, E. Carbonell, I. Rodríguez, G. Tobías, and I. Fernández-Hernández, 'First Experimentation Results with the Full Galileo CS Demonstrator', Sep. 2016, pp. 2870–2877, doi: 10.33012/2016.14728.
- [67] C. Sarto *et al.*, 'Implementation and Testing of OSNMA for Galileo', Sep. 2017, pp. 1508–1519, doi: 10.33012/2017.15184.
- [68] 'NACSET- Navigation Authentication through Commercial Service-Enhanced Terminals', *Internal Market, Industry, Entrepreneurship and SMEs - European Commission*, Sep. 08,

2020. https://ec.europa.eu/growth/sectors/space/research/horizon-2020/nacset_en (accessed Mar. 30, 2021).
- [69] 'Septentrio AsteRx-U Receiver'. <https://www.septentrio.com/en/products/gnss-receivers/rover-base-receivers/integrated-gnss-receivers/asterx-u> (accessed Mar. 26, 2021).
- [70] T. LANGE, 'Pilot living labs at the JRC', *EU Science Hub - European Commission*, Jun. 20, 2019. <https://ec.europa.eu/jrc/en/research-facility/living-labs-at-the-jrc> (accessed Apr. 07, 2021).
- [71] 'FLIR PTU-D300E Pan/Tilt Unit for side-mounted payloads up to 70 lbs | FLIR Systems'. <https://www.flir.com/products/ptu-d300e/> (accessed Apr. 28, 2021).
- [72] F. S. T. Van Diggelen, *A-GPS: assisted GPS, GNSS, and SBAS*. Boston: Artech House, 2009.
- [73] A. C. García, S. Maier, and A. Phillips, *Location-based services in cellular networks from GSM to 5G NR*. 2020.

List of Abbreviations

ADC	Analog-to-Digital Converter
ADKD	Authentication Data and Key Delay
AVAR	Allan Variance
ATLAS	Air Traffic Laboratory for Advanced Systems
AWGN	Additive White Gaussian Noise
BER	Bit Error Rate
CAS	Commercial Authentication Service
CDF	Cumulative Distribution Function
COG	Corse Over Ground
CSTTFF	Cold Start Time-To-First-Fix
CW	Continuous Wave
C/N₀	Carrier-to-Noise Power Spectral density ratio (C/N ₀)
DAC	Digital-to-Analog Converter
DC	Direct Current
DHCP	Dynamic Host Configuration Protocol
DG	Directorate General
DNS	Domain Name System
DSSS	Direct-Sequence Spread Spectrum
DUT	Devices Under Test
EC	European Commission
EGNOS	European Geostationary Overlay System
EMSL	European Microwave Signature Laboratory
EU	European Union
FANTASTIC	Field Aware Navigation and Timing Authentication Sensor for Timing Infrastructure and Centimeter level positioning
FDE	Fault Detection and Exclusion
GAUSS	Galileo-EGNOS as an Asset for UTM Safety and Security
GFE	Galileo Fundamental Elements
GGTO	Galileo to GPS Time Offset
GNSS	Global Navigation Satellite System
GSA	European GNSS Agency
GSC	Galileo Service Centre
GUI	Graphical User Interface
HAS	High Accuracy Service
HE	Horizon Europe: The EU Research and Innovation Programme in the Multi-Annual Financial Framework 2021-2027
HW	Hardware
H2020	Horizon 2020: The EU Research and Innovation Programme in the Multi-Annual Financial Framework 2014-2020
ICD	Interface Control Document
IEC	International Electrotechnical Committee
IEEE	Institute of Electrical and Electronics Engineers
IF	Intermediate Frequency
IMO	International Maritime Organisation
IMU	Inertial Measurement Unit
IOD	Issue Of Data
JRC	Joint Research Centre
J/S	Jammer over Signal
KPI	Key Performance Indicator
LBS	Location-Based Service
LHCP	Left Hand Circularly Polarised
MAS	Mission And Services
MEMS	Micro Electro Mechanical System
NAS	Network Attached Storage

NMEA	National Marine Electronics Association
NTP	Network Time Protocol
OBU	On-board Unit
OSNMA	Open Service Navigation Message Authentication
OTA	Over The Air
PATROL	Position Authenticated Tachograph foR OSNMA Launch
PCI	Peripheral Component Interconnect
PDOP	Position Dilution Of Precision
PLC	Programmable Logic Controller
PPP	Precise Point Positioning
PPK	Post Processing Kinematic
PPS	Pulse Per Second
PVT	Position Velocity and Time
RAIM	Receiver Autonomous Integrity Monitoring
RF	Radio Frequency
RFI	Radio Frequency Interference
RHCP	Right Hand Circularly Polarised
RINEX	Receiver Independent Exchange
RMS	Root Mean Squared
RTK	Real Time Kinematic
RX	Receive
SAR	Synthetic Aperture Radar
SARA	Search and Rescue Aid
SBAS	Satellite Based Augmentation System
SCER	Security Code Estimation and Replay
SDR	Software Defined Receiver
SGP4	Standard General Perturbations Satellite Orbit Model 4
SIS	Signal In Space
SOG	Speed Over Ground
SPAN	Synchronous Position Attitude and Navigation
STD	STandard Deviation
ST	Smart Tachograph
SW	Software
TC	Test Case
TCP/IP	Transmission Control Protocol / Internet Protocol
TESLA	Timed Efficient Stream Loss-Tolerant Authentication
TLE	Two Lines Element
TTFF	Time-To-First-Fix
TX	Transmit
USRП	Universal Software Radio Peripheral
VNA	Vector Network Analyser

List of Figures

Figure 1. 3-D sketch of an exploded view of the EMSL with a car on top of the rotating tower (left). A photograph of the rotating tower with an antenna under test (right).....	11
Figure 2. Close view of the antennas, video camera and laser pointer in the sleds A (left) and B (right) of the EMSL laboratory.....	12
Figure 3. Sketch of the side view (left) and top view (right) of the two circular scans in an antenna measurement in the EMSL, which correspond to the zenith and azimuth angles.	13
Figure 4. 3D sketches identifying the four mechanical axes of the EMSL (left) and the spherical grid of measurement points in an antenna measurement with combined azimuth/zenith scans (right).....	13
Figure 5. Sketches of the set-up of a calibration measurement with the vector network analyser: reference antenna with known gain on transmit (left) and receive (right) modes... .	14
Figure 6. Two vertical cuts of the LHCP and RHCP gain of a choke-ring antenna at the frequency of 1578.0 MHz: vertical cuts at azimuth 0 deg (left) and azimuth 90 deg (right)... .	15
Figure 7. RHCP gain versus frequency of a choke-ring antenna measured at boresight in the EMSL	15
Figure 8. Sketch of the laboratory set-up to characterise an antenna using a GNSS simulator as a signal source (left) and photograph of the GNSS simulation rack behind the dome of the EMSL (right).	16
Figure 9. a sketch of the multi-port microwave switch (left) and a photograph of a 7-element antenna array mounted on the measurement tower of the EMSL (right).	17
Figure 10. Close view of the 7-element antenna array interfaced with the microwave switch driver (left); vertical cuts of the RHCP gain pattern of the central and a peripheral element at azimuth 0 deg (center); horizontal cuts of the gain of the central and a peripheral element at 40 deg elevation (right).	17
Figure 11. 3-D sketch of the signal routing network of the array of the 36 fixed antennas on the outer surface of the dome (top), and photograph showing the arrangement of the fixed probe antennas as seen inside the anechoic chamber (bottom).	18
Figure 12. Schematic representation of the set-up developed for eCall conformance testing at the JRC.	20
Figure 13. Barplot of the average, minimum and maximum CSTTFF values of the eCall devices measured at the signal power levels of -130 and -140 dBm.	21
Figure 14. Sketch of simulated vehicle trajectory used in the dynamic scenario with limited sky visibility and repeated periods of GNSS signals obscuration for the eCall tests.....	21
Figure 15. Skyplot showing the satellites in view for the second dynamic scenario with a limited sky view and the mask applied to the antenna pattern of the eCall device under test. .	22
Figure 16. Horizontal positioning accuracy for eCall modules in dynamic and dynamic shadow mode for the combined configuration GPS+GAL+SBAS is shown in terms of STD, maximum and mean values. The limit fixed in the regulation is also indicated.....	22
Figure 17. Photograph of the set-up used in the measurement campaign of the ship-borne receivers. The movable platform holds an RF signal generator and an antenna to generate RF interference signals.	24
Figure 18. Sketch illustrating the calibration of the GNSS signal power levels in the radiated tests. Using the amplified RF output of the simulator and a programmable attenuator, C/N ₀ values observed with a reference receiver in the radiated tests (left) are fully aligned with those measured with the same receiver in conducted mode (right) using the calibrated RF output of the simulator.	25

Figure 19. Two photographs with a close view of the set-up used with the programmable vector signal generator and a TX standard gain horn antenna on the movable platform of the EMSL	25
Figure 20. Pseudorange ramps and horizontal positioning error as a function of the time in the RAIM/FDE test case.	26
Figure 21. Experimental set-up adopted for the smartphone static test. a) Schematic representation of the test set-up. b) Views of the actual implementation of the set-up.....	27
Figure 22. Cumulative Distribution Function of the Range and Range Rate error considering two smartphones equipped with different Android versions.	28
Figure 23. Frequency stability of an Android smartphone in open-sky conditions	28
Figure 24. Pedestrian data collection set-up. On the left a schematic representation of the set-up. On the right side the trajectory and view of the actual implementation of the kinematic tests.	29
Figure 25. Photograph of the set-up used in the vehicular tests with the smartphones.	29
Figure 26. Schematic representation of the test set-up for smartphone testing using simulated GNSS signals.	29
Figure 27. Views of the actual set-up for smartphone testing using simulated GNSS signals, in the RF shielded room (left) and in the control room (right).	30
Figure 28. Novatel SPAN-CPT system of the reference navigation system available at the JRC.	31
Figure 29. (Left side) Experimental set-up of the cart used for the dynamic test in the frame of the FANTASTIC project [35]; (Right Side) Picture of the cart used for the dynamic tests carrying the SPAN-CPT system on the top (Extracted from FANTASTIC White Paper [36]). ...	32
Figure 30. Cart carrying the devices under test during a dynamic data collection in a vineyard [35].	32
Figure 31. Reference trajectory obtained by post processing the SPAN-CPT and the reference station data.	33
Figure 32. CDF of the horizontal position errors estimated for different devices under test and using the provided post-processed SPAN-CPT trajectory as reference [35].....	33
Figure 33. (Left Side) High-end geodetic antenna placed under open sky at the ATLAS facility, connected to a high geodetic receiver to serve as reference station during flight tests with drones (Right Side) Tucan drone used in the frame of the GAUSS Project (images courtesy of the GAUSS project).	34
Figure 34. Reference trajectory computed for one of the flight performed by the Tucan drone with Novatel Inertial Explorer.	34
<i>Figure 35. Surveying of the measurement points using a GNSS receiver (left) and the total station (right).</i>	35
<i>Figure 36: Survey results for the test carried out with the total station in the JRC Campus. ...</i>	36
<i>Figure 37: Multi-frequency high-grade GNSS geodetic antenna placed on the roof of the JRC laboratory. A geodetic receiver using this antenna is the source of the RTK corrections.</i>	37
<i>Figure 38: Multi-frequency antenna connected to a high grade mid-grade receiver that was used as the RTK rover.</i>	38
<i>Figure 39: JRC van equipped with an antenna on the roof and receivers acting as moving rover for RTK.</i>	38
Figure 40. Robotic cart used for the dynamic tests of the Fantastic Project (photograph taken during a demo organised at the occasion of a project review meeting on 30/10/2018, in Torino)....	39

Figure 41. Example PPK solution for a dynamic test carried out in the frame of the FANTASTIC Project	39
<i>Figure 42. Setting for the definition of the Galileo signals in the GNSS simulator.</i>	40
<i>Figure 43: Loss of lock analysis for the different Galileo modulations analysed during the test with simulated signals.</i>	41
<i>Figure 44: BER as a function of the C/N₀ extracted from a commercial receiver for all simulated Galileo signals including the Galileo E6 signal.</i>	41
<i>Figure 45: Views of the experimental setup used for the dynamic test: (upper left side) Internal view of the van with the USRP 2, connected to an external rubidium clock, and the COTS receiver; (upper right side) External view of the van with the high geodetic antenna mounted on the roof;(lower left and right sides) Views of the environment selected for the dynamic test. The path is characterised by the presence of tall trees with rich foliage and sporadic buildings.</i>	42
<i>Figure 46: C/N₀ time series obtained from the COTS receiver (dashed red lines) and data-only KF tracking with 20 ms integration time (continuous line) for the dynamic test.</i>	42
Figure 47. (On the right) Schematic representation of the process used for local clock characterisation. (On the left) Different navigation solution used for computing receiver clock bias.	43
Figure 48. Set-up used for GNSS receiver local clock characterisation.	44
Figure 49. Set-up used for assessing the impact of RFI on GNSS timing. (On the right) Set-up used for evaluating the impact of jamming mitigation technique. (On the left) Set-up developed in the anechoic chamber to assess RFI impact on GPS timing receivers.	44
Figure 50. Sample results for local clock stability results using the two set-ups available at the JRC.....	45
Figure 51. Test set-up used for monitoring PPS signal output. The GNSS simulator is used to generate both genuine and spoofed satellite signals during the test (taken from the Final Report of the FANTASTIC Project [33]).....	45
Figure 52 Snapshot of the multi-channel oscilloscope showing the true PPS (yellow) and PPS signals of other receivers under test (taken from the Final Report of the FANTASTIC Project [33]).	46
Figure 53. Evaluation of the Allan variance using GPS/Galileo inter-system bias and its drift estimates. a) Pseudorange-derived Allan variance. b) Doppler-derived Allan variance.	47
Figure 54. In the upper box:GPS to Galileo Inter-system bias time series obtained using a mass market receiver. In the lower plot:GPS-Galileo inter-system stability.	47
Figure 55. Photograph of the setup used in the EMSL for the compatibility assessment with LightSquared (left). Observed loss of C/No versus power of the LTE signals with the three receivers tested and one of the proposed band allocations (right).	48
Figure 56. Snapshot of the real time spectrum analyser showing the narrow-band pulse interference signal, its power spectrum, power versus time, and power spectrogram.	49
Figure 57. Timeline showing the time intervals where the wide-band interference signal was present.	49
Figure 58. Snapshot of the real time spectrum analyser showing the wide-band AWGN signal, its power spectrum, power versus time, and power spectrogram.	50
Figure 59. Spectrogram and power spectral density of a narrow-band sawtooth FM waveform, with a bandwidth of 10 MHz and a sweep time of 20 usec.....	50
Figure 60. Spectrogram and power spectral density of a wide-band sawtooth FM waveform, with a bandwidth of 40 MHz and a sweep time of 20 usec.....	51
Figure 61. Spectrogram and power spectral density of a narrow-band triangular FM waveform, with a bandwidth of 10 MHz and a sweep time of 20 usec.....	51

Figure 62. Flowchart diagram illustrating the methodology used to create the IF datasets with the spoofing threats for the ST test battery.	52
Figure 63. Photographs of the test equipment used to create the battery of test scenarios with jamming and spoofing threats.....	53
Figure 64. GUI of the software tool used to merge the two IF datasets, weighting the relative power level of one of them in accordance with a pre-defined profile.....	53
Figure 65. Sketch of the targeted spoofing attack with the GNSS simulator on board the truck (top); 2D genuine and counterfeit trajectories (bottom left) and speed profiles (bottom right) corresponding to the same test case.	54
Figure 66. Photographs of the JRC's van with the record and replay system used in the OSNMA test drives: outer (left) and inside (right) views of the van, showing the laptop, USRP device, rubidium clock, and PCI-to-Thunderbolt 3 adapter.	55
Figure 67. Block diagram of the record and replay system in the configuration to function as a GNSS repeater with an adjustable time delay.....	56
Figure 68. GUI of the OSNMA-enabled SW Receiver.	58
Figure 69. TESLA chain parameters, including number of MACK sections (NMACK), Hash function (HF), MAC function (MF), MACK Offset (MO) and public key ID (PKID).	59
Figure 70. ADKD status for Galileo SVID14.	59
Figure 71. OSNMA testing capabilities.	60
Figure 72. Satellite high-resolution image of the campus of JRC Ispra Site (source: Google Earth).	61
Figure 73. Examples of the test environments available on the JRC Ispra Campus.	62
Figure 74. Representation of the LI P57 "No Fly Zone" on the ENAV aeronautical map. This spatial area is under the control of JRC Ispra Site Manager.	62
Figure 75. Tethered drone used in the flight trial (top-left), drone flying on the campus (top-right) and view from the on-board camera used for traffic monitoring (bottom). All photographs taken during the demonstration of the SARA Project in the campus of the JRC Ispra Site, on 1/10/2020.	63
Figure 76. Example of repeatability test. On the left side the navigation device under test. On the right side, the reconstruction of the four laps performed by the user.	64
Figure 77. Example of indoor accuracy test. On the left side the navigation device under test. On the right side, the displacement of the control points.	64
Figure 78. North coordinate evolution as a function of time. The red dotted line indicates the position of the control points.	65
Figure 79. Photographs of the pan-tilt antenna positioner mounted on the measurement tower of the EMSL during one of the integration tests; (left) side and (right) front views of the pan-tilt antenna positioner.	66

List of Tables

Table 1. Typical interactions between JRC and the project consortium requesting the facilitation of testing and demonstration activities.....	8
Table 2. Specification of the positioning ranges and accuracies of the four mechanical axes of the EMSL.....	12

GETTING IN TOUCH WITH THE EU

In person

All over the European Union there are hundreds of Europe Direct information centres. You can find the address of the centre nearest you at: https://europa.eu/european-union/contact_en

On the phone or by email

Europe Direct is a service that answers your questions about the European Union. You can contact this service:

- by freephone: 00 800 6 7 8 9 10 11 (certain operators may charge for these calls),
- at the following standard number: +32 22999696, or
- by electronic mail via: https://europa.eu/european-union/contact_en

FINDING INFORMATION ABOUT THE EU

Online

Information about the European Union in all the official languages of the EU is available on the Europa website at: https://europa.eu/european-union/index_en

EU publications

You can download or order free and priced EU publications from EU Bookshop at: <https://publications.europa.eu/en/publications>. Multiple copies of free publications may be obtained by contacting Europe Direct or your local information centre (see https://europa.eu/european-union/contact_en).



The European Commission's science and knowledge service

Joint Research Centre

JRC Mission

As the science and knowledge service of the European Commission, the Joint Research Centre's mission is to support EU policies with independent evidence throughout the whole policy cycle.



EU Science Hub
ec.europa.eu/jrc



@EU_ScienceHub



EU Science Hub - Joint Research Centre



EU Science, Research and Innovation



EU Science Hub



Publications Office
of the European Union

doi:10.2838/93444

ISBN 978-92-76-39185-2